NATIONAL ADVISORY COMMITTEE FOR AERONAUTICS

TECHNICAL NOTE 2495

WIND-TUNNEL INVESTIGATION OF EFFECTS OF VARIOUS AERODYNAMIC BALANCE SHAPES AND SWEEPBACK ON CONTROL-SURFACE CHARACTERISTICS OF SEMISPAN TAIL SURFACES WITH NACA 0009, 0015, 66-009, 66(215)-014, AND CIRCULAR-ARC AIRFOIL SECTIONS

By John J. Harper

Georgia Institute of Technology

Washington
October 1951

NATIONAL ADVISORY COMMITTEE FOR AERONAUTICS

TECHNICAL NOTE 2495

WIND-TUNNEL INVESTIGATION OF EFFECTS OF VARIOUS AERODYNAMIC BALANCE SHAPES AND SWEEPBACK ON CONTROL-SURFACE CHARACTERISTICS OF SEMISPAN TAIL SURFACES WITH NACA 0009, 0015, 66-009, 66(215)-014, AND CIRCULAR-ARC AIRFOIL SECTIONS

By John J. Harper

SUMMARY

A summary of force data on unswept and sweptback airplane control surfaces is presented. Lift and hinge-moment characteristics were determined for four unswept, semispan control surfaces, and lift, drag, hinge moment, and pitching moment were determined for two semispan, sweptback control surfaces. These control surfaces were tested in the 9-foot wind tunnel of the Daniel Guggenheim School of Aeronautics at the Georgia Institute of Technology and were of the wide-chord type suitable for use as elevators or rudders.

Measured values of the various parameters are compared with those obtained from section data by application of lifting-surface and lifting-line theory.

INTRODUCTION

The data presented herein are the results of two wind-tunnel investigations in the Georgia Institute of Technology 9-foot wind tunnel. These tests were conducted under the sponsorship and with the financial assistance of the National Advisory Committee for Aeronautics as part of an extensive wind-tunnel investigation to determine the aerodynamic characteristics of balanced control surfaces in order to supply data for design purposes.

Force-test measurements were made in three-dimensional flow to determine the aerodynamic characteristics of the following control-surface arrangements:

(1) A series of tail models having NACA 0009, 66-009, 0015, and 66(215)-014 profiles, a sweep angle of 13.5° at the 25-percent-chord line, a tail aspect ratio of 3.36, and a taper ratio of 0.4 with various unswept trailing-edge flap configurations. The flap configurations tested included 30-percent-chord elliptic and sharp-nosed aerodynamically balanced flaps and internal-balance flaps, as well as some 30-percent-chord plain (radius-nose) flaps. The balanced flaps had a nose balance overhang of 35 percent of the local flap chord and a constant flap nose gap. Plain tabs and two sizes of unshielded horn balances were tested with some of the models.

The NACA 66-009 and 66(215)-014 airfoil models were also constructed without the cusp to give straight-contour flaps.

(2) A series of tail models having NACA 0009 or 9-percent-thick circular-arc profiles, a sweep angle of 40° at the 25-percent-chord line, a tail aspect ratio of 3.30, and a taper ratio of 0.4 with balanced and plain flaps which were swept back 30.7° at the hinge line. The model flaps were 30 percent of the tail chord measured parallel to the air stream and had a 35-percent-flap-chord overhang. The flap nose gap was held constant for the various overhangs tested. Only one size of shielded horn was tested in conjunction with the plain flap.

A more complete description of the models is given in the section entitled "Apparatus, Models, and Tests."

SYMBOLS

A	aspect ratio $\left(b^2/S\right)$
B	horn balance coefficient $\left(\sqrt{\frac{\text{Horn area} \times \text{horn mean chord}}{\text{Flap area} \times \text{flap mean chord}}}\right)$
b	twice span of semispan model, measured perpendicular to plane of symmetry, feet
b_f	twice span of semispan model flap, measured perpendicular to plane of symmetry, feet
C_D	airfoil drag coefficient $(2D/qS)$
ΔC_{h_b}	increment of hinge-moment coefficient contributed by internal balance

C_{h_f} flap hinge-moment coefficient $\left(H_f/q\bar{c}_f^2 b_f\right)$

C_L airfoil lift coefficient $(2L/qS)$

ΔC_{L_f} increment of lift coefficient due to deflection of flap

C_m airfoil pitching-moment coefficient $(2M/qS\bar{c})$

c airfoil chord, measured in free-stream plane, feet

$\bar{c}$ mean aerodynamic chord, feet $\left(\dfrac{\int_0^{b/2} c^2\,db}{\int_0^{b/2} c\,db}\right)$

c' chord measured perpendicular to hinge axis, feet

c_b chord of balance overhang, measured in free-stream plane, feet

$\bar{c}_{bp}$ root-mean-square chord of balance plate, feet

c_f chord of flap at any section, measured in free-stream plane, feet

$\bar{c}_f$ root-mean-square chord of flap, measured perpendicular to hinge axis, feet

c_f' flap chord measured perpendicular to hinge axis, feet

c_{h_f} flap section hinge-moment coefficient $\left(h_f/qc_f^2\right)$

c_l airfoil section lift coefficient (l/qc)

D measured total drag force, pounds

H_f flap hinge moment, foot-pounds

h_f flap section hinge moment, foot-pounds

L measured total lift force, pounds

l section lift, pounds

M measured pitching moment about quarter chord of mean aerodynamic chord, foot-pounds

m_s ratio of moment contributed by flexible seal to moment contributed by balance plate

P_R resultant pressure coefficient

q dynamic pressure, pounds per square foot

R Reynolds number $(\rho V\bar{c}/\mu)$

S twice area of semispan model, square feet

t thickness of control surface at hinge

$\bar{t}$ root-mean-square thickness of overhang, measured at hinge line

V velocity, feet per second

α model angle of attack, degrees

δ control-surface or tab deflection, measured in plane perpendicular to hinge axis, degrees

Λ sweepback angle, measured at quarter-chord line, degrees

λ taper ratio $\left(\frac{\text{Tip chord}}{\text{Root chord}}\right)$

μ coefficient of viscosity

ρ mass density of air, slugs per cubic foot

ϕ trailing-edge angle, measured in plane perpendicular to hinge axis, degrees

$$C_{h_\alpha} = \left(\frac{\partial C_{h_f}}{\partial \alpha}\right)_{\delta_f,\delta_t}$$

$$c_{h_\alpha} = \left(\frac{\partial c_{h_f}}{\partial \alpha}\right)_{\delta_f,\delta_t}$$

$$C_{h_\delta} = \left(\frac{\partial C_{h_f}}{\partial \delta_f}\right)_{\delta_f,\delta_t}$$

$$c_{h_\delta} = \left(\frac{\partial c_{h_f}}{\partial \delta_f}\right)_{\alpha,\delta_t}$$

$$C_{L_\alpha} = \frac{\partial C_L}{\partial \alpha}$$

$$c_{l_\alpha} = \frac{\partial c_l}{\partial \alpha}$$

$$C_{L_\delta} = \frac{\partial C_L}{\partial \delta_f}$$

$$c_{l_\delta} = \frac{\partial c_l}{\partial \delta_f}$$

$$\alpha_\delta = \left(\frac{\partial \alpha}{\partial \delta}\right)_{C_L} = \frac{\left(\partial C_L/\partial \delta_f\right)_{\alpha,\delta_t}}{\left(\partial C_L/\partial \alpha\right)_{\delta_f,\delta_t}}$$

$\left(\frac{\partial C_m}{\partial C_L}\right)_{\alpha,\delta_t}$ slope of pitching-moment curve at constant angle of attack

$\left(\frac{\partial C_m}{\partial C_L}\right)_{\delta_f,\delta_t}$ slope of pitching-moment curve at constant flap deflection

Subscripts:

b	balance
e	effective
f	flap
t	tab
u	uncorrected

The subscripts outside the parentheses indicate the factors held constant in determining the parameter.

ACCURACY OF DATA

The accuracy of the experimental data depends upon the model contours, deflection of flap under load, and accuracy of force-measuring apparatus. The small hinge moments read when both angle of attack and flap deflection were zero indicate that inaccuracies in model contour were negligible. As the flap was controlled remotely, it could be set to any desired angle, and any deflection under load could be compensated for by simply resetting the flap to the original angle. The flap-angle-setting apparatus was completely separate from the strain-gage arm, and no deflections of the gage arm or torque shaft were registered. The accuracy of the flap angles and angles of attack was within $\pm 0.1^{\circ}$. The hinge moments were measured by means of strain gages used in conjunction with a commercial Wheatstone bridge control box. Frequent repeat runs indicated that lift and hinge-moment coefficients could be duplicated within ± 0.002 and ± 0.0002, respectively.

The jet-boundary corrections for the unswept models were supplied by the Langley Laboratory and are as follows:

$$\Delta\alpha = 1.386C_L - 0.208\,\Delta C_{L_f}$$

$$\Delta C_L = -0.021C_L$$

$$\Delta C_{h_f} = 0.0101C_L \quad \text{for 35-percent-}c_f\text{ overhang}$$

$$\Delta C_{h_f} = 0.0130C_L \quad \text{for plain flap}$$

As few data could be obtained for the wall corrections on the swept models, the corrections applied are similar to those for the unswept model. They are as follows:

$$\Delta\alpha = 1.10C_L - 0.20\,\Delta C_{L_f}$$

$$\Delta C_L = -0.018C_L$$

$$\Delta C_{h_f} = 0.0090C_L \quad \text{for 35-percent-}c_f\text{ overhang}$$

$$\Delta C_{h_f} = 0.0110C_L \quad \text{for plain flap}$$

Wake and solid blocking corrections (reference 1) have been applied to all data.

APPARATUS, MODELS, AND TESTS

All tests were conducted in the 9-foot wind tunnel of the Georgia Institute of Technology. This tunnel is a single-return type having a closed, circular test section 12 feet long. For panel testing a flat floor is installed which gives a jet height of approximately 8 feet. Speed changes are accomplished by means of a controllable-pitch propeller. The tunnel turbulence factor is 1.7.

Each model was mounted on a 50-inch-diameter plywood disk as shown in figure 1. This disk had less than 1/4-inch clearance between it and the tunnel floor. Model-plan-form dimensions are shown in figures 2 and 3. Following conventional practice, laminated mahogany was used to construct the models. The unswept flap models (actually the tail is swept 13.5° at $\bar{c}/4$) were equipped with 30-percent-chord flaps and a 20-percent-flap-chord plain tab of 50-percent-flap span. The flap nose gap was constant at 0.005c except on the sealed flap where the gap was zero. The tab used on the sealed flap had a gap of 0.001c. In order to obtain complete sealing for the internal balance, external hinges were employed. The effect of these external hinges was determined by means of dummies, and all data have been corrected for this effect. The nose overhangs tested are shown in figure 4.

The swept models were obtained by sweeping the quarter-chord axis 40° but maintaining the true airfoil parallel to the free stream. Development of the airfoil in a plane perpendicular to the hinge axis showed it to have a thickness ratio of 10.3 percent. Because of the fact that the swept models were designed to have the same flap and balance chord ratios in the free-stream plane as the unswept models (i.e., $c_f = 0.30c$, $c_b = 0.35c_f$), the values of c_f and c_b in the plane normal to the hinge axis (i.e., the chord upon which the hinge moment is based) were not the same as those for the unswept models. The values of c_f and c_b are shown in figure 3 to be $0.35c'$ and $0.319c_f'$, respectively. The prime indicates the airfoil chord measured normal to the flap hinge axis. With the exception of the sealed flap, the nose gap was 0.005c in the free-stream plane. The 20-percent-flap-chord tab was sealed by means of Scotch tape. The nose overhangs tested are shown in figure 5.

The unswept models had a taper ratio of 0.4 and an aspect ratio (including reflection) of 3.36. The swept models had a taper ratio

of 0.4 and an aspect ratio of 3.30. The airfoil sections tested were as follows:

Unswept models

NACA 0009

NACA 0015

NACA 66-009 } with true-contour and straight-contour flaps

NACA 66(215)-014 } with true-contour and straight-contour flaps

Swept models

NACA 0009 } in plane parallel to plane of symmetry

9-percent-thick circular arc } in plane parallel to plane of symmetry

The airfoil ordinates are given in table I, and the elliptic-overhang and horn dimensions are given in tables II and III, respectively.

The angle of attack and flap angle were both set by a remote-control arrangement which enabled the tunnel operator to detect any change in deflection of the flap under load and to correct for this. The model flaps generally were set at deflections from -6° to 21° in 3° increments, while the angle of attack was varied from zero to plus stall in 2° increments, except in some cases where the angle of attack was varied from minus stall to plus stall at zero flap deflection. On the unswept models the plain tab was tested in conjunction with the sealed flap (except on the NACA 0009 and 66(215)-014 models which were tested with the tab on the plain flap also) with the ratio of tab to flap deflection being -0.50. On the swept models the tab was tested with the sealed flap only with ratios of tab to flap deflection of 1.0, 0.50, -0.50, and -1.0.

Lift and hinge moments were measured on the unswept models, whereas lift, drag, pitching moment (about $\bar{c}/4$), and hinge moment were obtained for the swept models.

Tests on the models were made at a dynamic pressure of approximately 20.72 pounds per square foot which corresponds to an air velocity of about 90 miles per hour at standard sea-level conditions. Effective Reynolds numbers were 4,075,000 and 3,620,000 for the unswept and swept models, respectively.

DISCUSSION OF TEST RESULTS

Lift

A summary of the lift parameters C_{L_α} and α_δ for the various airfoils and flap configurations, as determined from the lift curves found in figures 6 to 38, 40 to 43, and 45 is given in table IV. These values were taken from unpublished data reports. In all cases the slope of the lift curve was greatest for the internal balance (sealed-gap condition). The NACA 66-009 airfoil model had slightly higher values of C_{L_α} than did the NACA 0009. These results are in qualitative agreement with reference 2, which reports the same trends. With a straight-contour flap (cusp removed) the lift-curve slopes of the 66-009 profile decreased slightly. The amount and shape of the balance overhang had little effect on C_{L_α}. This effect has been previously reported in reference 3. The slopes of the 9-percent-thick biconvex profile were considerably lower than those of the sweptback NACA 0009 model, and the lift curves were nonlinear. A comparison of the NACA 0009 unswept model with the NACA 0009 swept back 40° showed that the lift-curve slope decreased slightly with sweepback but not so much as theory predicts. The effect of sweeping the models by the method explained previously is to increase the thickness ratio slightly in a plane normal to the sweep reference line which would in itself tend to decrease C_{L_α} somewhat. References 4 and 5 show that C_{L_α} should decrease with sweep which agrees qualitatively with the results herein. It is believed that an unswept NACA 0010.3 airfoil model would have lift characteristics similar to those of an unswept 0009 model; therefore, the swept NACA 0009 (or actually a "swept" 0010.3) profile should have a smaller slope than the unswept configuration. The actual measured slopes for the swept and unswept models were very nearly the same; thus the swept model has lift characteristics almost identical with those of the unswept model. Therefore, an effort was made to determine whether or not Reynolds number had any effect on the characteristics of a sweptback panel. These data, presented in figure 46, are unpublished results on a 35° sweptback 9-percent-thick 6-series airfoil having virtually the same geometric characteristics as those of the models described herein. It appears that there is little Reynolds number effect over the range of test velocities. Other unpublished data from tests conducted at the Georgia Institute of Technology on a swept and an unswept panel have indicated that at $R \approx 3{,}500{,}000$ the swept panel had virtually the same lift characteristics as those of the unswept panel. Since these models of NACA 0009-64 modified airfoil section had a taper ratio of 0.53, an aspect ratio of 4.6, and were of approximately the same size as the models described in this report, it appears

that, within the Reynolds number range of the tests, the simplified theoretical sweepback corrections would overestimate the effects of sweep on the airfoils described in this report.

The NACA 66(215)-014 airfoil model with a true-contour flap had a lift-curve slope approximately the same as that of the NACA 0015 model, but when the cusp was removed on the 66(215)-014 section the lift-curve slope was reduced to values below that of the 0015 section. This reduction in C_{L_α} due to increasing the trailing-edge angle (using a straight-contour flap) on the 66(215)-014 airfoil model has been previously reported in reference 6. On the 6-series airfoil models both the elliptic and sharp-nosed overhangs gave minimum values of C_{L_α}. As the slopes of the curves of the 6-series profiles agreed favorably with those of the NACA 0009 and 0015 profiles when straight-contour flaps were used, it would appear that trailing-edge angle has more effect than airfoil profile. As with the 9-percent-thick airfoils, the amount and shape of balance overhang had little effect on C_{L_α}.

The minimum value of lift-curve slope on the NACA 0009 and 0015 profiles was obtained with the elliptic overhang, which agrees with the data presented in references 3 and 7.

The maximum value of the flap lift effectiveness α_δ for both the swept and unswept NACA 0009 profiles was generally obtained with the internal balance, with the plain nose yielding the next largest values. The elliptic and sharp-nosed overhangs generally gave values of α_δ slightly less than those for the plain nose. As indicated by theory, sweeping the NACA 0009 airfoil reduced the value of the lift-effectiveness parameter. The biconvex profile (with 40° sweepback) gave considerably lower values of α_δ than those for the 0009 profile, although the data are in good qualitative agreement. The data of reference 8 indicate this decrease in effectiveness due to sweepback.

Figures 6 to 10, 36 to 38, 40 to 43, and 45 indicate that for the tail surfaces with NACA 0009 (unswept), 0009 (swept back 40°), and biconvex (swept back 40°) sections the controls retained lift effectiveness throughout the angle-of-attack range tested for all deflections with but one exception, which was the sharp-nosed overhang on the unswept 0009 airfoil model. The figures also show that the lift effectiveness was reduced somewhat at the large flap deflections and at moderate and high positive angles of attack. This result is probably due to separation phenomena.

With reference to the unswept models, the NACA 66-009 airfoil model yielded the largest values of lift effectiveness; however, increasing the trailing-edge angle on this airfoil reduced α_δ. This effect is also reported in references 6 and 9. In the case of the NACA 66(215)-014 profile the true-contour flap with no aerodynamic balance (plain flap) gave values of α_δ larger than those for the NACA 0015 profile. This is not true for the other nose shapes as shown in table IV. With a straight-contour flap the absolute value of the lift effectiveness was reduced for all balance shapes. Figures 11 to 35 show that for the tail surfaces with NACA 0015 and both NACA 6-series airfoil sections the controls retained lift effectiveness for all flap deflections, although the flap was not so effective at the higher deflections.

Compared on a thickness basis, the lift effectiveness for the NACA 0009 and 66-009 profiles is slightly larger than that for the NACA 0015 and 66(215)-014 profiles. It is also indicated that airfoil shape has considerable effect as evidenced by the difference in values of α_δ for the NACA 66-009 (with a true-contour flap) and the NACA 0009 models, although the effect of trailing-edge angle cannot be eliminated as the pressure distribution over the flap changes with increase in trailing-edge angle. The values of lift due to flap deflection C_{L_δ} do not show so much variation since C_{L_δ} is proportional to both α_δ and C_{L_α}.

Hinge Moment

The curves of hinge-moment coefficient plotted against angle of attack for all models are shown in figures 6 to 38, 40 to 43, and 45. A summary of the hinge-moment parameters C_{h_α} and C_{h_δ} as determined from these figures is given in table IV. Unfortunately only two references (references 3 and 9) contained data on finite-span control surfaces with which the data in table IV could be compared. Results for a rectangular semispan NACA 0009 control surface of $A = 3$ are reported in reference 3. The values presented herein are considerably lower than those of reference 3; however, differences in plan form and aspect ratio may account in part for the discrepancy. Better agreement is obtained with the data of reference 9, which presents results for a tapered-plan-form model. Only fair quantitative agreement exists, however, possibly because the Reynolds number of reference 9 was about half that of the present tests.

On comparing the swept and unswept NACA 0009 surfaces, it is apparent that the hinge-moment parameters C_{h_α} and C_{h_δ} are

considerably more negative for the former. Although the simplified sweep theory predicts a reduction in the absolute values of C_{h_α} and C_{h_δ}, the discrepancy is attributed to the fact that the swept model had a 35-percent-flap chord (see fig. 3) and a 31.9-percent-c_f nose overhang measured in a plane perpendicular to the hinge axis. These values are comparable to $c_f = 0.30c$ and $c_b = 0.35c_f$ on the unswept model. Apparently this effect is enough to overcome any reductions in C_{h_α} and C_{h_δ} due to sweep and the increased trailing-edge angle; consequently, the hinge-moment parameters are considerably more negative for the sweptback 0009 surface. In the case of the swept biconvex airfoil all values of C_{h_α} and half of the values of C_{h_δ} were positive (see table IV). Here it is believed that the large trailing-edge angle (23.5°) measured perpendicular to the hinge line is responsible for the large balancing effect. A graphical presentation of the measured parameters for the two swept models and the 0009 unswept model is given in figure 47. This figure reveals the good qualitative agreement obtained for the various balance configurations.

With reference to the unswept models it can be pointed out that the hinge-moment parameter C_{h_α} is considerably more negative for the 9-percent-thick models than for the 15-percent-thick surfaces, except in the case of the NACA 66(215)-014 profile with a true-contour flap which gave values of C_{h_α} more negative than those for the NACA 0009 model or for the NACA 66-009 straight-contour model. The results in table IV also show that the 66-009 airfoil model with a true-contour flap yielded values of C_{h_α} which were more negative than those for the NACA 0009 profile. With a straight-contour flap (ϕ increased from 7° to 13°) the 66-009 profile had values of very nearly the same magnitude as those for the 0009 profile. Previous results for the 0009 section (reference 9) have shown that increasing the trailing-edge angle provides a balancing effect which reduces C_{h_α}. Reference 6 reports the same effect on the NACA 66(215)-014 profile.

A comparison of the NACA 0015 and 66(215)-014 (with a true-contour flap) profiles reveals that the former has more positive values of C_{h_α}. Use of a straight-contour flap on the 66(215)-014 airfoil model reduced the absolute value of C_{h_α}, again indicating the balancing effect of increased trailing-edge angle. These results indicate that airfoil profile apparently has small effect compared with the effect of trailing-edge angle.

The elliptic and sharp-nosed overhangs produced an unbalance on the 6-series airfoils with true-contour flaps, although both of these overhangs gave positive increments of C_{h_α} on the NACA 0009 and 0015 profiles. The internal balance was, in general, the most effective on the 6-series profiles. A comparison of measured increments of C_{h_α} for all models (with internal balance) with an empirically derived curve (reference 10) is presented in figures 48 and 49. The data do not correlate so well as might be expected from the data in reference 10.

The values of C_{h_δ} for the NACA 66-009 and 66(215)-014 profiles with true-contour flaps were more negative than those for the NACA 0009 and 0015 airfoil models. With a straight-contour flap on the 66(215)-014 profile, the values of C_{h_δ} were less negative than those for the 0009 and 0015 airfoil models employing straight flaps; however, the 66-009 profile with a straight-sided flap yielded values of C_{h_δ} more negative than those for the 0009 and 0015 profiles. On the NACA 0009 and 0015 airfoil models the elliptic overhang proved most effective, whereas the internal balance gave best results on the two 6-series profiles. The use of a balancing (lagging) tab in conjunction with the internal balance was the most effective balance configuration. Insofar as C_{h_δ} is concerned, the magnitude of the trailing-edge angle would appear to have more effect than airfoil section, as the values for the 6-series profiles compare favorably with those for the NACA 0009 and 0015 profiles when the trailing-edge angles are approximately the same. If the surface is to be closely balanced - that is, C_{h_δ} approaches zero - then C_{h_α} should be held as close to zero as possible, although any device that reduces C_{h_α} and C_{h_δ} the same amount should not be used because the unbalanced values of C_{h_α} are usually less negative than the unbalanced values of C_{h_δ}. If C_{h_α} is sufficiently large, positively, and C_{h_δ} is small, negatively, a steady oscillation could be set up. An internal balance used with a balancing tab would apparently be a satisfactory combination since C_{h_δ} is reduced much more than C_{h_α}. Small trailing-edge angles (such as those obtained on the 6-series models) should be avoided, as the relatively large values of C_{h_α} would tend to "heavy" the controls even though C_{h_δ} could be reduced by a balancing device.

The swept 0009 model had values of C_{h_δ} more negative than those for the unswept model, with the elliptic overhang being more effective than the internal balance. This increase in C_{h_δ} for the swept model is most likely attributable to the increased flap chord ($c_f = 0.35c'$) in a plane perpendicular to the flap hinge axis. The swept circular-arc section had values of C_{h_δ} which were considerably more positive than those of either the swept or unswept 0009 profiles. This result was probably due to the large trailing-edge angle.

In summarizing, the results presented herein indicate that the elliptic nose overhang is as effective as the internal balance on the 0009 and 0015 profiles, whereas the internal balance proved most effective on the 6-series profiles. The sharp-nosed overhang seems undesirable, as it was less effective than the elliptic overhang, and reference 11 indicates that the sharp nose would cause larger increments of drag. Comparisons of measured increments of C_{h_δ} for the internal balance with empirically derived values are presented in figures 48 and 49. The measured values fall below the correlation curve (reference 10), indicating that the internal balance was approximately one-third as effective as it should be; although a slight out-of-contour cover-plate effect may have occurred, this in itself does not appear to be responsible. Reference 12 presents results which show that out-of-contour cover plates or change in vent width can seriously affect the hinge-moment parameters; however, the data in figures 48 and 49 seem to be consistently grouped which would apparently eliminate the out-of-contour plate effect. The only other cause for a decrease in effectiveness would be seal leakage, but the model construction prevented any serious leakage from occurring. As there were no breaks in the seals for hinges, leakage alone does not appear to be the cause.

From the balance-chamber pressure coefficients given in the original wind-tunnel data for the swept models, the increment of hinge-moment coefficient contributed by the balance has been calculated for the internally balanced flap on the swept 0009 airfoil model and compared with measured values. This comparison is given in figures 48 and 49. In order to calculate ΔC_{h_b}, the methods and data of reference 13 are employed using the relation:

$$\Delta C_{h_b} = \frac{1}{2} P_R \left[\left(\frac{\bar{c}_{bp}}{\bar{c}_f} \right)^2 (1 + m_s) - \left(\frac{\bar{t}/2}{\bar{c}_f} \right)^2 \right] \frac{b_f}{b}$$

where

P_R resultant pressure coefficient

$\bar{c}_{bp}$ root-mean-square chord of balance plate

m_s ratio of moment contributed by flexible seal to moment contributed by balance plate

$\bar{t}$ root-mean-square thickness of overhang measured at hinge line

The results obtained by this equation show good quantitative agreement with measured values as indicated in figures 48 and 49. Since the values calculated from the pressure coefficients agree with the measured values, it does not seem likely that the experimental data would be in error. This still leaves considerable doubt as to why the internal balance was not so effective as other test data (reference 10) indicate. The only logical conclusion is that the decreased effectiveness is probably due to a combination of a small amount of leakage and cover-plate misalinement, or perhaps to the seal configuration itself.

The effect of fixed transition was determined on the NACA 0009 sweptback model with plain flap by means of a 0.050-inch-diameter wire placed along the surface at 3 percent chord. The effect of fixed transition, as also reported in reference 14, was to reduce the value of the parameters C_{h_α} and C_{h_δ} by shifting the hinge-moment-coefficient curves slightly. The effect was small, however, as it caused C_{h_α} to be reduced by 0.0005 and C_{h_δ}, by 0.001.

Effect of Horn Balance

The horn balances tested are shown in figures 2 and 3. The unshielded horn balance tested on the unswept models may be classified, according to reference 15, as type A horns, which are those formed by converting a spanwise portion of the fixed surface ahead of the hinge line into movable surface. On the sweptback models a shielded horn (see fig. 3) was tested. Horn dimensions and balance coefficients are given in table III. The positive increments of hinge-moment slopes for two sizes of unshielded horns (designated 1 and 2) have been compared (table V) with the correlated data of reference 15. These increments of C_{h_α} and C_{h_δ} are smaller than those predicted by means of the correlation curve of reference 15. This result may have been due in part to the rather small horn aspect ratios used.

One size of shielded horn balance was tested on the NACA 0009 and biconvex sweptback models. As may be seen from the results in table V, the shielded horn was less effective than the unshielded horns. This would be expected because the horn balance coefficient was much smaller. It would appear that a shielded horn alone could not be used to obtain a closely balanced surface.

Apparently the use of a horn balance would tend to increase the stick-free stability but at the same time would, during maneuvers, tend to heavy the control forces due to the positive value of C_{h_α} without a comparable change in C_{h_δ}. A properly designed horn balance would keep C_{h_α} near zero but the negative values of C_{h_δ} would most likely have to be reduced by the use of a balancing tab or other means. Experimental results indicating this effect have been previously given in reference 16.

Effect of Tab

All unswept surfaces were tested with a $0.20c_f$ lagging (balancing) tab used in conjunction with the internal balance, except for the NACA 0009 and 66(215)-014 (with a true-contour flap) profiles on which the plain flap was also tested with the tab. The plain tab was unsealed, and the ratio of tab to flap deflection δ_t/δ_f was -0.50. The use of the lagging tab reduced the flap lift effectiveness but also reduced C_{h_δ} on the NACA 0009 profile to about 50 percent of the unbalanced value for the plain flap. On the NACA 0015 profile, C_{h_α} was zero and C_{h_δ} had only a small negative value, indicating close balance. On the 6-series airfoils with straight-contour flaps, the tab was not so effective as on the true-contour models. On the 66(215)-014 profile with a true-contour flap (plain) the tab reduced C_{h_δ} to about 75 percent of the unbalanced value. The following increments of C_{h_δ} were obtained with the lagging tab:

	Increment
NACA 0009	
Plain flap	0.0032
Internal balance	.0023
NACA 66-009 with internal balance	
True-contour flap	.0030
Straight-contour flap	.0024
NACA 0015 with internal balance	.0031
NACA 66(215)-014 with internal balance	
True-contour flap	.0029
Straight-contour flap	.0008

The two swept models were tested with a sealed tab (Scotch tape seal) using ratios of tab to flap deflection of 1.0, 0.50, -0.50, and -1.0. The tab was used in conjunction with the internal balance only. The results (table IV) show that the tab was less effective on the circular-arc profile than on the swept NACA 0009 profile, as well as on some of the unswept airfoils. The tab also proved to be more effective on the swept 0009 model than on the unswept, although this result was probably due to sealing of the tab and to the fact that in a plane perpendicular to the flap hinge axis the tab chord was $0.214c_f$. The effect of tab deflection on hinge-moment coefficients is shown in figures 39 and 44. The tab produced larger increments in C_{h_δ} when deflected in same direction as the flap (unbalancing or leading). The following increments of C_{h_δ} were measured:

Airfoil	δ_t/δ_f	ΔC_{h_δ}
NACA 0009	1.0	-0.0072
	.5	-.0032
	-.5	.0032
	-1.0	.0061
9-percent-thick circular arc	1.0	-.0062
	.5	-.0030
	-.5	.0017
	-1.0	.0041

Drag

Drag data were obtained for the sweptback models only. The plots of drag coefficient against angle of attack are given in figures 36 to 38, 40 to 43, and 45. It is doubtful whether the drag coefficients can be considered absolute, but the incremental values should be relatively independent of tunnel-wall effect and end-plate tare and interference.

The incremental values of drag coefficient for different aerodynamic balance configurations are plotted in figure 50. The differences in ΔC_D

for the plain flap, elliptic overhang, and internal balance are small and in several instances are probably of the same order of magnitude as the experimental error. At $\alpha = 0^\circ$ the plain flap on the NACA 0009 model produced the smallest increments of drag, followed by the internal balance and the elliptic overhang. The data for the biconvex airfoil are somewhat scattered and, as before, the differences in ΔC_D for the various configurations are small compared with the total value of ΔC_D. At $\alpha = 0^\circ$ the elliptic nose produced the smallest increments, while at $\alpha = 6^\circ$ the plain flap caused the least drag.

Pitching Moment

The values of the parameters $\left(\frac{\partial C_m}{\partial C_L}\right)_{\alpha,\delta_t}$ and $\left(\frac{\partial C_m}{\partial C_L}\right)_{\delta_f,\delta_t}$ are presented in table IV. These parameters were determined from the plots of pitching-moment coefficient C_m found in figures 36 to 38, 40 to 43, and 45. These values were obtained for the sweptback airfoils only. When the lift was varied by changing the angle of attack with the flap at $\delta_f = 0^\circ$, the aerodynamic center was approximately at 28 percent chord for all flap configurations on the NACA 0009 airfoil model and at 25 percent chord on the biconvex profile. Actually, with plain flap and horn balance, the aerodynamic center moved back to the 29-percent-chord line on the NACA 0009 profile.

The following table gives the position of the aerodynamic center of lift due to flap deflection:

Aerodynamic Center of Lift due to Flap Deflection

[In fractions of the chord]

Flap configuration	NACA 0009	Circular arc
Plain	0.56	0.56
Plain with horn	.53	.53
Plain with fixed transition	.55	----
Elliptic overhang	.57	.57
Internal balance	.46	.58

PREDICTION OF FINITE-SPAN PARAMETERS FROM SECTION DATA

Finite-span parameters may be obtained by application of lifting-line or lifting-surface theories to section data. Both methods were employed and compared with measured parameter values in order to determine which method gives better agreement with experimental data. These comparisons are presented in table IV. Lifting-line-theory results as set forth in reference 17 and lifting-surface-theory corrections as given in reference 18 have been applied to section data obtained from reference 10. Because of the lack of section data it was impossible to calculate the finite-span-parameter values for all models and configurations, particularly in the case of the 6-series airfoils for which few section data could be found.

The result of comparing the two theories indicates that the lifting-surface theory generally gives better agreement with test data; however, both methods will sometimes give errors that are not generally tolerable for use in the design of a closely balanced surface. It is noted that discrepancies appear in both cases, mostly in C_{h_δ}; however, slight variations in trailing-edge angle, turbulence, separation, and aspect ratio all have considerable effect on the various parameters. Nonagreement may therefore be due to these variables.

The effects of sweepback are accounted for by applying sweep corrections to either lifting-line or lifting-surface results. Theory provides a means of estimating the effects of sweep (reference 19) on the lift-curve slope by use of the following relation:

$$\left(C_{L_\alpha}\right)_\Lambda = \left(C_{L_\alpha}\right)_{\Lambda=0} \cos \Lambda$$

Although the above relationship gives good agreement with test data for infinite and high aspect ratios, it overestimates the effect of sweep on low-aspect-ratio tail surfaces. Some unpublished data from tests $\left(R \approx 4 \times 10^6\right)$ conducted at the Georgia Institute of Technology on a swept and an unswept panel have shown that the swept configuration had a lift-curve slope only slightly smaller than that of the unswept configuration. The maximum lift coefficient was slightly higher for the swept configuration. As the data of reference 4 show excellent agreement with the cosine law, even for low aspect ratio at low Reynolds number (163,000 to 326,000), it would appear that there is some Reynolds number effect which may affect results obtained by using the theoretical sweep corrections. The method of DeYoung (reference 20) will give C_{L_α}

directly for various values of aspect ratio, taper ratio, and sweep, the data being presented in the form of charts.

Although it is implied that once the value of C_{L_α} is obtained either from lifting-line or lifting-surface theory the sweep corrections may be applied, the nature of the sweep correction is important. It has already been indicated (reference 21) that the full cosine effect is not realized at low aspect ratios; hence it appears that the use of the square root of the cosine would give better results. The following modification to the lifting-line theory gives results that correlate well with test data:

$$\left(C_{L_\alpha}\right)_\Lambda = 0.95\left(\frac{c_{l_\alpha}}{1 + \frac{57.3c_{l_\alpha}}{\pi A}}\right)\sqrt{\cos\Lambda}$$

For the NACA 0009 airfoil model with 40° sweep (plain flap) the above relationship gives $C_{L_\alpha} = 0.0525$. The method of DeYoung yields the same value. The measured value (table IV) is 0.052. A comparison of measured values with those obtained by means of the above equation is given in figure 51(a). The lift-curve slopes for the various test configurations were taken from the data of references 5 and 22. The use of the simple cosine correction as used in table IV is not to be recommended for small aspect ratios since it overestimates the effect of sweep.

The simple sweep theory gives the following relations for the other control-surface parameters:

$$\left(\alpha_\delta\right)_\Lambda = \left(\alpha_\delta\right)_{\Lambda=0}\cos\Lambda$$

$$\left(C_{h_\alpha}\right)_\Lambda = \left(C_{h_\alpha}\right)_{\Lambda=0}\cos\Lambda$$

$$\left(C_{h_\delta}\right)_\Lambda = \left(C_{h_\delta}\right)_{\Lambda=0}\cdot\cos^2\Lambda$$

It would be expected that these corrections would also overestimate the effects of sweep for low aspect ratios. The results in table IV were obtained by applying the foregoing corrections to parameter values calculated for an unswept surface by lifting-line or lifting-surface theory. The method of reference 21 corrects for sweep by modifying the

lifting-line theory to account for the sweep of the hinge line. Induced-camber effects are also considered, although this is a lifting-surface correction which is included in any results obtained by means of the lifting-surface method. It would appear that the method of reference 21 would give better agreement of estimated and test values than the simple corrections used in this report; therefore, it is to be recommended even though it, too, is subject to the limitations of both lifting-line and lifting-surface theories.

Although the flap lift effectiveness parameter C_{L_δ} may be obtained if C_{L_α} and α_δ are known, it may be estimated by the method of reference 8. This method applies to controls starting at the tip and will not strictly apply to controls beginning at the root. The value of C_{L_δ} obtained by the method of reference 8 is 0.0194 as compared with measured values of 0.0218 and 0.017 for the NACA 0009 and circular-arc airfoil models with plain flaps. The data of reference 8 were obtained from wings swept by rotating the wing about the intersection of the 50-percent-chord line with the plane of symmetry. A graphical comparison of this method with experimental data obtained from lifting-surface theory using the $\cos^2$ correction is presented in figure 51(b).

In computing finite-span parameters for the swept NACA 0009 airfoil model from section data, it was assumed that the NACA 0010.3 airfoil model normal to the hinge axis would have characteristics almost identical with those of the 0009 airfoil model. Thus 0009 section data were corrected for the increased flap chord, decreased overhang, and increased trailing-edge angle in the plane normal to the hinge axis.

CONCLUSIONS

The results of tests of tail models having NACA 0009, 66-009, 0015, and 66(215)-014 profiles and various unswept trailing-edge flap configurations and of tail models having NACA 0009 and 9-percent-thick circular-arc profiles with 40° sweepback at the quarter chord and trailing-edge flap configurations swept back 30.7° at the hinge line indicate the following conclusions:

1. The slope of the lift curve C_{L_α} is little affected by airfoil section but does vary with thickness as indicated by theory. Sweeping the airfoil back reduces the lift-curve slope, but the decrease due to sweep is not so much as that given by theory for low aspect ratios. The amount and shape of the balance overhang had little effect on C_{L_α}, although the internal balance generally resulted in the highest values of C_{L_α}, whereas the elliptic overhang generally gave the lowest values. The effect of increasing the trailing-edge angle is to decrease C_{L_α}.

2. For a given thickness ratio, it is indicated that airfoil profile has considerable effect on the flap lift effectiveness α_δ. In general, the internal balance gave the largest values of flap lift effectiveness, with the plain nose yielding the next largest values. The elliptic and sharp-nosed overhangs generally gave values of α_δ slightly less than those for the plain nose. Increasing the trailing-edge angle on the NACA 66-009 and 66(215)-014 profiles reduced α_δ for all balance configurations.

3. For a given thickness ratio the hinge-moment coefficient C_{h_α} is not greatly affected by airfoil section when compared with changes in trailing-edge angle. In all cases where the trailing-edge angle was increased, the absolute value of C_{h_α} was reduced considerably, thus indicating that trailing-edge angle has a much greater effect than airfoil profile. The effect of sweep (obtained by shearing the airfoil back) on the NACA 0009 airfoil was to increase the absolute values of C_{h_α}, although theory predicts a reduction in C_{h_α}. The elliptic and sharp-nosed overhangs produced an unbalance on the 6-series profiles with true-contour flaps, although both of these overhangs gave positive increments of C_{h_α} on the NACA 0009 and 0015 airfoil models. The internal balance was, in general, the most effective on the 6-series profiles.

4. Insofar as the hinge-moment coefficient C_{h_δ} is concerned, the magnitude of the trailing-edge angle would appear to have more effect than airfoil section, as the values for the 6-series profiles compare favorably with those of the NACA 0009 and 0015 profiles when the trailing-edge angles are approximately the same. The elliptic overhang was most effective on the 0009 and 0015 profiles, whereas the internal balance proved most effective on the 6-series airfoils. The sharp-nosed overhang seems undesirable because of its smaller effectiveness. The swept 0009 profile had values of C_{h_δ} more negative than those for the unswept model, with the elliptic overhang again being more effective than the internal balance. The swept circular-arc airfoil model yielded values of C_{h_δ} considerably less negative than those for the 0009 model probably because of the large trailing-edge angle.

5. The plain tab tested on the unswept models yielded about the same increment of C_{h_δ} on the NACA 0009 and 0015 profiles with the internal balance. Although the lagging tab reduced the flap lift effectiveness, it reduced C_{h_δ} to about 50 percent of the unbalanced value for the plain flap on the NACA 0009 model. On the 6-series airfoils, the tab was not so effective on the straight-sided flaps as on the true-contour

flaps. On the NACA 66(215)-014 airfoil model with a plain true-contour flap, the tab reduced C_{h_δ} to about 75 percent of the unbalanced value. On the swept profiles the tab was less effective on the circular-arc section than on the swept NACA 0009 profile, as well as on some of the unswept profiles. For the same value of the ratio of tab to flap deflection, the tab was more effective on the swept NACA 0009 model than on the unswept model, although this result was probably due to sealing of the tab and to the fact that the tab chord was 0.214 of the flap chord in the plane normal to the hinge axis.

6. The results of comparing lifting-line- and lifting-surface-theory results indicate that the lifting-surface method generally gives better agreement with test data; however, both methods will sometimes give errors that are not generally tolerable for use in design of a closely balanced surface.

Georgia Institute of Technology
Atlanta, Ga., August 2, 1949

REFERENCES

1. Glauert, H.: Wind Tunnel Interference on Wings, Bodies and Airscrews. R. & M. No. 1566, British A.R.C., 1933.

2. Gillis, Clarence L., and Lockwood, Vernard E.: Wind-Tunnel Investigation of Control-Surface Characteristics. XIII - Various Flap Overhangs Used with a 30-Percent-Chord Flap on an NACA 66-009 Airfoil. NACA ACR 3G20, 1943.

3. Garner, I. Elizabeth: Wind-Tunnel Investigation of Control-Surface Characteristics. XX - Plain and Balanced Flaps on an NACA 0009 Rectangular Semispan Tail Surface. NACA ARR L4I11f, 1944.

4. Bennett, Charles V., and Johnson, Joseph L.: Experimental Determination of the Damping in Roll and Aileron Rolling Effectiveness of Three Wings Having 2°, 42°, and 62° Sweepback. NACA TN 1278, 1947.

5. Letko, William, and Goodman, Alex: Preliminary Wind-Tunnel Investigation at Low Speed of Stability and Control Characteristics of Swept-Back Wings. NACA TN 1046, 1946.

6. Purser, Paul E., and Riebe, John M.: Wind-Tunnel Investigation of Control-Surface Characteristics. XV - Various Contour Modifications of a 0.30-Airfoil-Chord Plain Flap on an NACA 66(215)-014 Airfoil. NACA ACR 3L20, 1943.

7. Sears, Richard I., and Hoggard, H. Page, Jr.: Wind-Tunnel Investigation of Control-Surface Characteristics. VII - A Medium Aerodynamic Balance of Two Nose Shapes Used with a 30-Percent-Chord Flap on an NACA 0015 Airfoil. NACA ARR, July 1942.

8. Lowry, John G., and Schneiter, Leslie E.: Estimation of Effectiveness of Flap-Type Controls on Sweptback Wings. NACA TN 1674, 1948.

9. Hoggard, H. Page, Jr., and McKinney, Elizabeth G.: Wind-Tunnel Investigation of Control-Surface Characteristics of Plain and Balanced Flaps with Several Trailing-Edge Angles on an NACA 0009 Tapered Semispan Wing. NACA TN 1248, 1947.

10. Sears, Richard I.: Wind-Tunnel Data on the Aerodynamic Characteristics of Airplane Control Surfaces. NACA ACR 3L08, 1943.

11. Sears, Richard I., and Hoggard, H. Page, Jr.: Wind-Tunnel Investigation of Control-Surface Characteristics. XI - Various Large Overhang and Internal-Type Aerodynamic Balances for a Straight-Contour Flap on the NACA 0015 Airfoil. NACA ARR, Jan. 1943.

12. Hoggard, H. Page, Jr.: Wind-Tunnel Investigation of Control-Surface Characteristics. XII - Various Cover-Plate Alinements on the NACA 0015 Airfoil with a 30-Percent-Chord Flap and Large Sealed Internal Balance. NACA ARR, Jan. 1943.

13. Fischel, Jack: Hinge Moments of Sealed-Internal-Balance Arrangements for Control Surfaces. II - Experimental Investigation of Fabric Seals in the Presence of a Thin-Plate Overhang. NACA ARR L5F30a, 1945.

14. Lowry, John G., Turner, Thomas R., and Liddell, Robert B.: Aerodynamic Characteristics of Several Modifications of a 0.45-Scale Model of the Vertical Tail of the Curtiss XP-62 Airplane. NACA MR L6F27, 1946.

15. Lowry, John G.: Resume of Hinge-Moment Data for Unshielded Horn-Balanced Control Surfaces. NACA RB 3F19, 1943.

16. Lowry, John G., Maloney, James A., and Garner, I. Elizabeth: Wind-Tunnel Investigation of Shielded Horn Balances and Tabs on a 0.7-Scale Model of XF6F Vertical Tail Surface. NACA ACR 4C11, 1944.

17. Ames, Milton B., Jr., and Sears, Richard I.: Determination of Control-Surface Characteristics from NACA Plain-Flap and Tab Data. NACA Rep. 721, 1941.

18. Swanson, Robert S., and Crandall, Stewart M.: Lifting-Surface-Theory Aspect-Ratio Corrections to the Lift and Hinge-Moment Parameters for Full-Span Elevators on Horizontal Tail Surfaces. NACA TN 1175, 1947.

19. Ringleb, F.: Some Aerodynamic Relations for an Airfoil in Oblique Flow. NACA TM 1158, 1947.

20. DeYoung, John: Theoretical Additional Span Loading Characteristics of Wings with Arbitrary Sweep, Aspect Ratio, and Taper Ratio. NACA TN 1491, 1947.

21. Toll, Thomas A., and Schneiter, Leslie E.: Approximate Relations for Hinge-Moment Parameters of Control Surfaces on Swept Wings at Low Mach Numbers. NACA TN 1711, 1948.

22. Shortal, Joseph A., and Maggin, Bernard: Effect of Sweepback and Aspect Ratio on Longitudinal Stability Characteristics of Wings at Low Speeds. NACA TN 1093, 1946.

TABLE I.- AIRFOIL ORDINATES

Station (a)	NACA 0009 (a)	NACA 0015 (a)	NACA 66-009 (a)	NACA 66(215)-014 (a)	NACA 0009 swept back 40° (b)	Station (a)	9-percent-thick circular arc (a)
0	0	0	0	0	0	0	0
1.25	1.42	2.37	1.05	1.535	1.25	3.70	.648
2.5	1.96	3.27	1.41	2.080	2.12	8.33	1.39
5.0	2.67	4.44	1.94	2.880	3.22	12.96	2.04
7.5	3.15	5.25	2.34	3.506	3.86	17.59	2.64
10	3.51	5.85	2.67	4.048	4.26	22.22	3.13
15	4.01	6.68	3.19	4.904	4.79	26.85	3.54
20	4.30	7.17	3.59	5.566	5.01	31.48	3.89
25	4.46	7.43	3.91	6.081	5.15	36.11	4.17
30	4.50	7.50	4.16	6.470	5.15	40.74	4.35
40	4.35	7.25	4.44	6.920	4.94	45.37	4.47
50	3.97	6.62	4.49	6.962	4.52	50.00	4.51
60	3.42	5.70	4.21	6.497	3.86		
70	2.75	4.58	3.46	5.224	3.10		
80	1.97	3.28	2.22	3.375	2.21		
90	1.09	1.81	.92	1.389	1.25		
95	.60	1.01	.37	.523	.68		
100	(.10)	(.16)	(.10)	(.095)	(.137)		
100	0	0	0	0	0		
L.E. radius	0.89	2.48	0.558	1.206		L.E. radius	0

[a]Stations and ordinates in percent chord.
[b]Measured in plane perpendicular to hinge axis.

TABLE II.- ELLIPTIC-OVERHANG ORDINATES

Unswept models (a)						Swept models (b)		
Station	NACA 0009	NACA 0015	Station	NACA 66-009	NACA 66(215)-014	Station	NACA 0009	Circular arc
0	0	0	0	0	0	0	0	0
1.09	1.25	2.03	1.04	2.34	1.51	.43	.78	1.04
2.14	1.69	2.81	2.08	3.18	2.03	1.01	1.18	1.81
3.16	1.93	3.25	3.12	3.75	2.34	2.20	1.70	2.32
4.22	2.24	3.62	4.17	4.12	2.76	3.38	2.03	2.79
5.26	2.34	3.90	5.20	4.43	2.81	4.57	2.29	3.13
6.30	2.47	4.17	6.25	4.69	2.99	5.75	2.48	3.41
7.34	2.55	4.35	7.29	4.95	3.28	6.93	2.58	3.55
8.38	2.60	4.45	8.33	5.05	3.33	8.12	2.65	3.67
9.42	2.66	4.50	9.37	5.13	3.39	9.30	2.70	3.76
10.46	2.73	4.53	10.46	5.16	3.40	10.50	2.72	3.79

[a]In percent chord measured from leading edge of overhang.

[b]Measured parallel to free stream.

TABLE III.- DATA FOR HORN BALANCES

Horn number	Airfoil section	Horn span (in.)	Horn area (sq in.)	Horn mean chord (in.)	Flap area (sq in.)	Flap mean chord (in.)	B
1	NACA 0009	4.36	60.16	13.6	517.4	10.17	0.388
1	NACA 0015	4.94	65.92	13.4	518.4	10.12	.404
2	NACA 0009	6.36	89.28	14.25	517.4	10.17	.484
2	NACA 0015	6.94	96.00	13.95	518.4	10.12	.496
[a]1	NACA 66-009	4.36	58.10	13.85	516	10.05	.392
1	NACA 66(215)-014	4.84	63.10	13.82	517.17	10.10	.408
[a]2	NACA 66-009	6.36	88.0	14.26	516	10.05.	.492
2	NACA 66(215)-014	6.84	93.0	14.22	517.17	10.10	.503
[b]1a	Swept NACA 0009	4.46	33.40	7.25	434.0	9.15	.244
[b]1a	Swept circular arc	4.46	32.88	7.25	434.0	9.15	.244

[a]Horns are same for straight-contour flaps on both 6-series airfoils.
[b]Shielded horn used on swept models.

TABLE IV.- MEASURED AND PREDICTED PARAMETER VALUES

Model dimensions and characteristics			Section parameters					Finite-span parameters																
								C_{l_α}			C_{l_β}			C_{h_α}			C_{h_β}							
Balance shape	c_b/c_f	δ_t/δ_f	a_{l_α}	c_{l_β}	c_{l_δ}	a_{h_α}	a_{h_β}	Lifting line	Lifting surface	Measured	Lifting line	Lifting surface	Measured	Lifting line	Lifting surface	Measured	Lifting line	Lifting surface	Measured	Lifting line	Lifting surface	Measured	$\left(\frac{\partial c_m}{\partial \alpha}\right)_{\delta_f,\delta_t}$	$\left(\frac{\partial c_m}{\partial \alpha}\right)_{\alpha,\delta_t}$
NACA 0009 airfoil; A = 3.36; A(at $\bar{c}/4$) = 13.5°; ϕ = 11°																								
Plain	———	0	0.097	-0.522	0.0506	-0.00618	-0.0128	0.0545	0.056	0.056	-0.522	-0.549	-0.570	0.0284	0.0307	0.032	-0.00349	-0.00256	-0.0016	-0.00933	-0.0097	-0.0068	———	———
Elliptic	0.35	0	.087	-.575	.0500	-.00288	-.00569	.0505	.051	.055	-.575	-.600	-.561	.0282	.0306	.031	.00168	.0008	0	-.0096	-.0038	-.0032	———	———
Sharp	.35	0	.089	-.562	.0500	-.00383	-.00744	.0531	.052	.0552	-.562	-.586	-.561	.0286	.0305	.031	-.00229	-.00151	-.0003	-.00657	-.00587	-.0041	———	———
Internal	.35	0	———	———	———	———	———	———	———	.0575	———	———	-.573	———	———	.033	———	———	-.0009	———	———	-.0037	———	———
Internal	.35	-.50	———	———	———	———	———	———	———	.0575	———	———	-.561	———	———	.030	———	———	-.0009	———	———	-.0014	———	———
Horn 1	———	0	———	———	———	———	———	———	———	.057	———	———	-.543	———	———	.031	———	———	.0039	———	———	-.0040	———	———
Horn 2	———	0	———	———	———	———	———	———	———	.057	———	———	-.543	———	———	.031	———	———	.0084	———	———	-.0009	———	———
Plain	———	-.50	———	———	———	———	———	———	———	.057	———	———	-.543	———	———	.031	———	———	-.0016	———	———	-.0036	———	———
NACA 0009 airfoil; A = 3.30; A(at $\bar{c}/4$) = 40°; ϕ = 14° (measured in plane perpendicular to hinge line)																								
Plain	———	0	0.097	-0.603	0.0585	-0.0070	-0.0123	0.0412	0.489	0.052	-0.462	-0.482	-0.419	0.019	0.0208	0.0218	-0.00297	-0.00276	-0.0028	-0.00600	-0.0056	-0.0078	-0.0318	-0.307
Elliptic	a.319	0	.087	-.638	.0669	.0033	-.0061	.0383	.0414	.0505	-.488	-.508	-.467	.0188	.021	.0235	-.00145	-.00085	-.0012	-.00350	-.00252	-.0049	-.0318	-.317
Internal	a.319	0	———	———	———	———	———	———	———	.0545	———	———	-.458	———	———	.025	———	———	-.0020	———	———	-.0063	-.025	-.214
Internal	a.319	1.0	———	———	———	———	———	———	———	.0545	———	———	-.680	———	———	.035	———	———	-.0020	———	———	-.0136	———	———
Internal	a.319	.50	———	———	———	———	———	———	———	.0545	———	———	-.55	———	———	.030	———	———	-.0020	———	———	-.0095	———	———
Internal	a.319	-.50	———	———	———	———	———	———	———	.0545	———	———	-.413	———	———	.0225	———	———	-.0020	———	———	-.0051	———	———
Internal	a.319	-1.0	———	———	———	———	———	———	———	.0545	———	———	-.367	———	———	.020	———	———	-.0020	———	———	-.0002	———	———
Horn	———	0	———	———	———	———	———	———	———	.051	———	———	-.406	———	———	.0207	———	———	-.0020	———	———	-.0064	-.0392	-.284
Transition fixed (plain flap)	———	0	———	———	———	———	———	———	———	.0505	———	———	-.386	———	———	.0195	———	———	-.0023	———	———	-.0068	-.0347	-.296
Circular-arc airfoil; A = 3.30; A(at $\bar{c}/4$) = 40°; ϕ = 29.5° (measured in plane perpendicular to hinge line)																								
Plain	———	0	———	———	———	———	———	———	———	0.047	———	———	-0.364	———	———	0.017	———	———	0.0040	———	———	-0.0012	———	———
Elliptic	a.319	0	———	———	———	———	———	———	———	.0456	———	———	-.362	———	———	.0165	———	———	.0039	———	———	.0065	0	0.306
Internal	a.319	0	———	———	———	———	———	———	———	.048	———	———	-.417	———	———	.020	———	———	.0037	———	———	.0012	α	.318
Internal	a.319	1.0	———	———	———	———	———	———	———	.048	———	———	-.532	———	———	.0275	———	———	.0037	———	———	-.0050	q	.330
Internal	a.319	.50	———	———	———	———	———	———	———	.048	———	———	-.479	———	———	.025	———	———	.0037	———	———	-.0018	———	———
Internal	a.319	-.50	———	———	———	———	———	———	———	.048	———	———	-.354	———	———	.0170	———	———	.0037	———	———	.0029	———	———
Internal	a.319	-1.0	———	———	———	———	———	———	———	.048	———	———	-.312	———	———	.015	———	———	.0037	———	———	.0053	———	———
Horn	———	0	———	———	———	———	———	———	———	.0462	———	———	-.369	———	———	.0180	———	———	.0056	———	———	-.0005	0	.284
NACA 66-009 (true-contour flap) airfoil; A = 3.36; A(at $\bar{c}/4$) = 13.5°; ϕ = 7°																								
Plain	———	0	0.095	-0.620	0.059	-0.00737	-0.01351	0.0535	0.0540	0.0575	-0.620	-0.649	-0.574	0.0332	0.035	0.033	-0.00415	-0.0034	-0.0036	-0.01151	-0.0108	-0.0100	———	———
Elliptic	0.35	0	———	———	———	———	———	———	———	.057	———	———	-.561	———	———	.032	———	———	-.0037	———	———	-.0082	———	———
Sharp	.35	0	———	———	———	———	———	———	———	.056	———	———	-.580	———	———	.0325	———	———	-.0038	———	———	-.0086	———	———
Internal	.35	0	———	———	———	———	———	———	———	.058	———	———	-.604	———	———	.035	———	———	-.0022	———	———	-.0068	———	———
Internal	.35	-.50	———	———	———	———	———	———	———	.058	———	———	-.535	———	———	.031	———	———	-.0023	———	———	-.0032	———	———
Horn 1	———	0	———	———	———	———	———	———	———	.057	———	———	-.579	———	———	.033	———	———	.0018	———	———	-.0069	———	———
Horn 2	———	0	———	———	———	———	———	———	———	.057	———	———	-.614	———	———	.035	———	———	.0060	———	———	-.0043	———	———

[a]Percent chord measured perpendicular to hinge line.

TABLE IV.- MEASURED AND PREDICTED PARAMETER VALUES - Concluded

Model dimensions and characteristics			Section parameters					Finite-span parameters													
								c_{l_α}			a_b			c_{l_β}			c_{h_α}			c_{h_β}		
Balance shape	c_b/c_f	b_t/b_f	c_{l_α}	a_b	c_{l_β}	c_{h_α}	c_{h_β}	Lifting line	Lifting surface	Measured	Lifting line	Lifting surface	Measured	Lifting line	Lifting surface	Measured	Lifting line	Lifting surface	Measured	Lifting line	Lifting surface	Measured
NACA 66-009 (straight-contour flap) airfoil; A = 3.36; Λ(at $\bar{c}/4$) = 13.5°; β = 13°																						
Plain	———	0	———	———	———	———	———	———	———	0.056	———	———	-0.571	———	———	0.032	———	———	0	———	———	-0.0059
Elliptic	0.35	0	———	———	———	———	———	———	———	.054	———	———	-.509	———	———	.0275	———	———	-.0002	———	———	-.0054
Sharp	.35	0	———	———	———	———	———	———	———	.0545	———	———	-.560	———	———	.0305	———	———	-.0003	———	———	-.0054
Internal	.35	0	———	———	———	———	———	———	———	.0565	———	———	-.601	———	———	.034	———	———	-.0003	———	———	-.0042
Internal	.35	-.50	———	———	———	———	———	———	———	.056	———	———	-.571	———	———	.032	———	———	-.0006	———	———	-.0018
Horn 1	———	0	———	———	———	———	———	———	———	.056	———	———	-.571	———	———	.032	———	———	.0025	———	———	-.0045
NACA 0015 airfoil; A = 3.36; Λ(at $\bar{c}/4$) = 13.5°; β = 17°																						
Plain	———	0	0.087	-0.48	0.050	-0.00178	-0.00610	0.0514	0.052	0.0545	-0.460	-0.480	-0.55	0.0236	0.025	0.030	-0.00104	-0.00008	0	-0.00575	-0.005	-0.0048
Elliptic	0.35	0	.080	-.45	.036	-.00022	-.00313	.0478	.0485	.0535	-.45	-.466	-.561	.0215	.0226	.030	.000132	.00066	.0006	-.00309	.00249	-.0036
Sharp	.35	0	———	———	———	———	———	———	———	.054	———	———	-.556	———	———	.030	———	———	.0004	———	———	-.0040
Internal	.35	0	———	———	———	———	———	———	———	.055	———	———	-.582	———	———	.032	———	———	0	———	———	-.0037
Internal	.35	-.50	———	———	———	———	———	———	———	.055	———	———	-.518	———	———	.0285	———	———	0	———	———	-.0006
Horn 1	0	0	———	———	———	———	———	———	———	.055	———	———	-.546	———	———	.030	———	———	.0054	———	———	-.0019
NACA 66(215)-014 (true-contour flap) airfoil; A = 3.36; Λ(at $\bar{c}/4$) = 13.5°; β = 7.5°																						
Plain	———	0	0.094	-0.590	0.0555	-0.0088	-0.0146	0.0531	0.054	0.0535	-0.59	-0.616	-0.587	0.0314	0.033	0.0315	-0.00497	-0.00196	-0.0022	-0.0123	-0.0116	-0.0110
Elliptic	0.35	0	———	———	———	———	———	———	———	.053	———	———	-.510	———	———	.027	———	———	-.0034	———	———	-.0094
Sharp	.35	0	———	———	———	———	———	———	———	.053	———	———	-.537	———	———	.029	———	———	-.0044	———	———	-.0112
Internal	.35	0	———	———	———	———	———	———	———	.0548	———	———	-.553	———	———	.033	———	———	-.0028	———	———	-.0068
Internal	.35	-.50	———	———	———	———	———	———	———	.056	———	———	-.537	———	———	.030	———	———	-.0028	———	———	-.0039
Horn 1	———	0	———	———	———	———	———	———	———	.054	———	———	-.555	———	———	.030	———	———	.0025	———	———	-.0076
Horn 2	———	0	———	———	———	———	———	———	———	.054	———	———	-.574	———	———	.031	———	———	.0054	———	———	-.0040
Plain	———	-.50	———	———	———	———	———	———	———	.0535	———	———	-.635	———	———	.034	———	———	-.0026	———	———	-.0082
NACA 66(215)-014 (straight-contour flap) airfoil; A = 3.36; Λ(at $\bar{c}/4$) = 13.5°; β = 19.5°																						
Plain	———	0	0.085	-0.530	0.045	0	-0.0059	0.0498	0.0505	0.0515	-0.530	-0.550	-0.499	0.0264	0.028	0.025	0	0.00104	0.001	-0.0054	-0.0050	-0.0019
Elliptic	0.35	0	———	———	———	———	———	———	———	.0505	———	———	-.416	———	———	.021	———	———	.0013	———	———	-.0022
Sharp	.35	0	———	———	———	———	———	———	———	.050	———	———	-.459	———	———	.023	———	———	.0008	———	———	-.0027
Internal	.35	0	———	———	———	———	———	———	———	.052	———	———	-.524	———	———	.0275	———	———	.0013	———	———	-.0012
Internal	.35	-.50	———	———	———	———	———	———	———	.052	———	———	-.483	———	———	.025	———	———	.0013	———	———	-.0004
Horn 1	———	0	———	———	———	———	———	———	———	.0515	———	———	-.448	———	———	.0235	———	———	.0056	———	———	0
Horn 2	———	0	———	———	———	———	———	———	———	.0515	———	———	-.457	———	———	.024	———	———	.0097	———	———	.0011

TABLE V.- CORRELATION OF HORN DATA

Airfoil	Horn configuration	Horn coefficient B	Measured ΔC_{h_α}	Predicted ΔC_{h_α} (reference 15)	Measured ΔC_{h_δ}	Predicted ΔC_{h_δ} (reference 15)
NACA 0009	[a]1	0.388	0.0055	0.0065	0.0028	0.0055
NACA 0009	2	.484	.010	.011	.0059	.0075
NACA 66-009	1	.39	.0048	.0065	.0031	.0055
(true-contour flap)	2	.492	.0096	.0115	.0057	.0075
NACA 66-009 (straight-contour flap)	1	.392	.0036	.0065	.0014	.0055
NACA 0015	1	.404	.0054	.0070	.0028	.0060
NACA 66(215)-014	1	.408	.0047	.0070	.0034	.0060
(true-contour flap)	2	.50	.0086	.012	.0070	.0078
NACA 66(215)-014	1	.40	.0045	.0066	.0019	.0050
(straight-contour flap)	2	.50	.0087	.012	.0030	.0078
NACA 0009, 40° sweepback	Shielded[b]	.244	.0008	------	.0014	------
Circular arc, 40° sweepback	Shielded[b]	.244	.0016	------	.0007	------

[a]See fig. 2.
[b]See fig. 3.

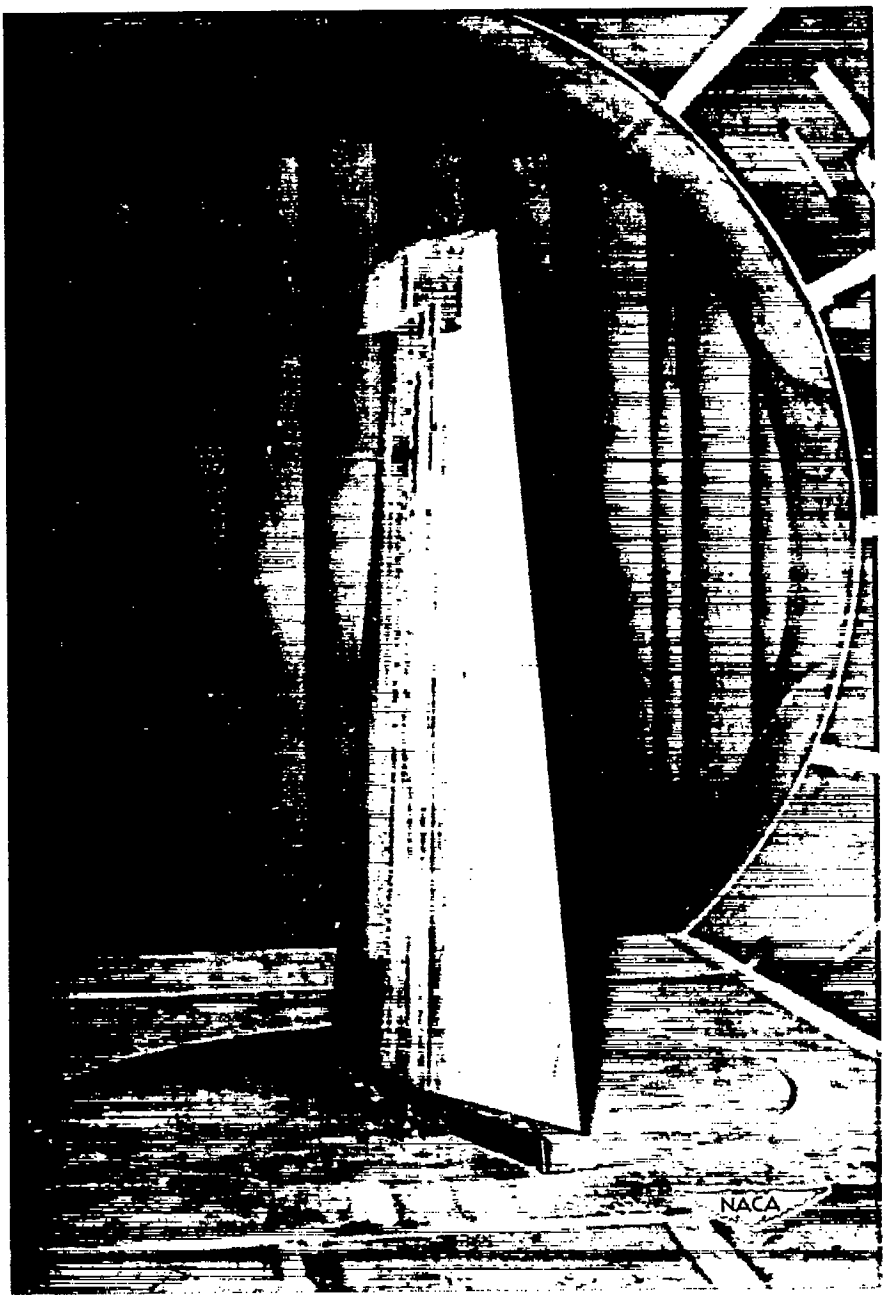

(a) Unswept model.

Figure 1.- Models mounted in tunnel.

(b) Swept model.

Figure 1.- Concluded.

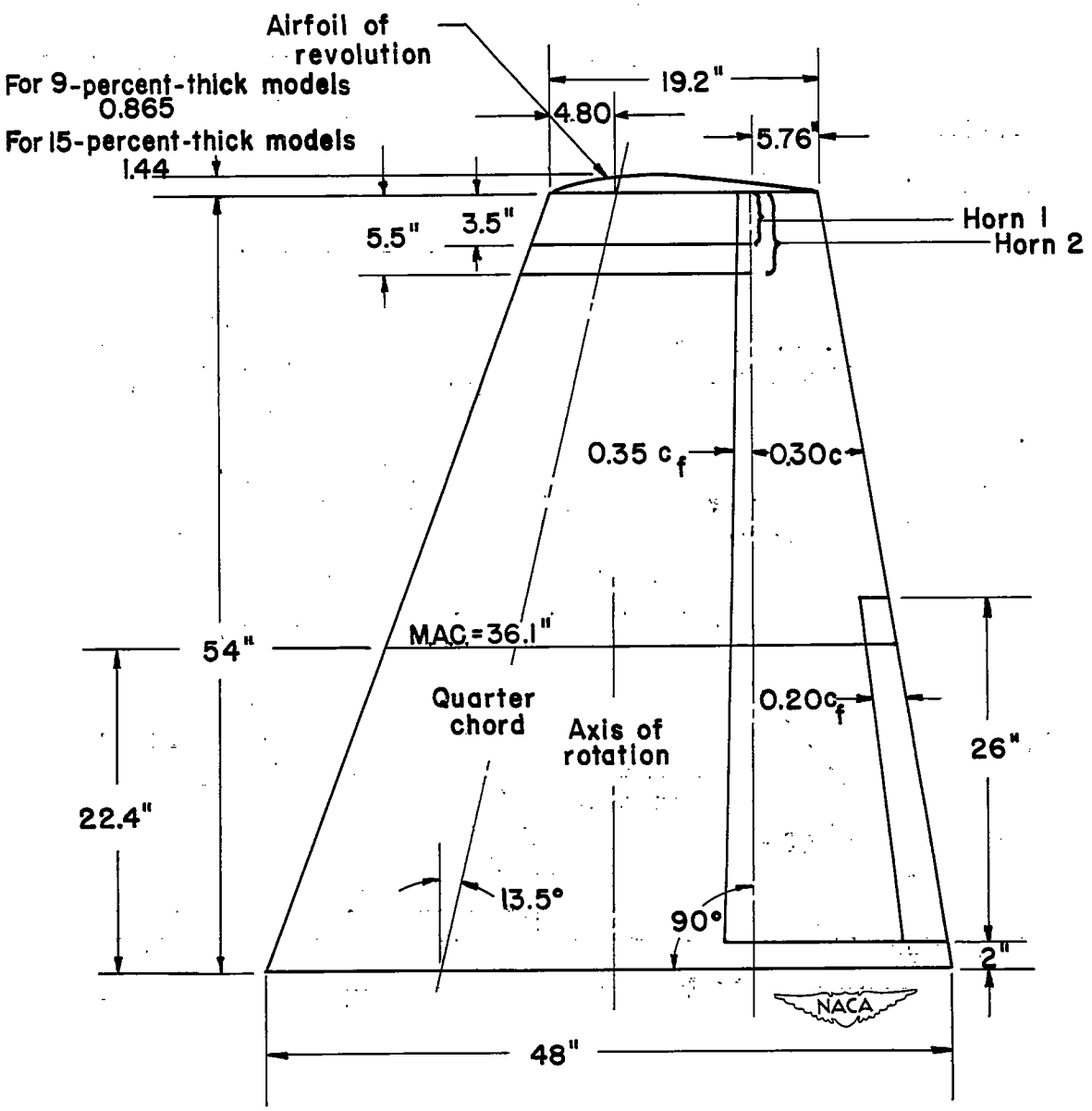

Figure 2.- Plan-form dimensions of unswept models. Aspect ratio A, 3.36; taper ratio λ, 0.4; area S/2, 12.69 square feet; area rearward of hinge line, 3.60 square feet; root-mean-square chord of flap $\bar{c}_f$, 0.71 foot.

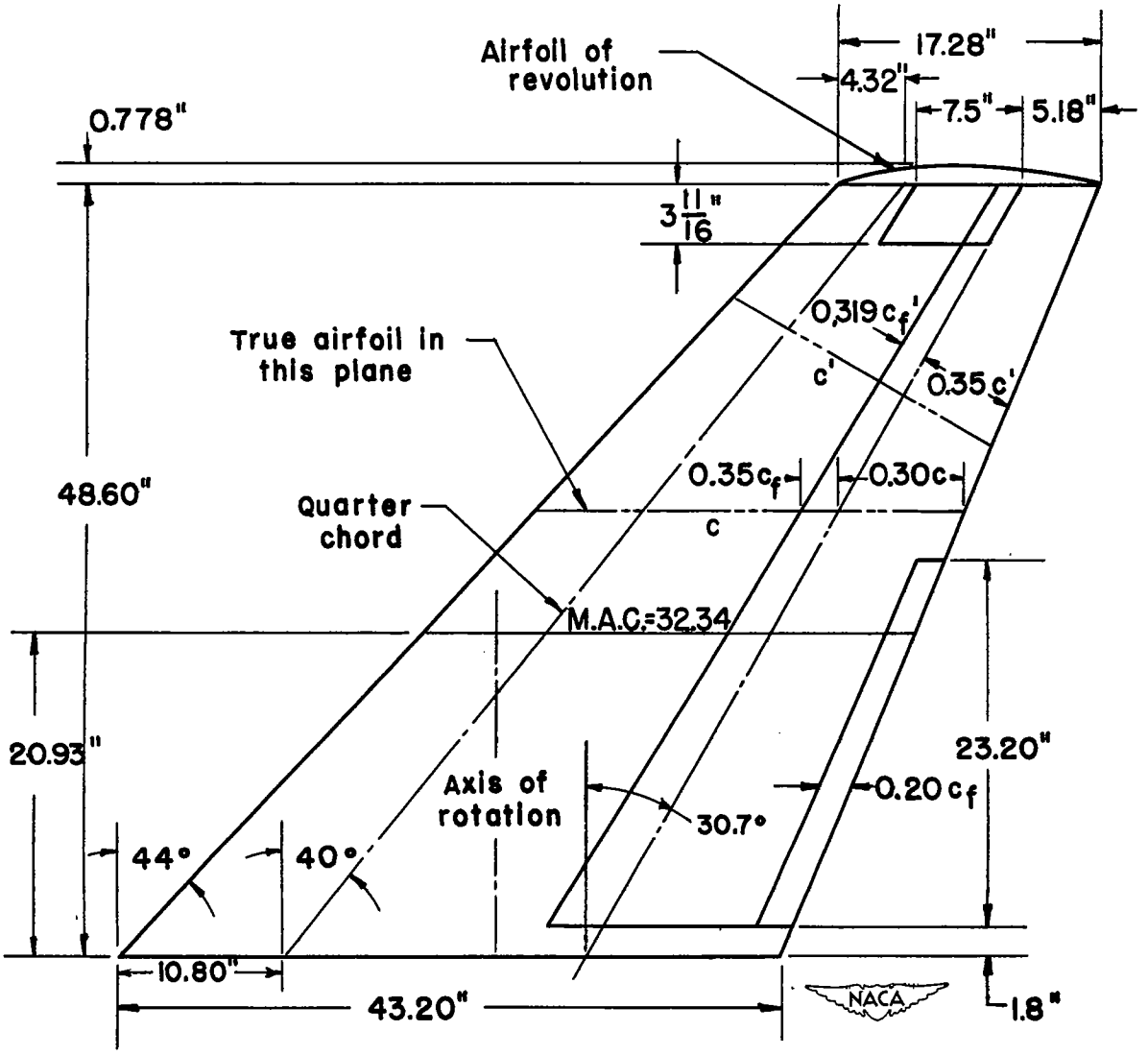

Figure 3.- Plan-form dimensions of swept models. NACA 0009 and circular-arc profiles; aspect ratio A, 3.30; taper ratio λ, 0.4; area S/2, 10.27 square feet; area rearward of hinge line, 2.91 square feet; root-mean-square chord of flap $\bar{c}_f$, 0.667 foot.

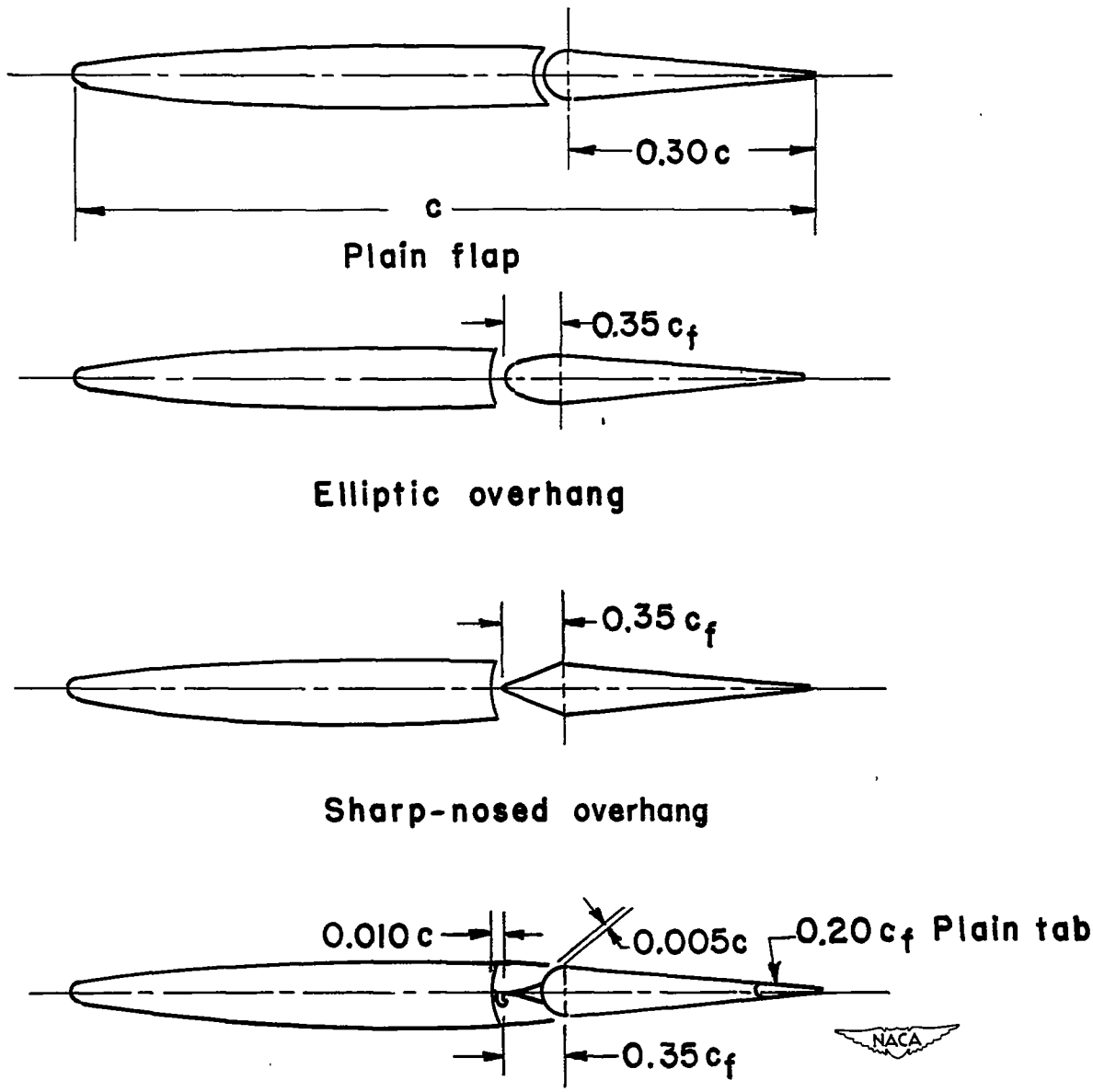

Figure 4.- Balance configurations tested on unswept models. All nose gaps 0.005c except as noted; all chords measured parallel to free stream.

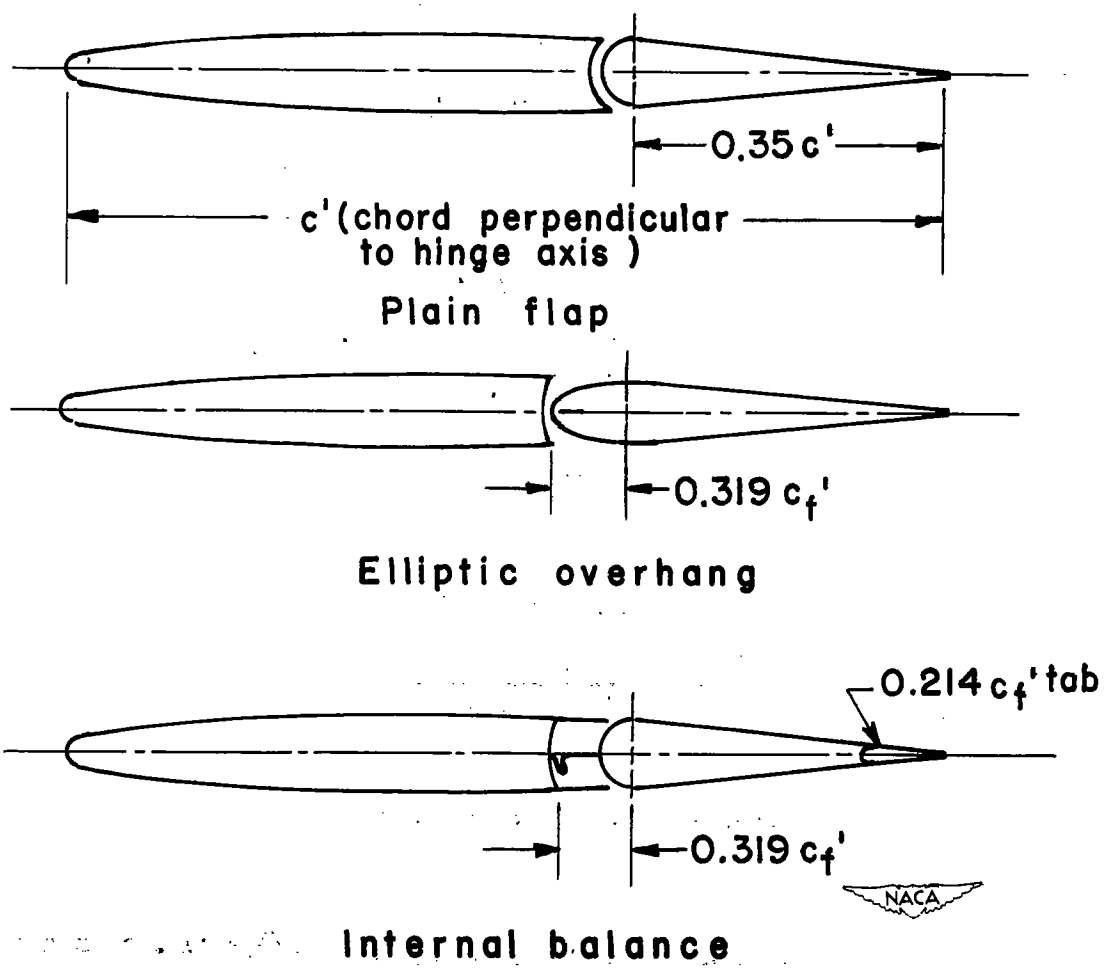

Figure 5.- Balance configurations tested on sweptback models. 0.005c gap maintained parallel to free stream; also see figure 3 for chords measured parallel to free stream.

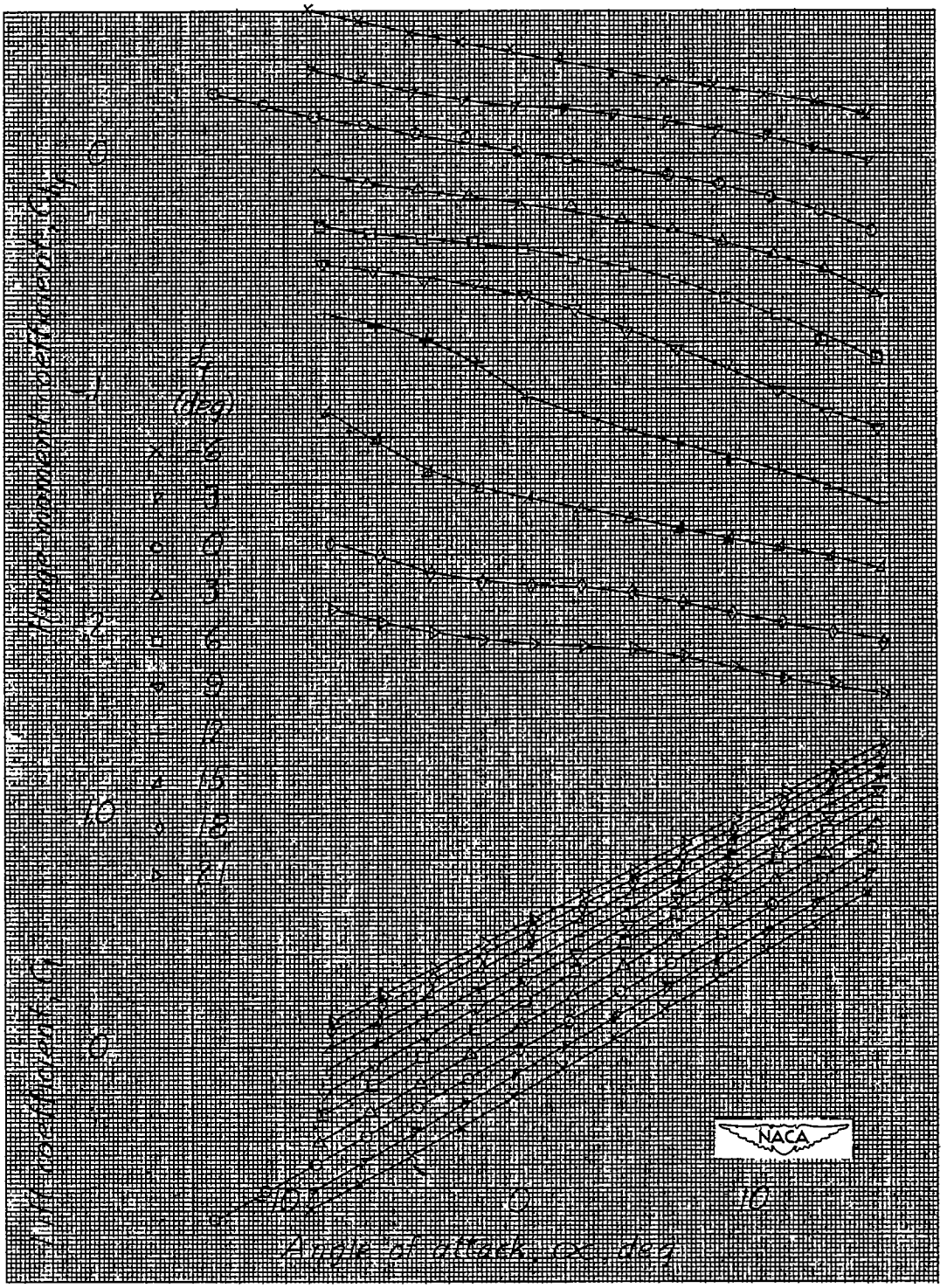

(a) $\delta_t/\delta_f = 0$.

Figure 6.- NACA 0009 semispan tail surface. Taper ratio λ, 0.4; aspect ratio A, 3.36; 0.30c plain flap; 0.005c gap.

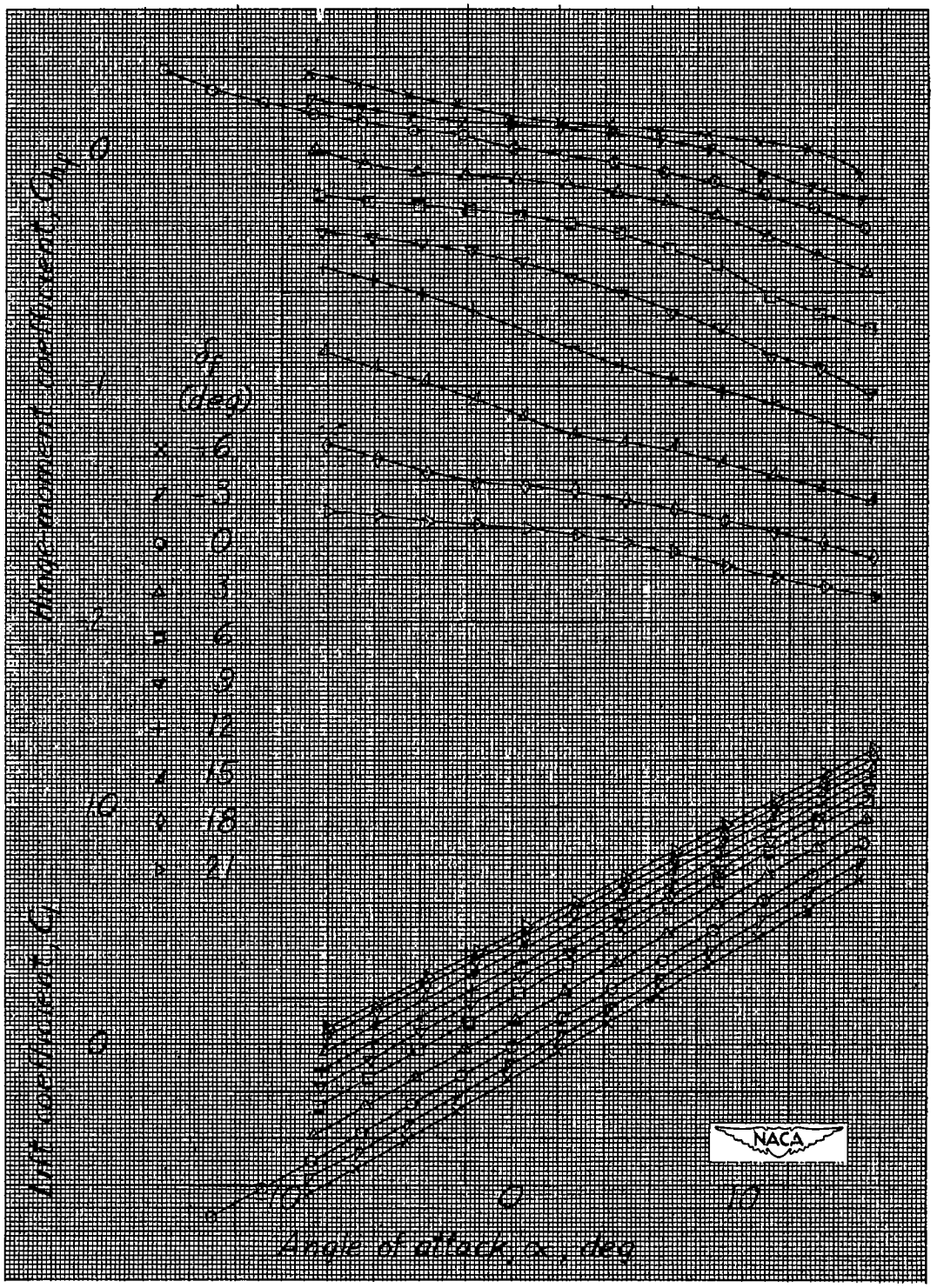

(b) $\delta_t/\delta_f = -0.5$.

Figure 6.- Concluded.

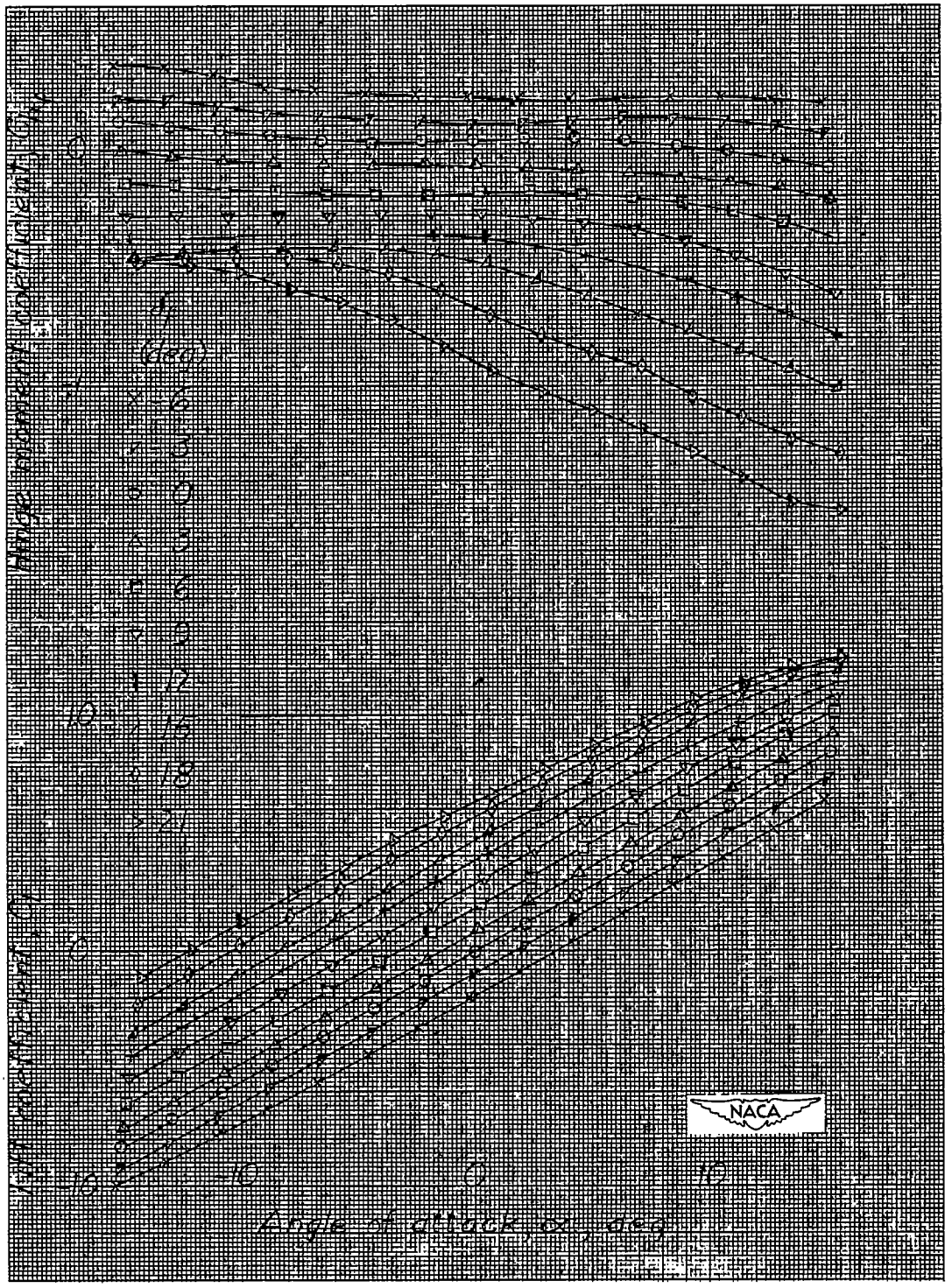

Figure 7.- NACA 0009 semispan tail surface. Taper ratio λ, 0.4; aspect ratio A, 3.36; 0.30c flap with $0.35c_f$ elliptic overhang; 0.005c gap; δ_t/δ_f, 0.

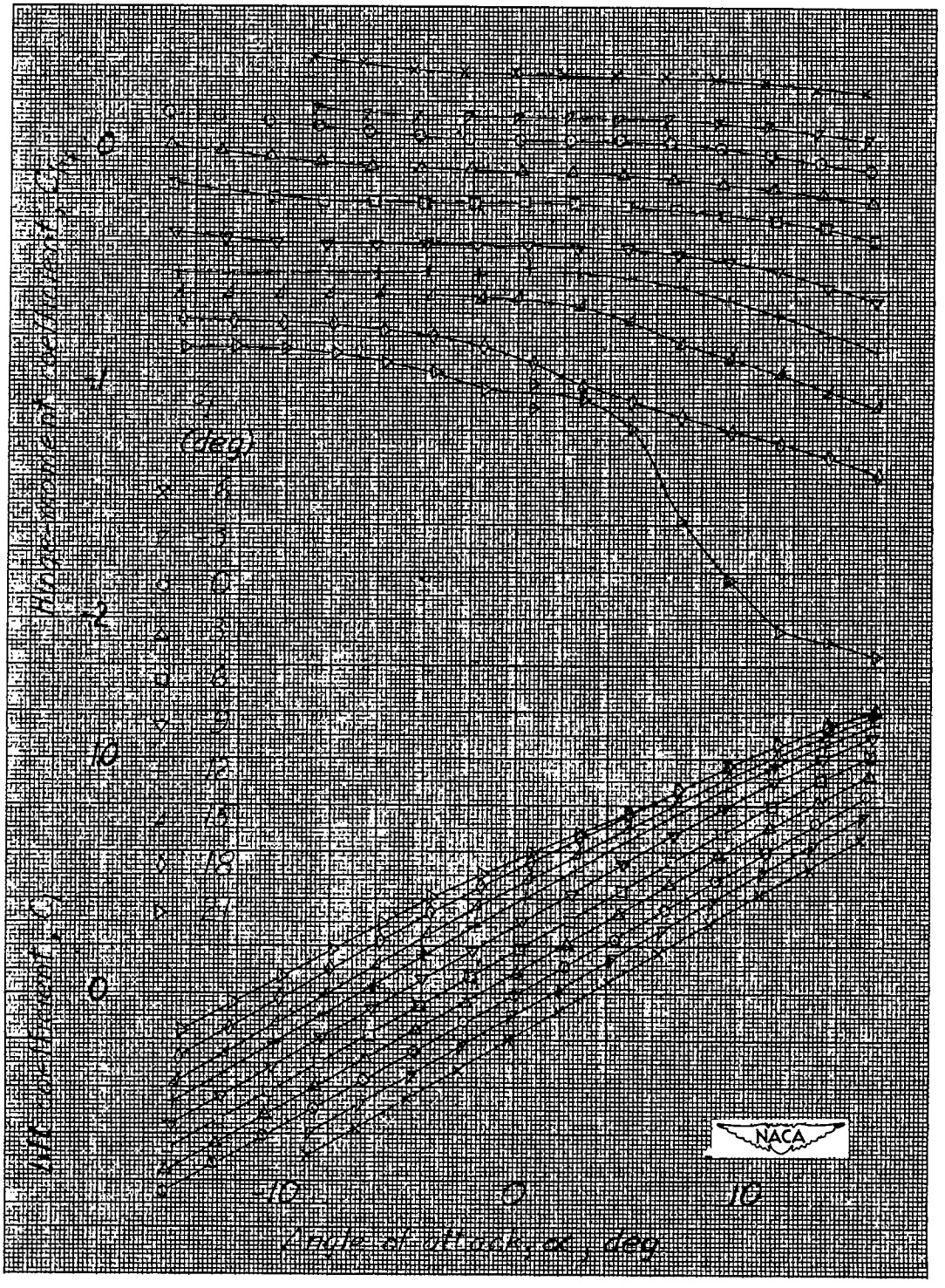

Figure 8.- NACA 0009 semispan tail surface. Taper ratio λ, 0.4; aspect ratio A, 3.36; 0.30c flap with $0.35c_f$ sharp-nosed overhang; 0.005c gap; δ_t/δ_f, 0.

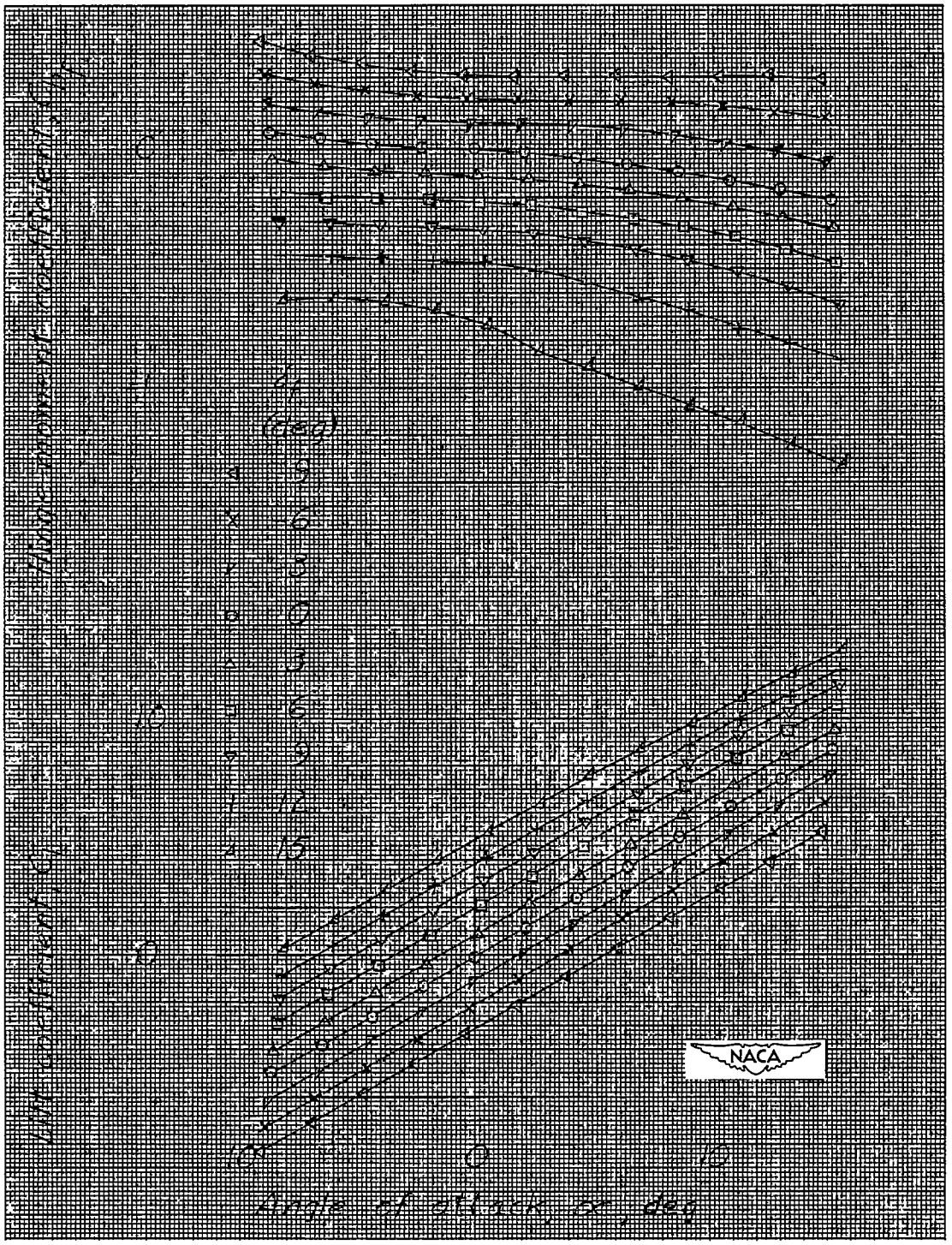

(a) $\delta_t/\delta_f = 0.$

Figure 9.- NACA 0009 semispan tail surface. Taper ratio λ, 0.4; aspect ratio A, 3.36; 0.30c flap with $0.35c_f$ internal balance; sealed gap.

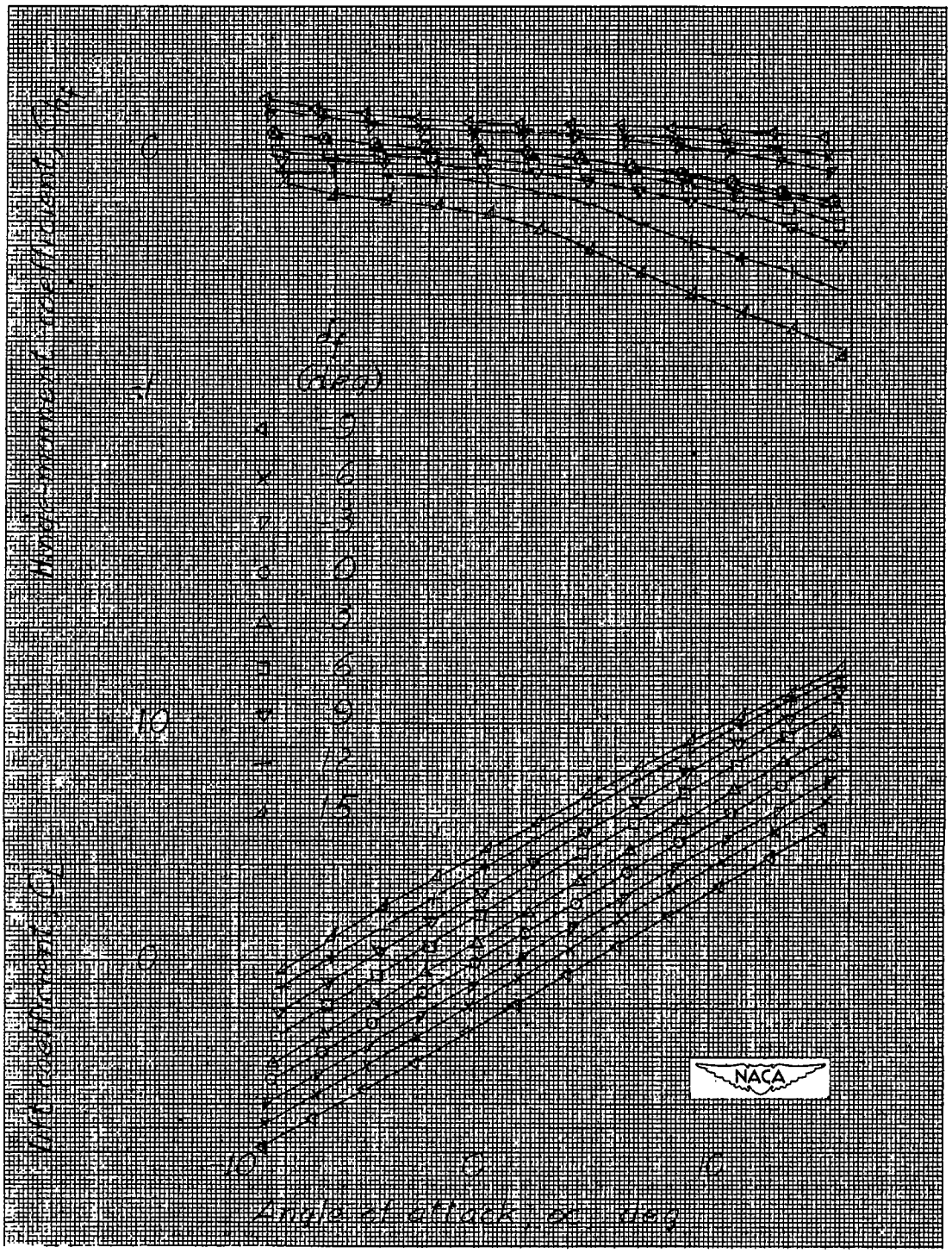

(b) $\delta_t/\delta_f = -0.5$.

Figure 9.- Concluded.

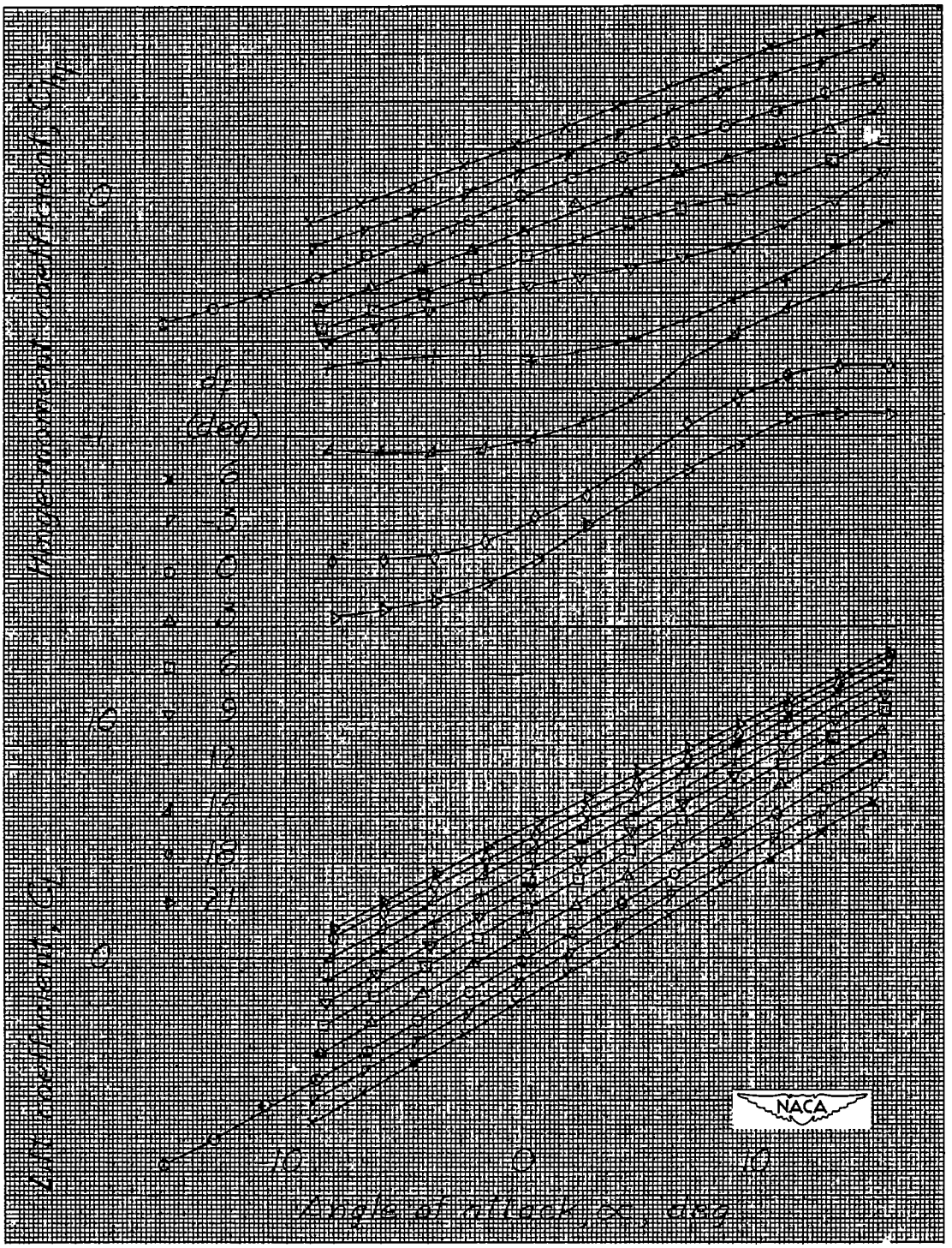

(a) Horn 1.

Figure 10.- NACA 0009 semispan tail surface. Taper ratio λ, 0.4; aspect ratio A, 3.36; 0.30c plain flap; 0.005c gap; δ_t/δ_f, 0.

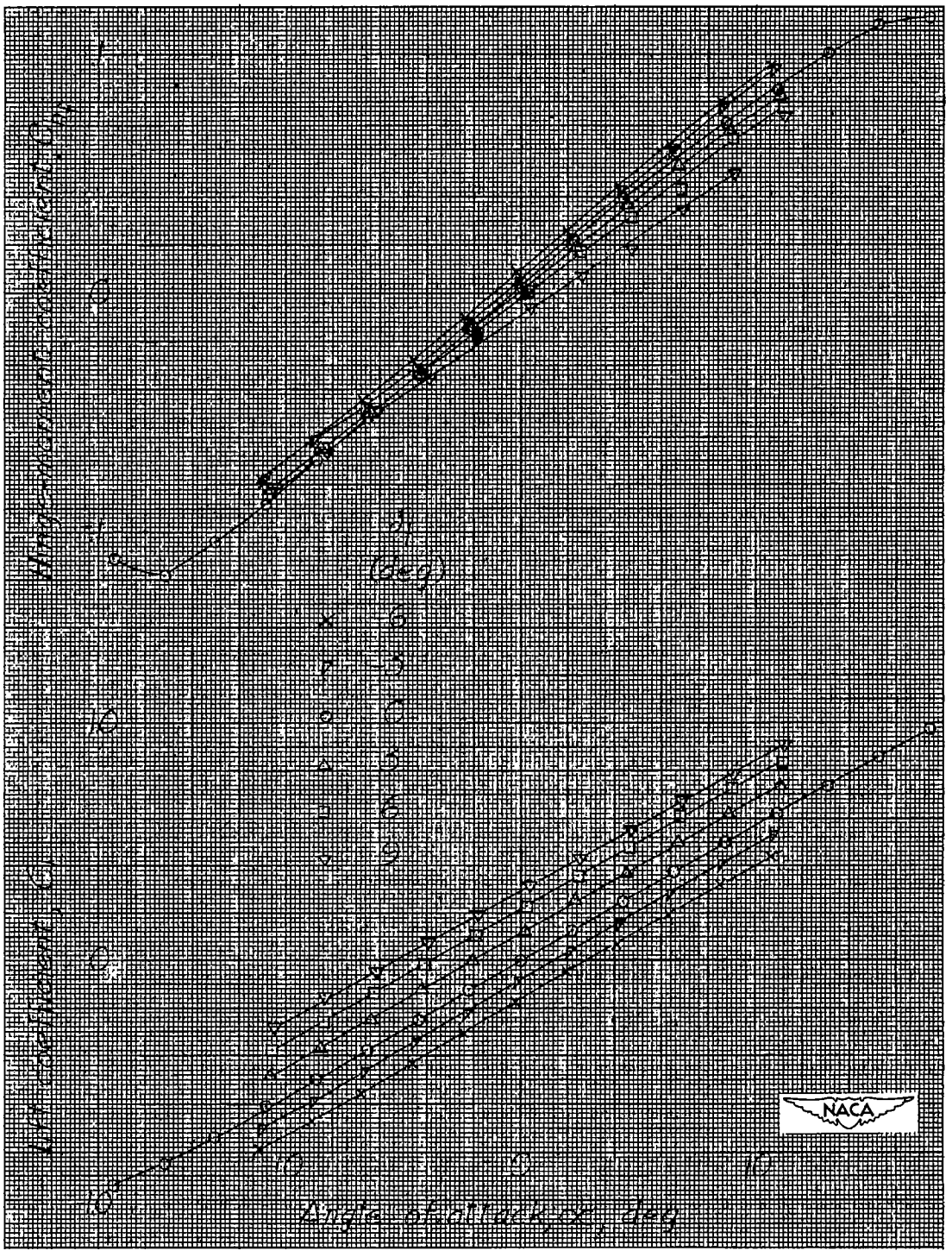

(b) Horn 2.

Figure 10.- Concluded.

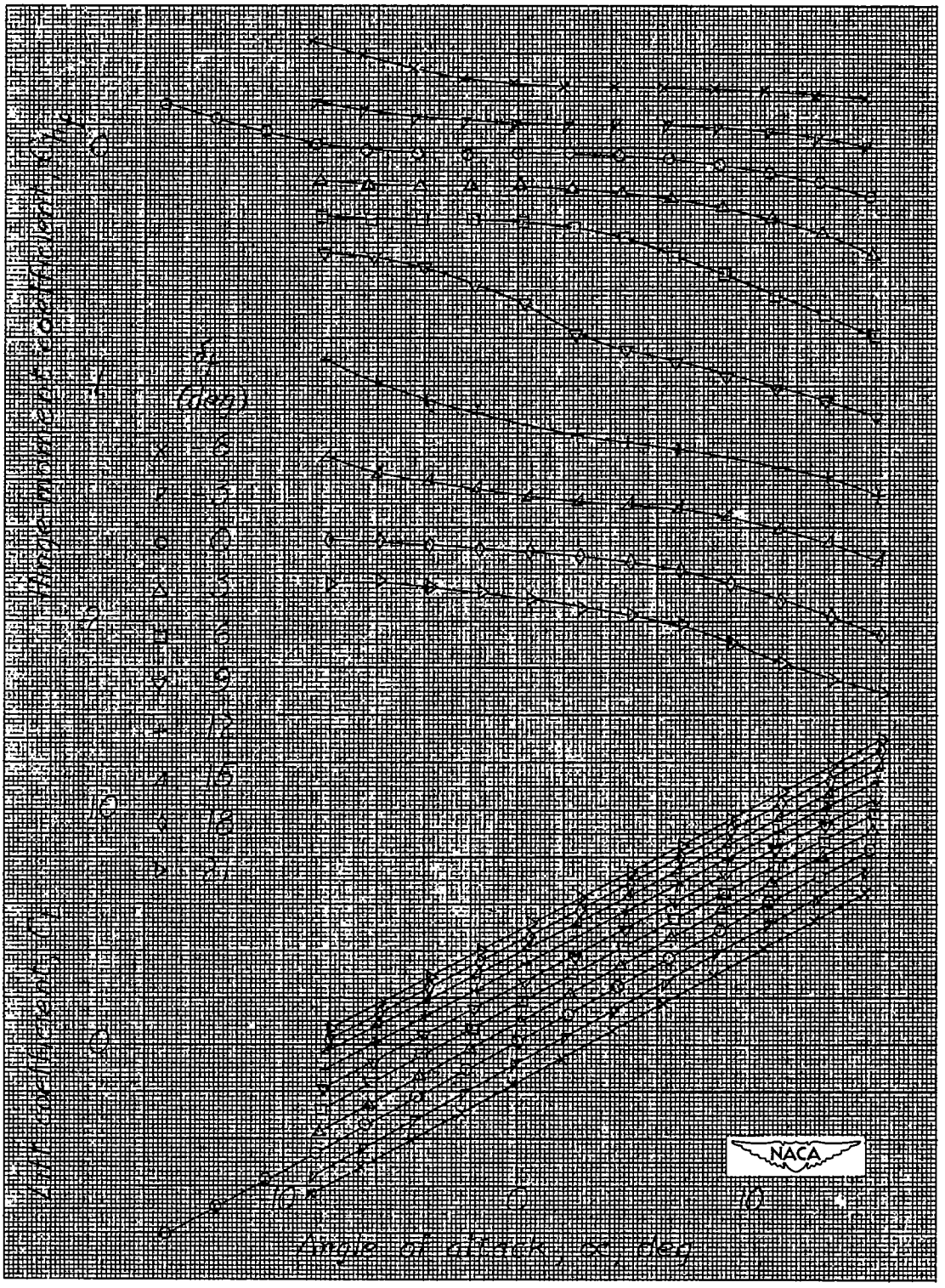

Figure 11.- NACA 0015 semispan tail surface. Taper ratio λ, 0.4; aspect ratio A, 3.36; 0.30c plain flap; 0.005c gap; δ_t/δ_f, 0.

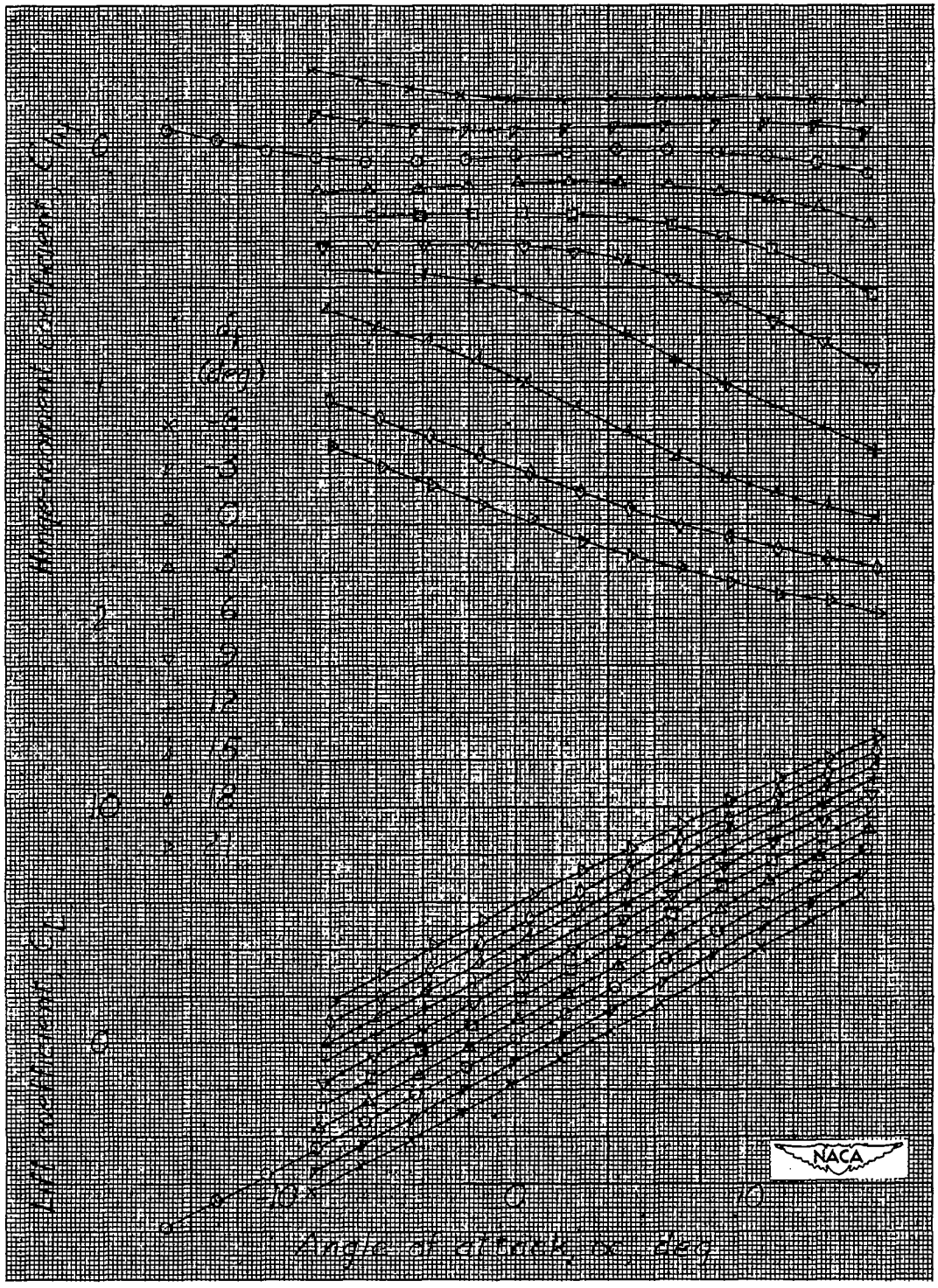

Figure 12.- NACA 0015 semispan tail surface. Taper ratio λ, 0.4; aspect ratio A, 3.36; 0.30c flap with $0.35c_f$ elliptic overhang; 0.005c gap; δ_t/δ_f, 0.

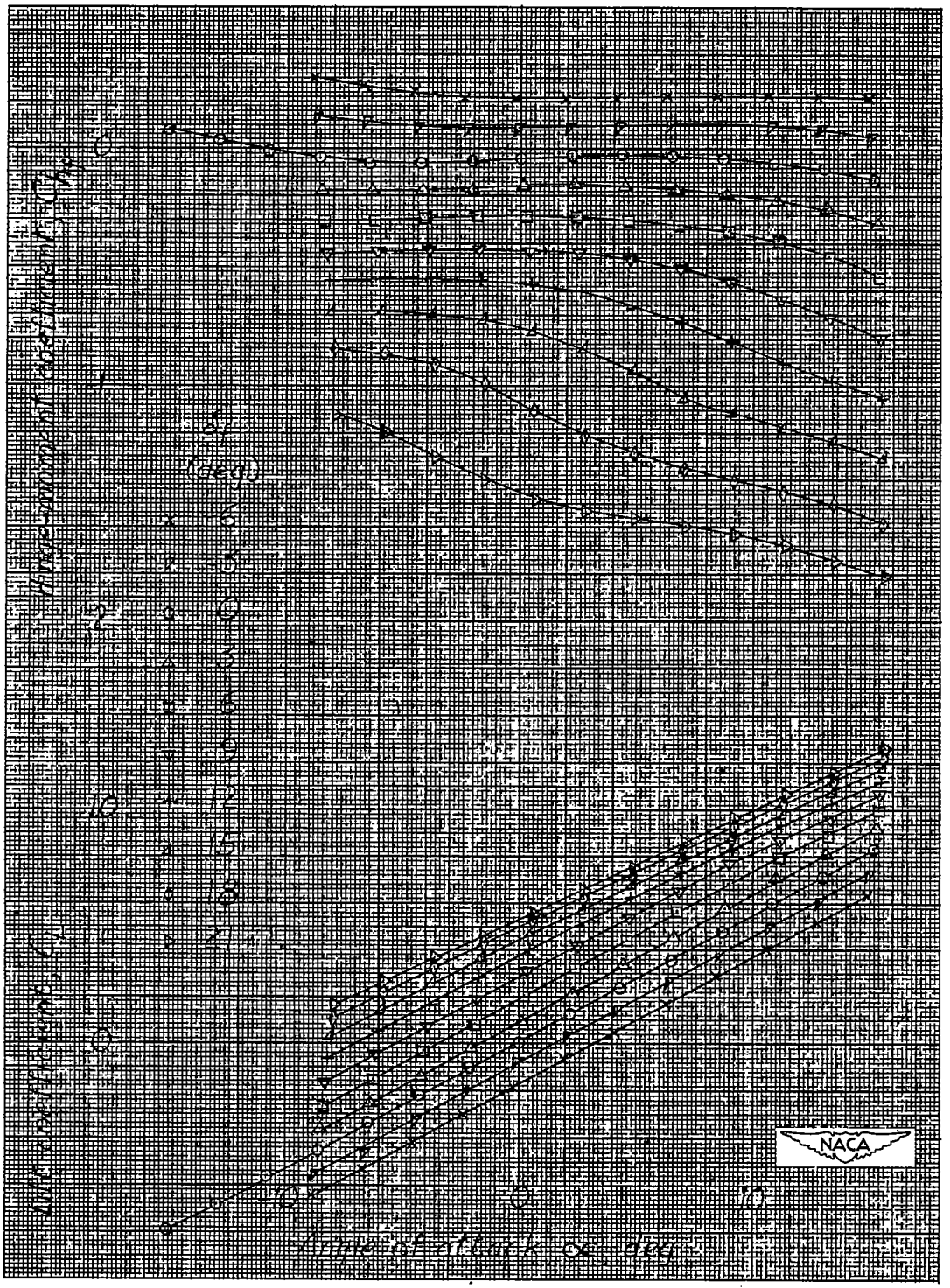

Figure 13.- NACA 0015 semispan tail surface. Taper ratio λ, 0.4; aspect ratio A, 3.36; 0.30c flap with $0.35c_f$ sharp-nosed overhang; 0.005c gap; δ_t/δ_f, 0.

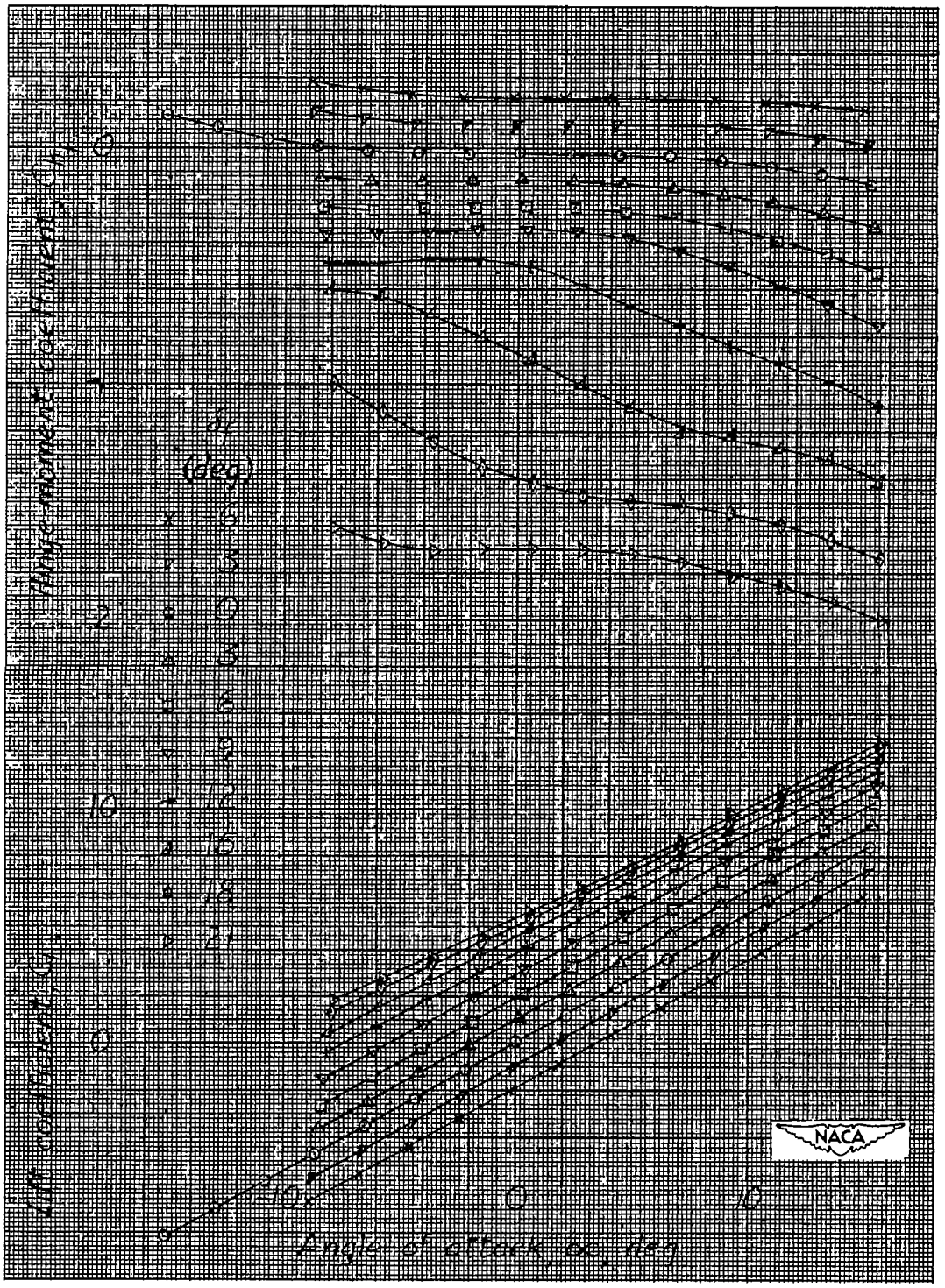

(a) $\delta_t/\delta_f = 0$.

Figure 14.- NACA 0015 semispan tail surface. Taper ratio λ, 0.4; aspect ratio A, 3.36; 0.30c flap with $0.35c_f$ internal balance; sealed gap.

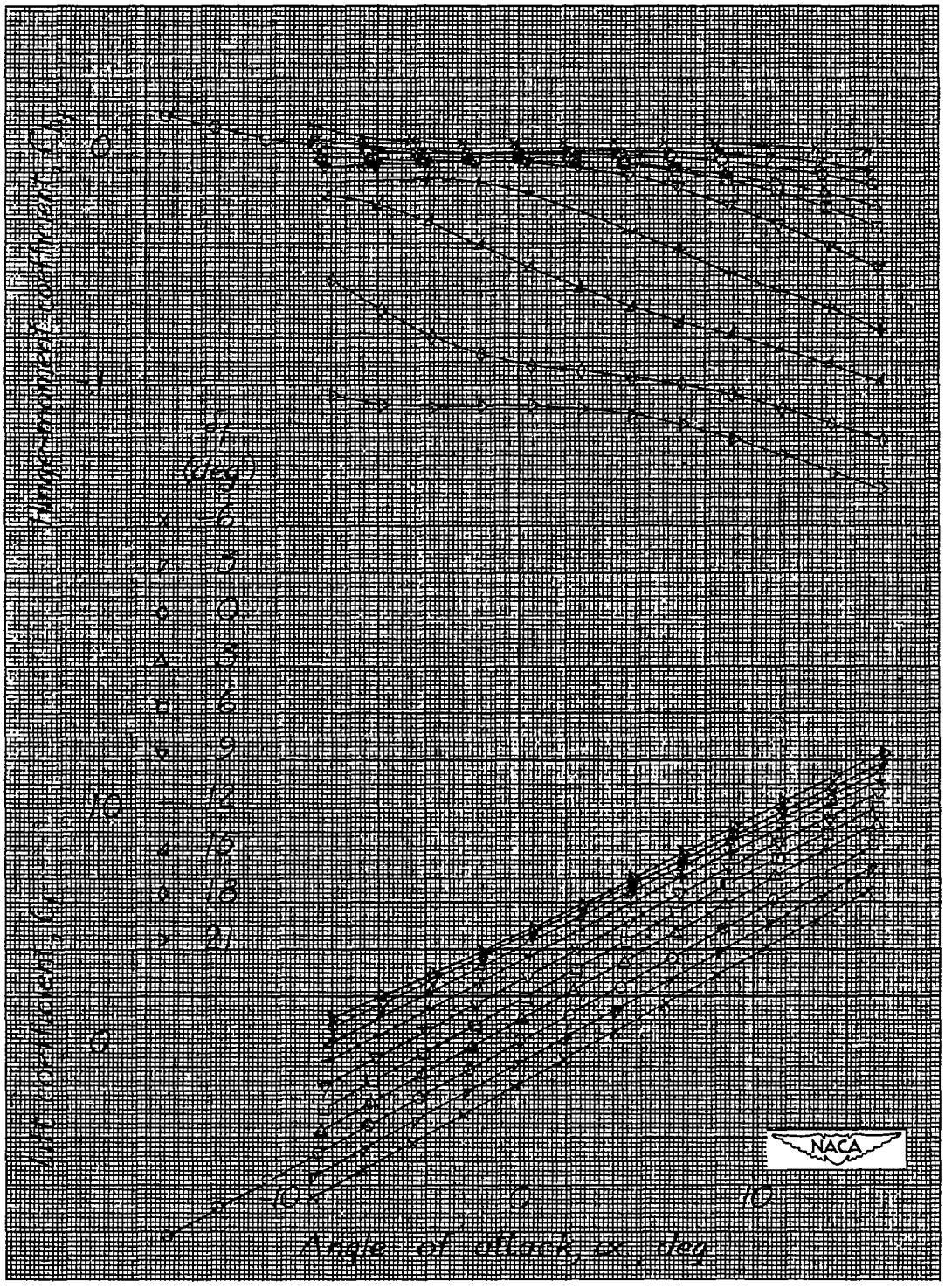

(b) $\delta_t/\delta_f = -0.5$.

Figure 14.- Concluded.

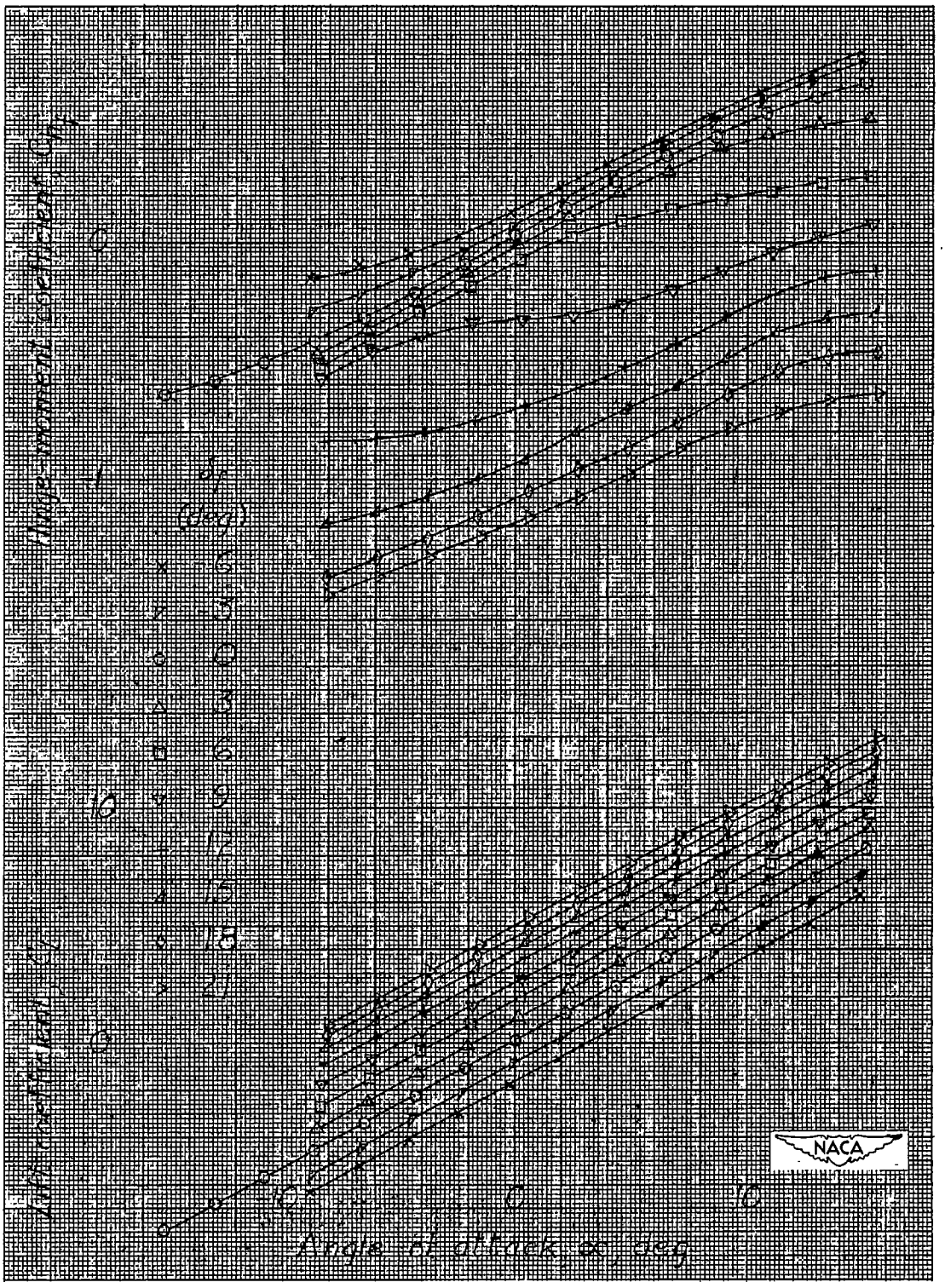

Figure 15.- NACA 0015 semispan tail surface. Taper ratio λ, 0.4; aspect ratio A, 3.36; 0.30c plain flap; 0.005c gap; horn 1; δ_t/δ_f, 0.

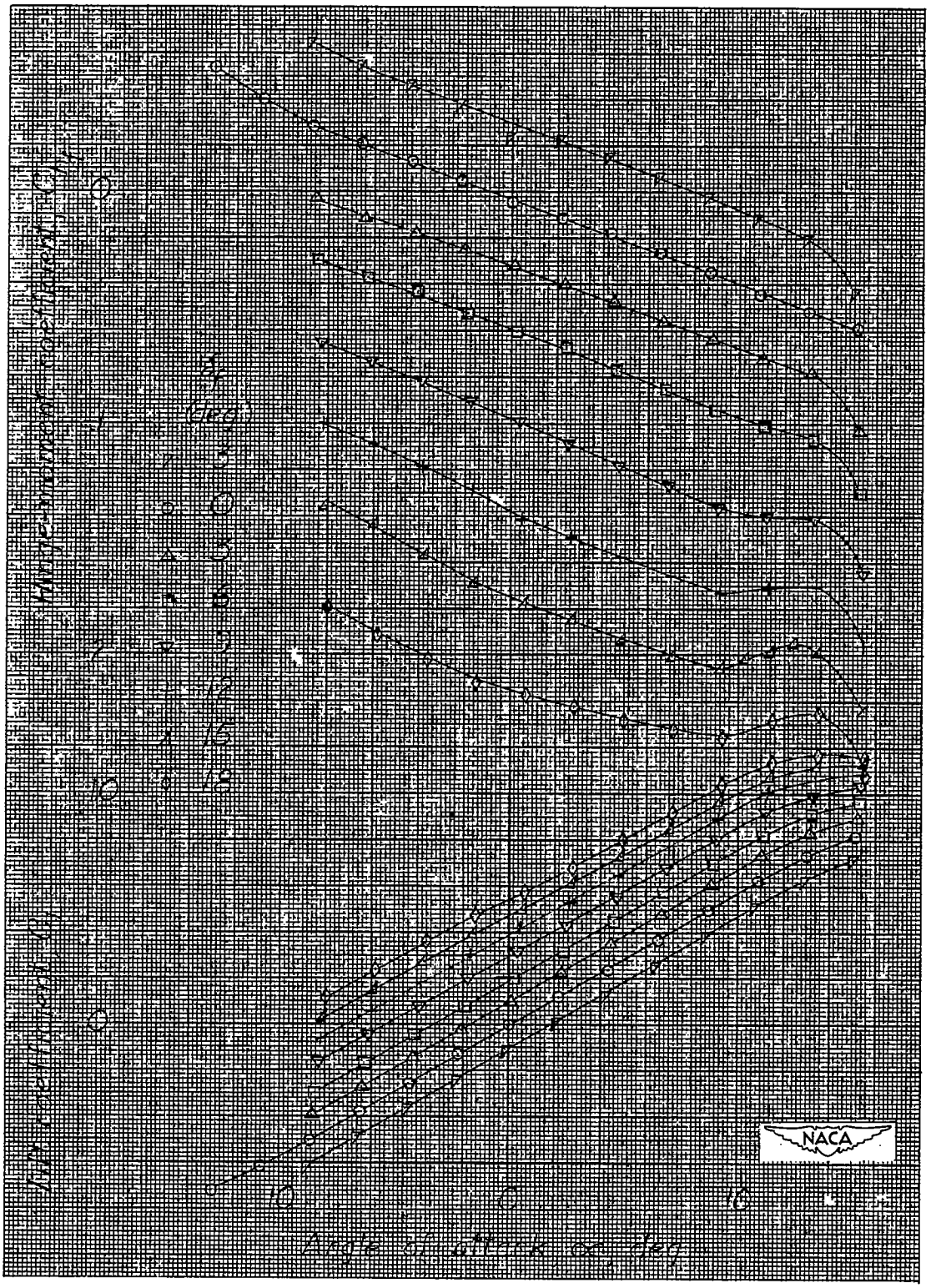

Figure 16.- NACA 66-009 semispan tail surface. Taper ratio λ, 0.4; aspect ratio A, 3.36; 0.30c plain flap; 0.005c gap; δ_t/δ_f, 0.

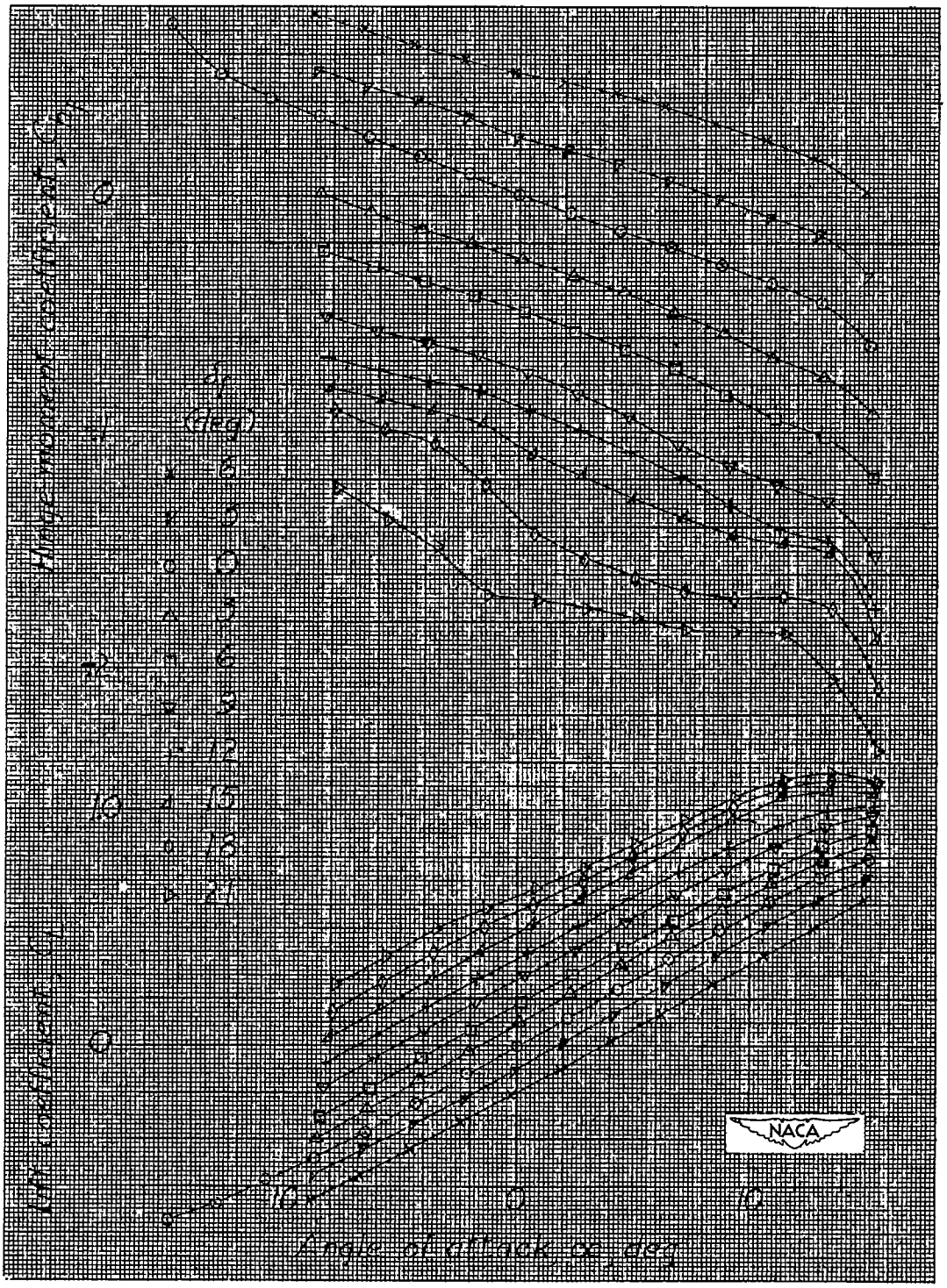

Figure 17.- NACA 66-009 semispan tail surface. Taper ratio λ, 0.4; aspect ratio A, 3.36; 0.30c flap with 0.35c_f elliptic overhang; 0.005c gap; δ_t/δ_f, 0.

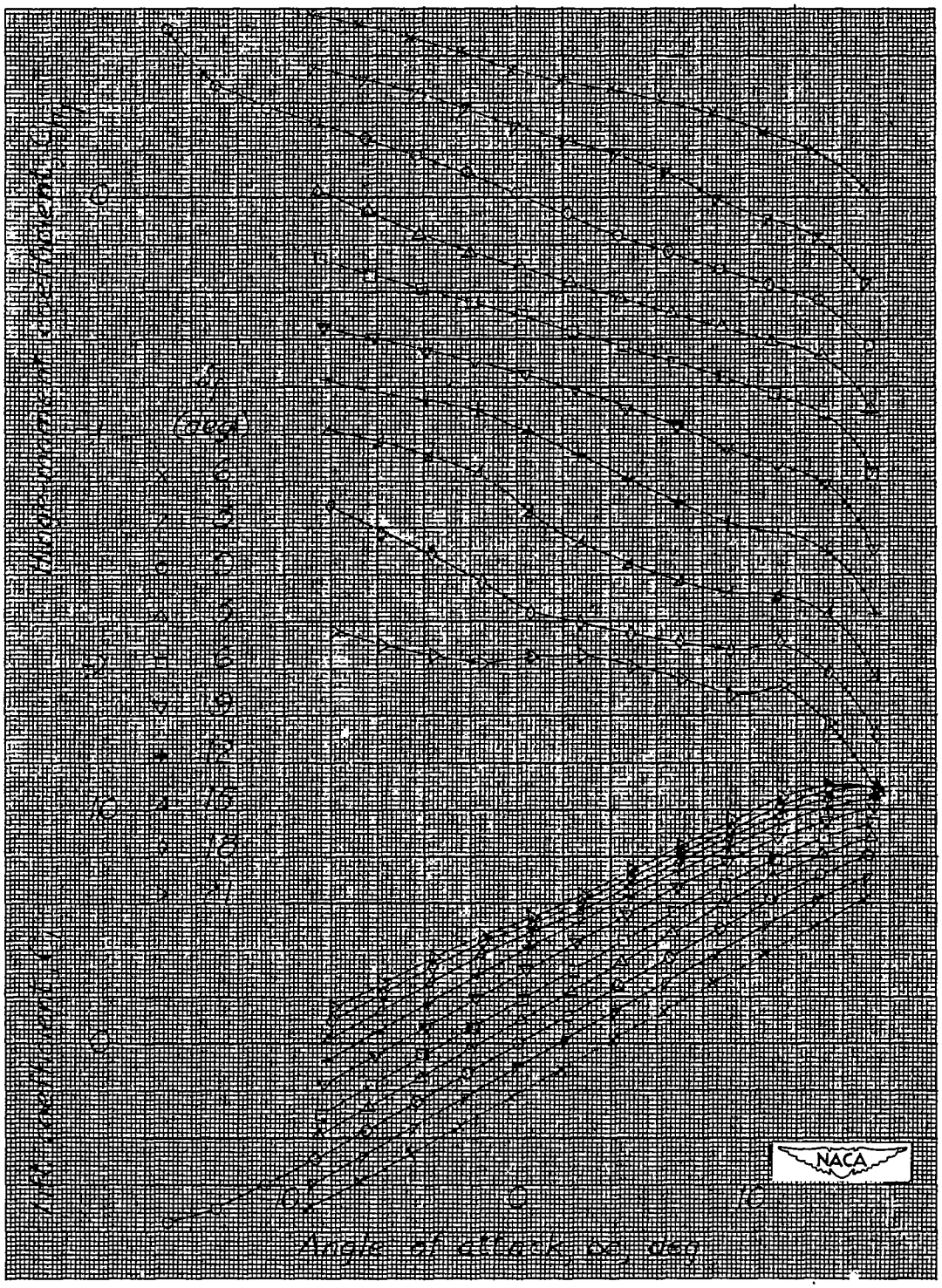

Figure 18.- NACA 66-009 semispan tail surface. Taper ratio λ, 0.4; aspect ratio A, 3.36; 0.30c flap with 0.35c_f sharp-nosed overhang; 0.005c gap; δ_t/δ_f, 0.

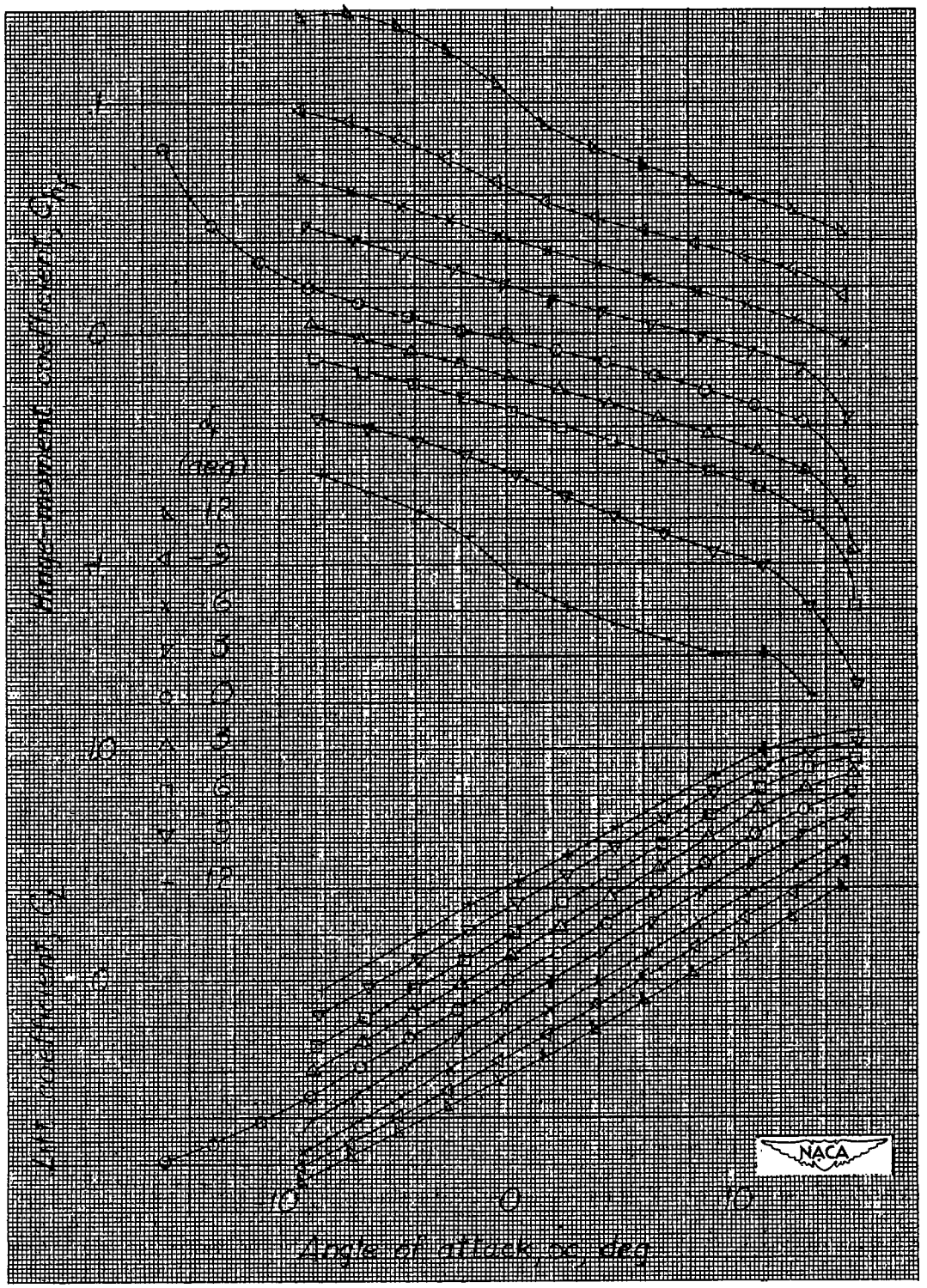

(a) $\delta_t/\delta_f = 0$.

Figure 19.- NACA 66-009 semispan tail surface. Taper ratio λ, 0.4; aspect ratio A, 3.36; 0.30c flap with $0.35c_f$ internal balance; sealed gap.

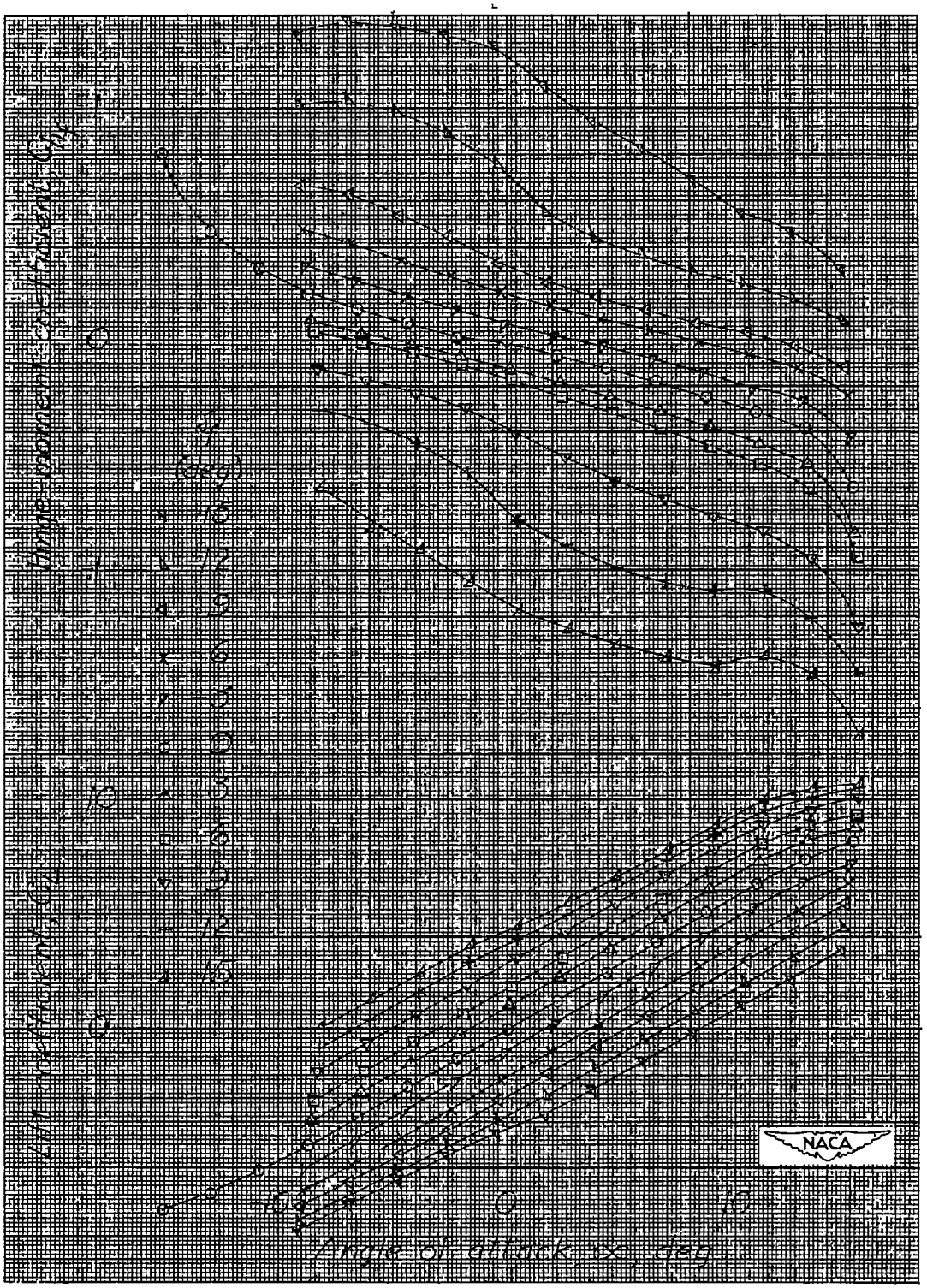

(b) $\delta_t/\delta_f = -0.5$.

Figure 19.- Concluded.

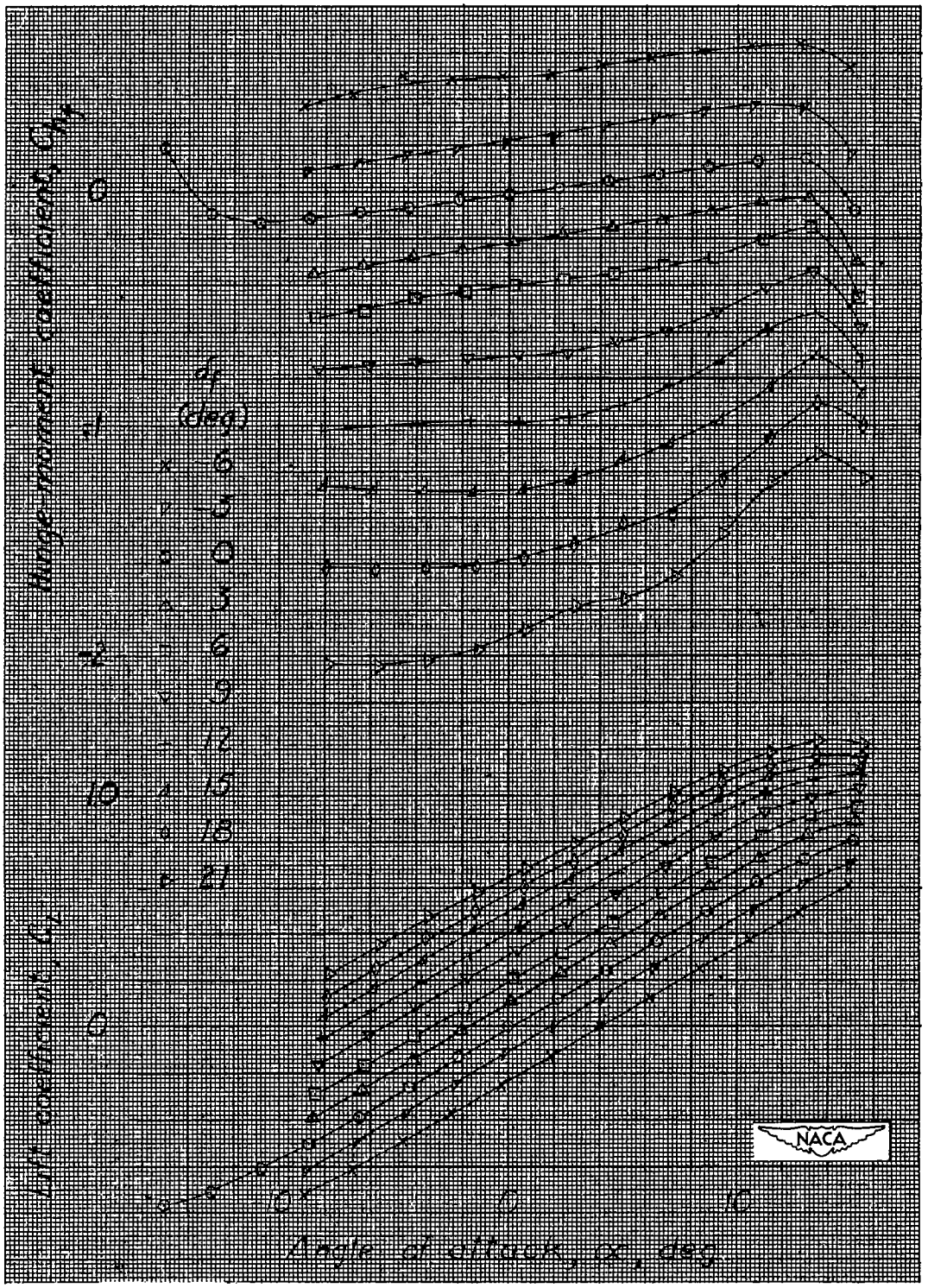

(a) Horn 1.

Figure 20.- NACA 66-009 semispan tail surface. Taper ratio λ, 0.4; aspect ratio A, 3.36; 0.30c plain flap; 0.005c gap; δ_t/δ_f, 0.

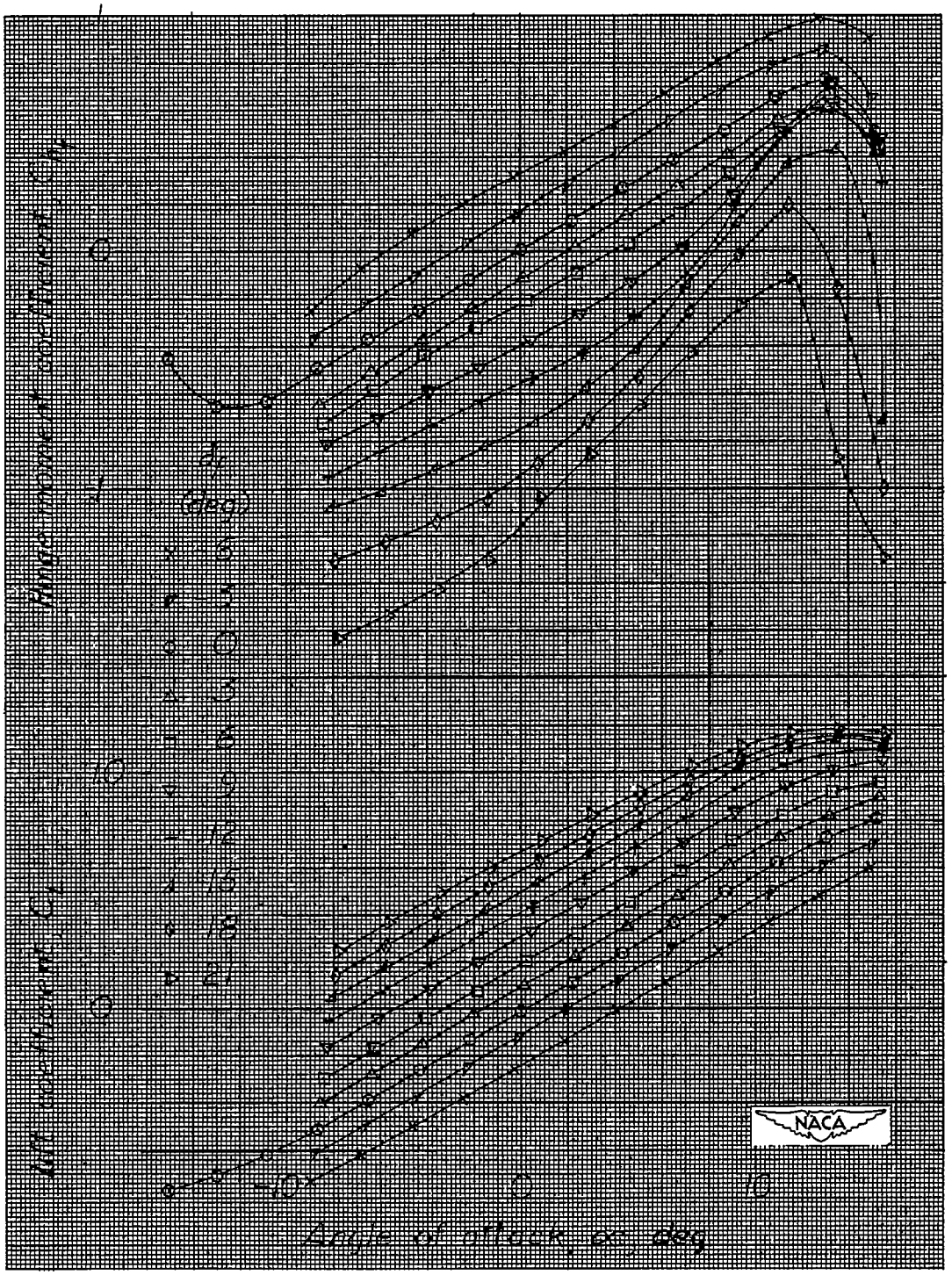

(b) Horn 2.

Figure 20.- Concluded.

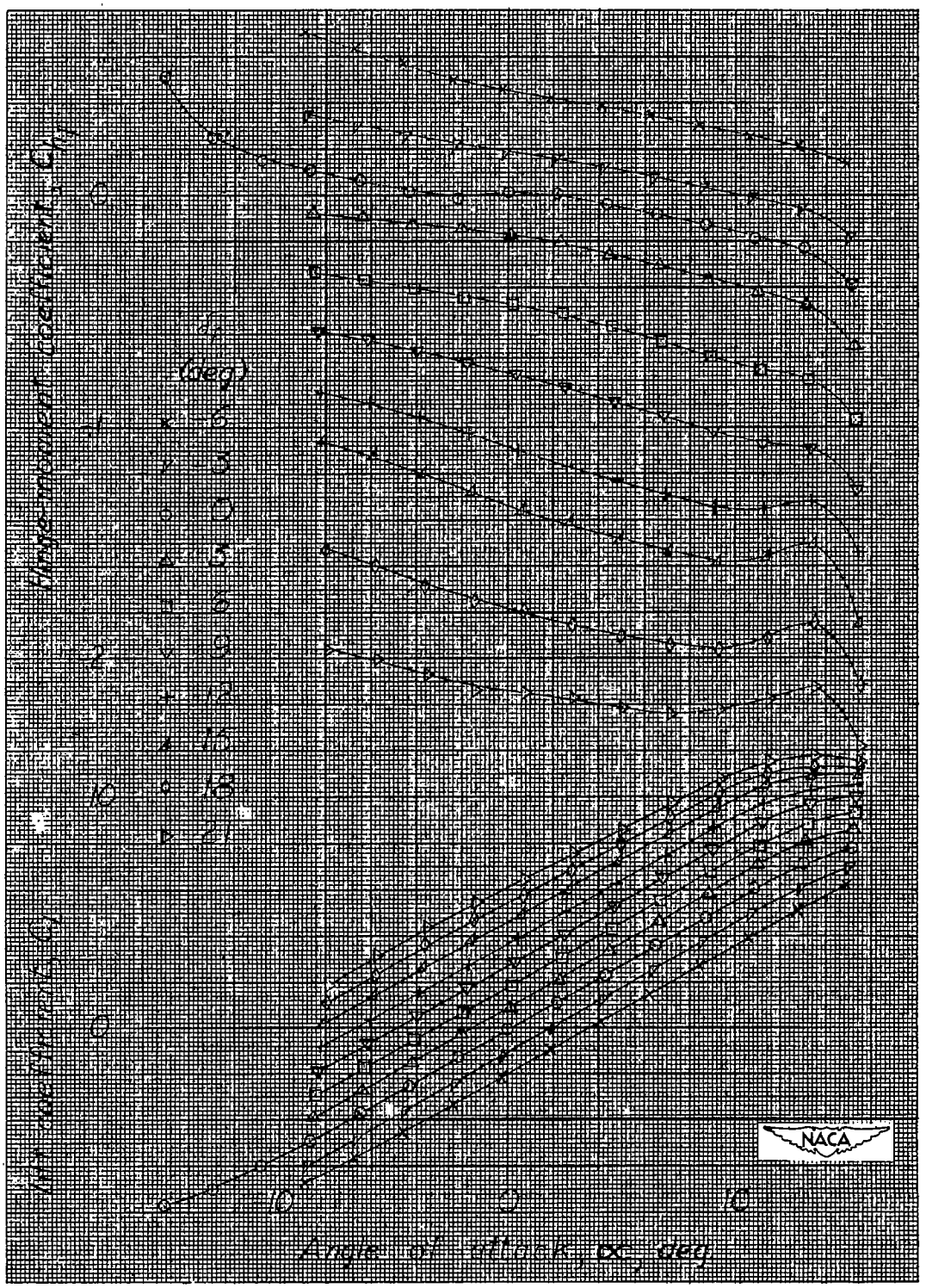

Figure 21.- NACA 66-009 semispan tail surface. Taper ratio λ, 0.4; aspect ratio A, 3.36; 0.30c straight-contour plain flap; 0.005c gap; δ_t/δ_f, 0.

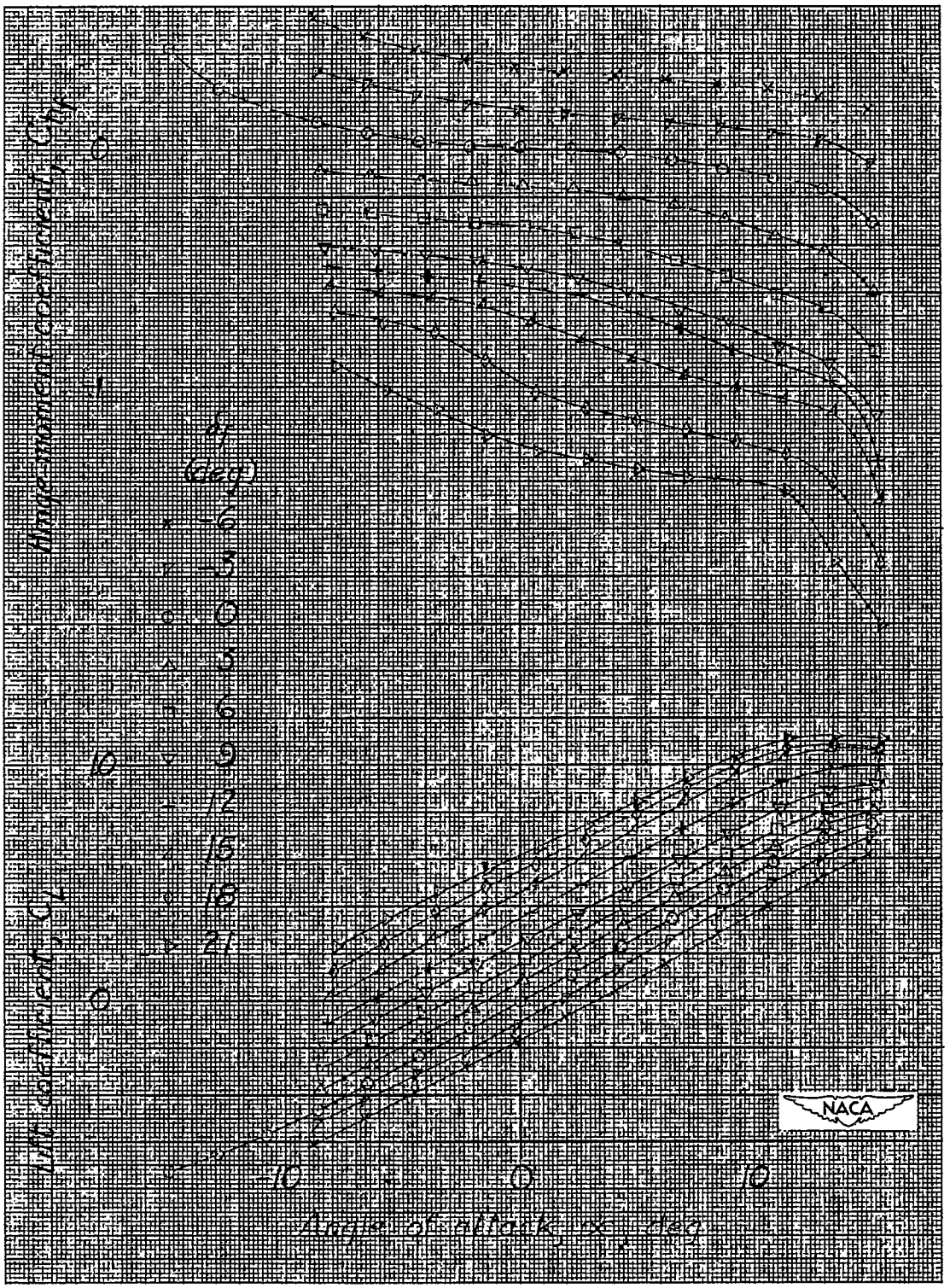

Figure 22.- NACA 66-009 semispan tail surface. Taper ratio λ, 0.4; aspect ratio A, 3.36; 0.30c straight-contour flap with 0.35c_f elliptic overhang; 0.005c gap; δ_t/δ_f, 0.

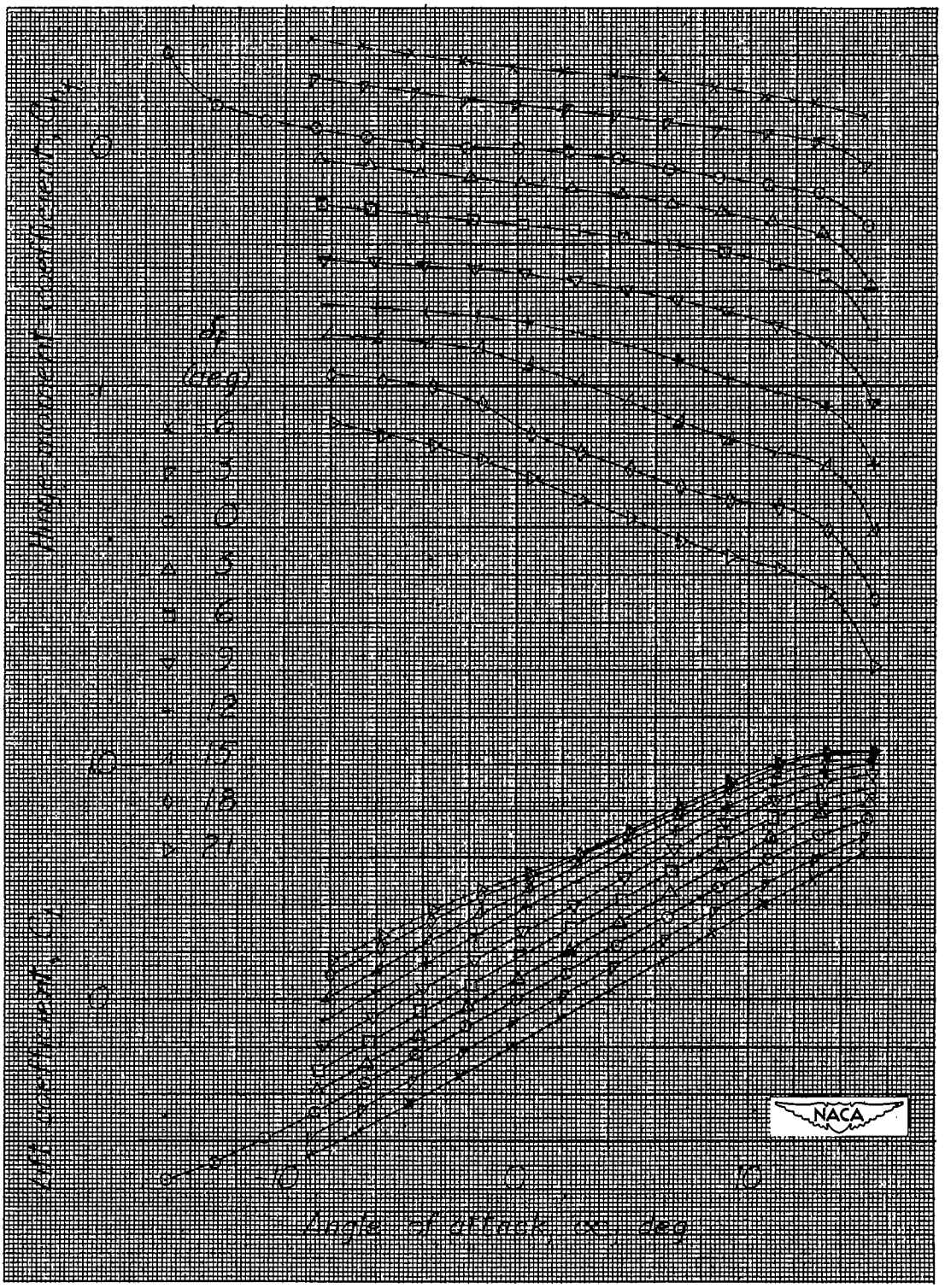

Figure 23.- NACA 66-009 semispan tail surface. Taper ratio λ, 0.4; aspect ratio A, 3.36; 0.30c straight-contour flap with 0.35c_f sharp-nosed overhang; 0.005c gap; δ_t/δ_f, 0.

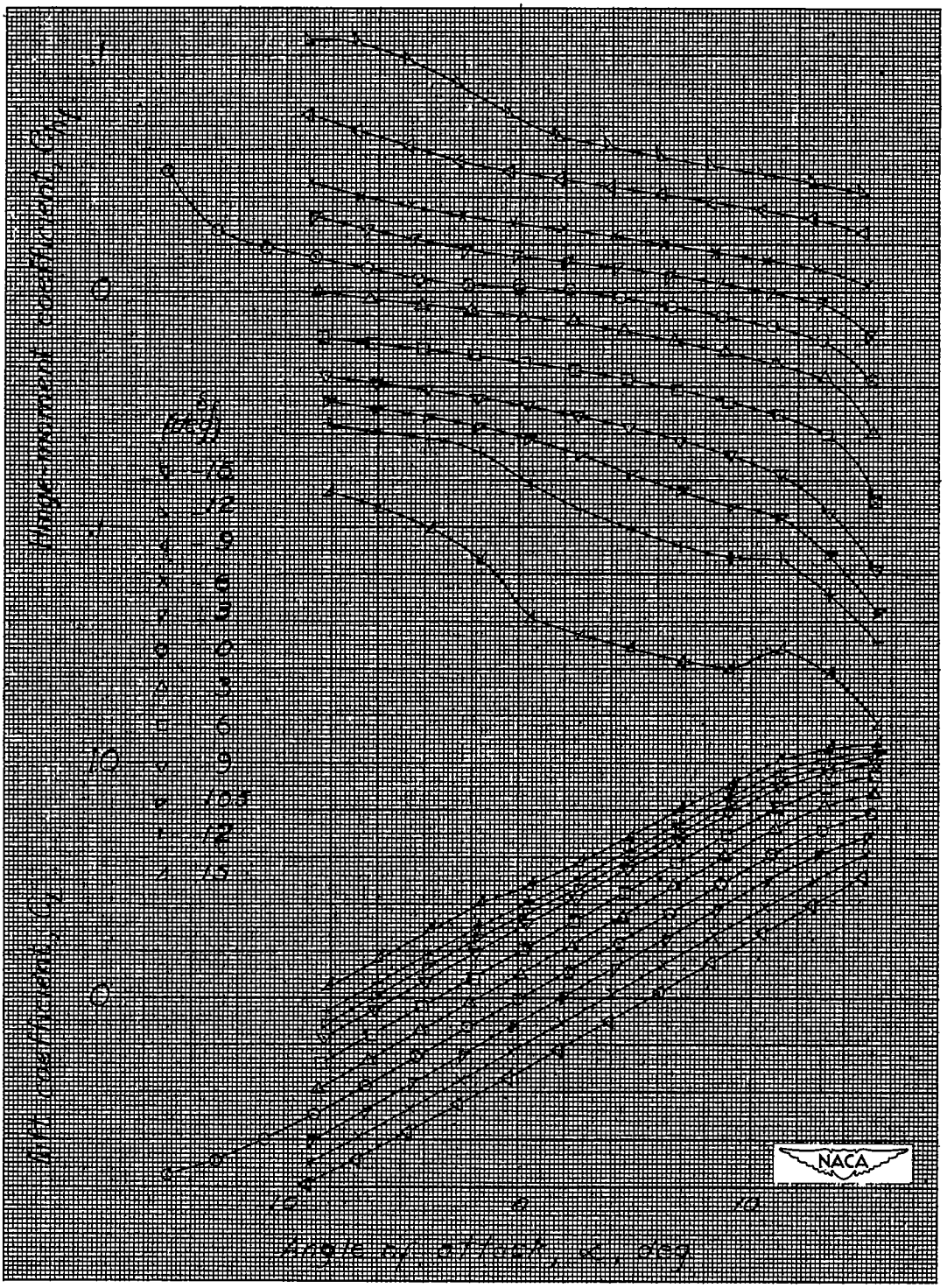

(a) $\delta_t/\delta_f = 0.$

Figure 24.- NACA 66-009 semispan tail surface. Taper ratio λ, 0.4; aspect ratio A, 3.36; 0.30c straight-contour flap with $0.35c_f$ internal balance; sealed gap.

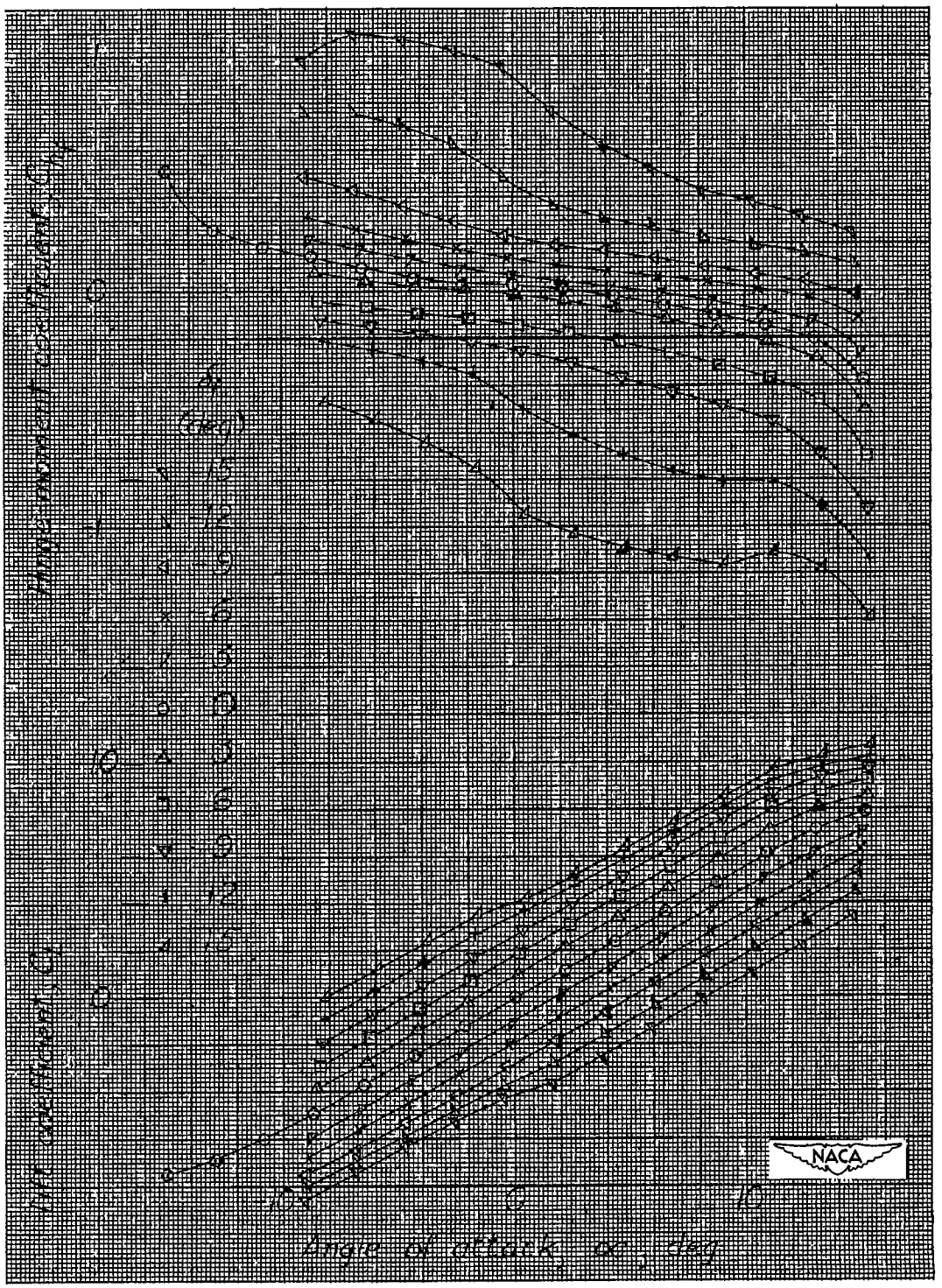

(b) $\delta_t/\delta_f = -0.5$.

Figure 24.- Concluded.

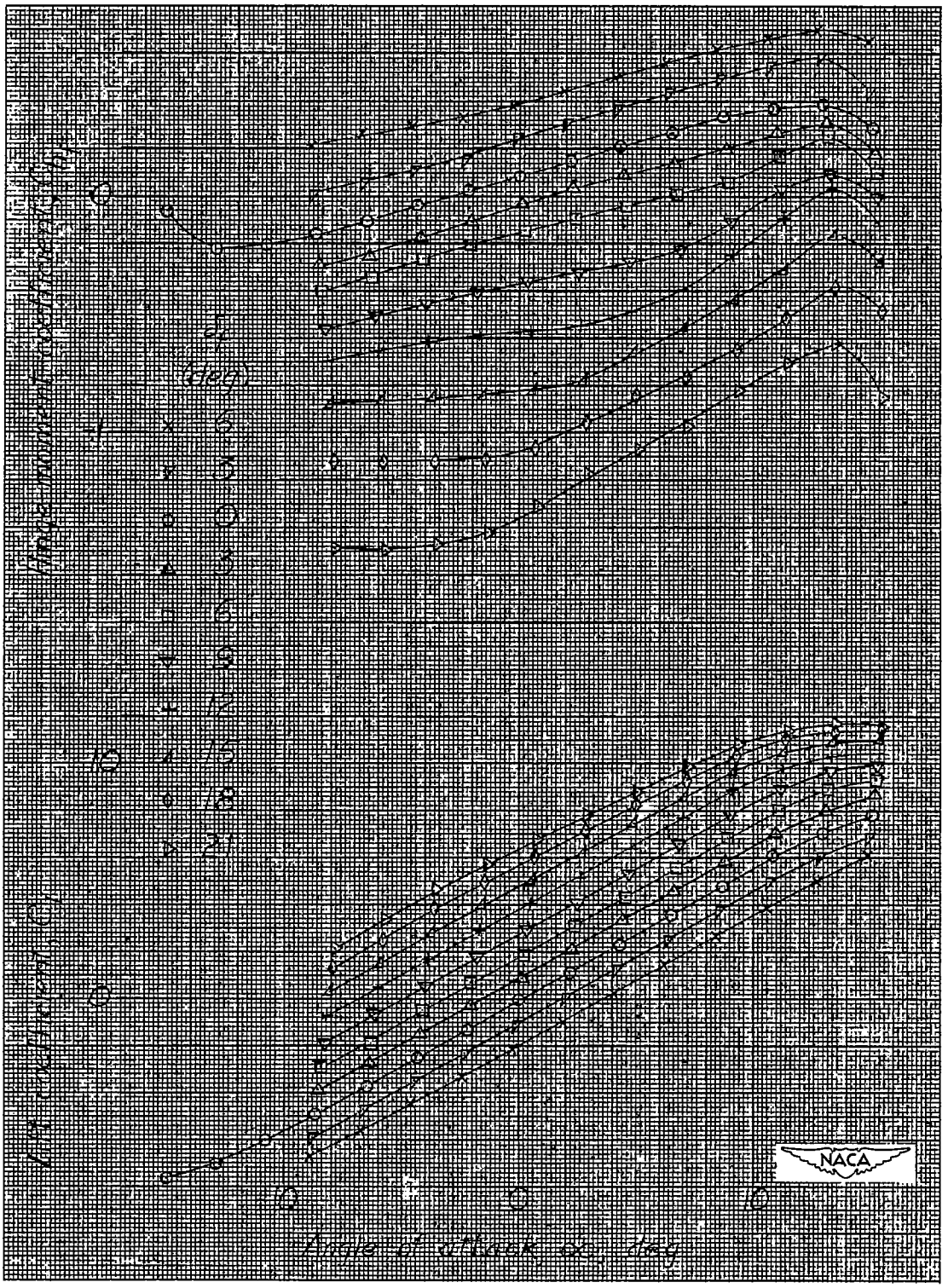

Figure 25.- NACA 66-009 semispan tail surface. Taper ratio λ, 0.4; aspect ratio A, 3.36; 0.30c straight-contour plain flap; 0.005c gap; horn 1; δ_t/δ_f, 0.

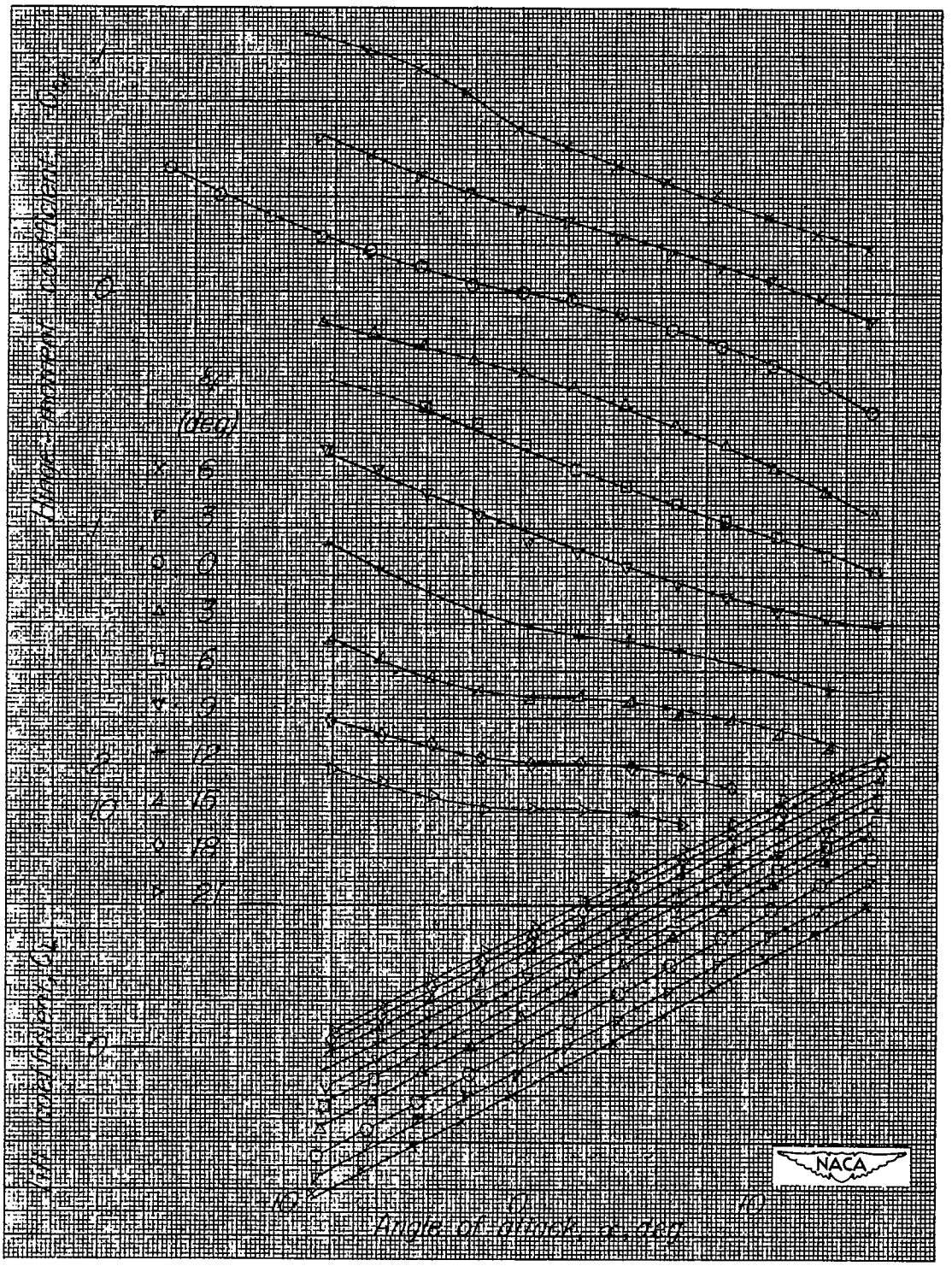

(a) $\delta_t/\delta_f = 0$.

Figure 26.- NACA 66(215)-014 semispan tail surface. Taper ratio λ, 0.4; aspect ratio A, 3.36; 0.30c flap; 0.005c gap.

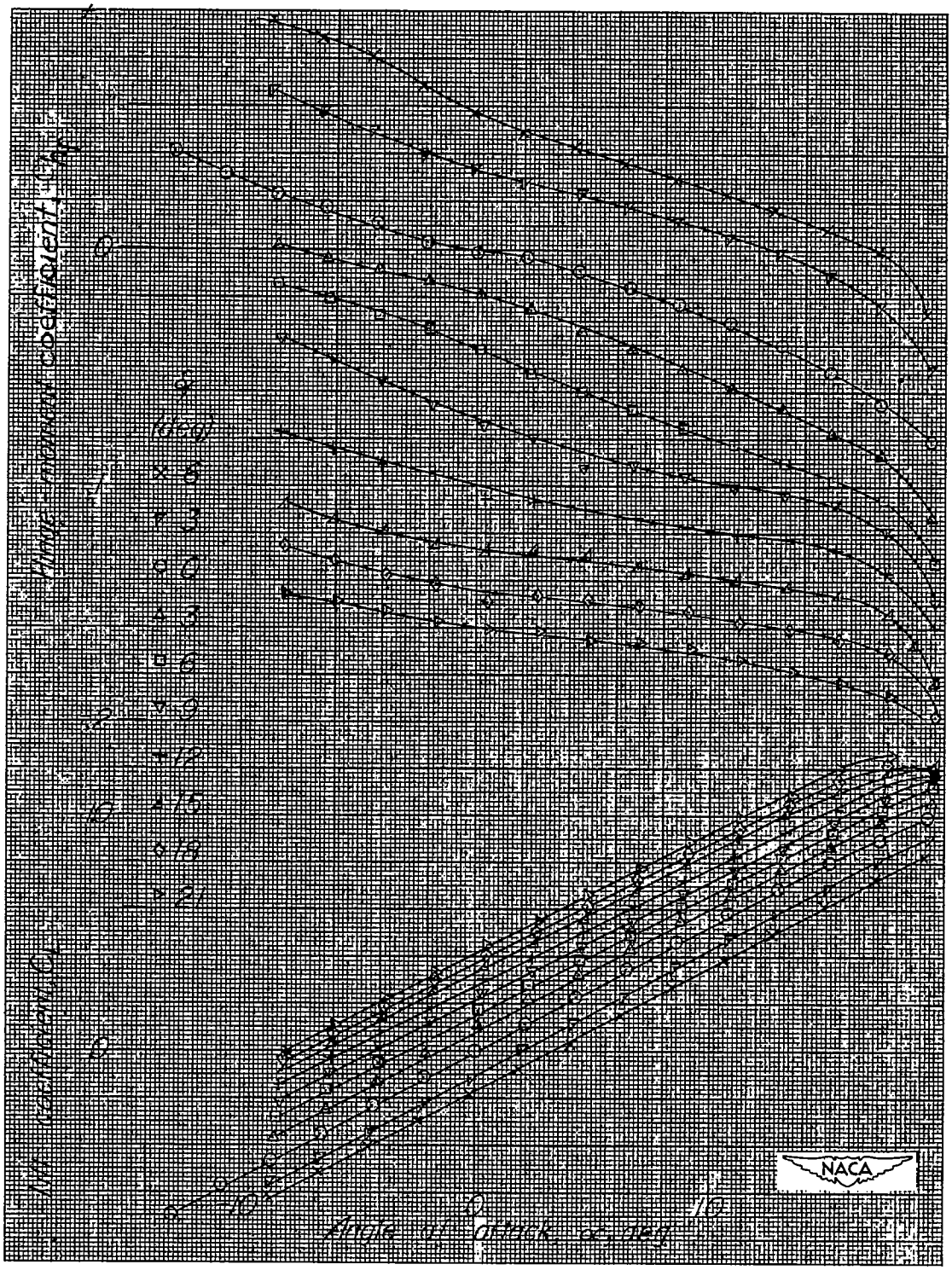

(b) $\delta_t/\delta_f = -0.5$.

Figure 26.- Concluded.

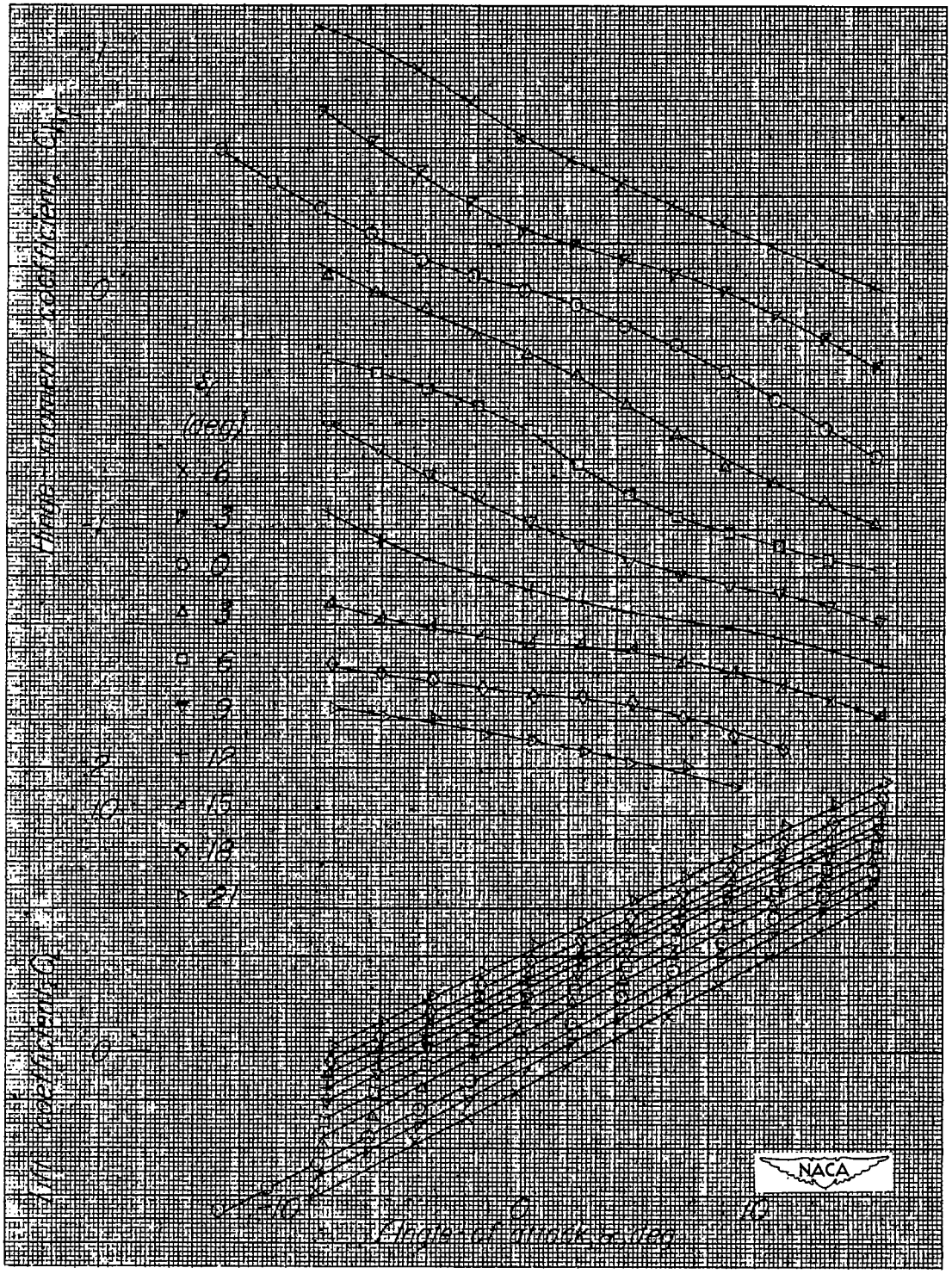

Figure 27.- NACA 66(215)-014 semispan tail surface. Taper ratio λ, 0.4; aspect ratio A, 3.36; 0.30c flap with $0.35c_f$ elliptic overhang; 0.005c gap; δ_t/δ_f, 0.

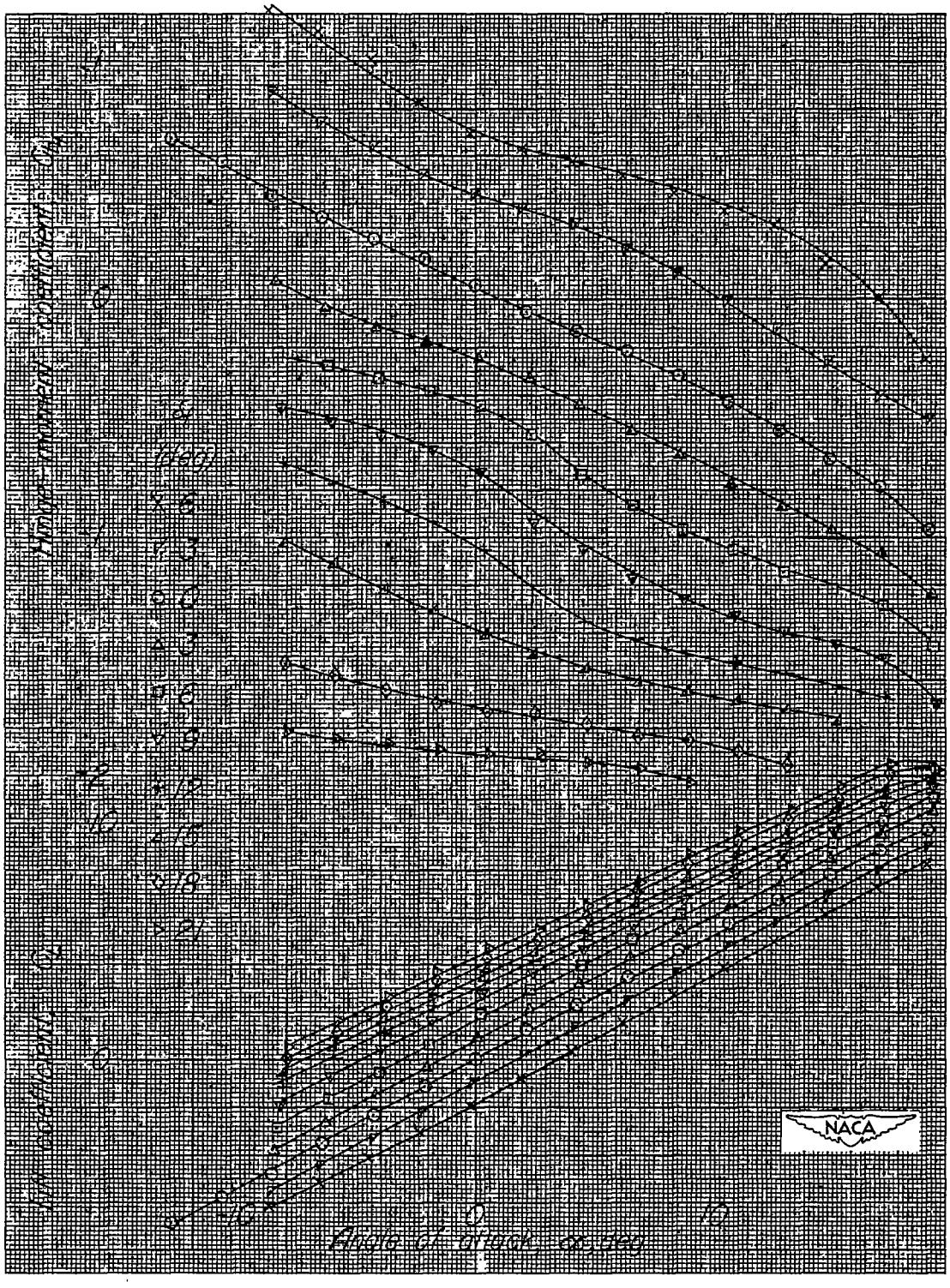

Figure 28.- NACA 66(215)-014 semispan tail surface. Taper ratio λ, 0.4; aspect ratio A, 3.36; 0.30c flap with $0.35c_f$ sharp-nosed overhang; 0.005c gap; δ_t/δ_f, 0.

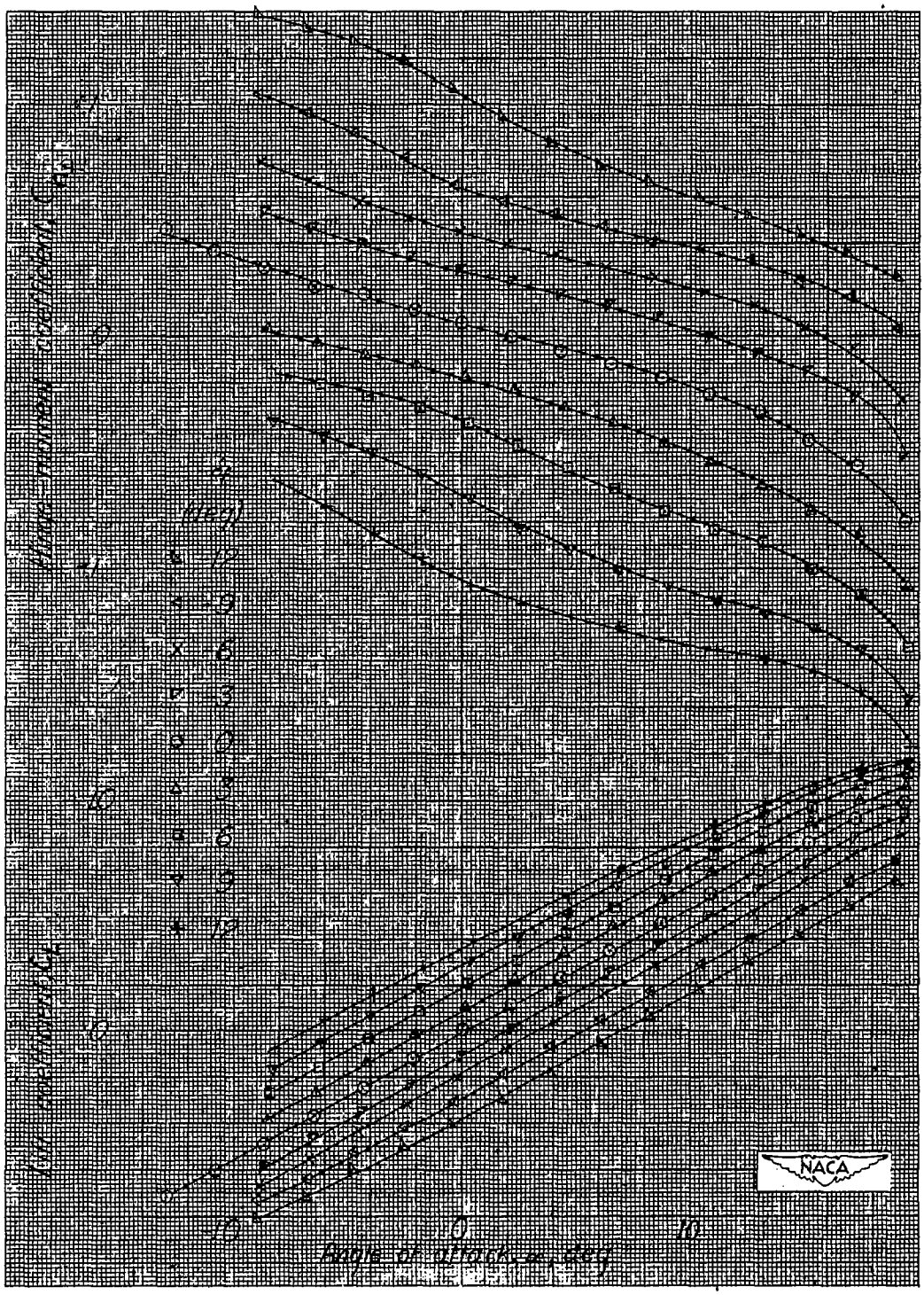

(a) $\delta_t/\delta_f = 0.$

Figure 29.- NACA 66(215)-014 semispan tail surface. Taper ratio λ, 0.4; aspect ratio A, 3.36; 0.30c flap with 0.35c_f internal balance; sealed gap.

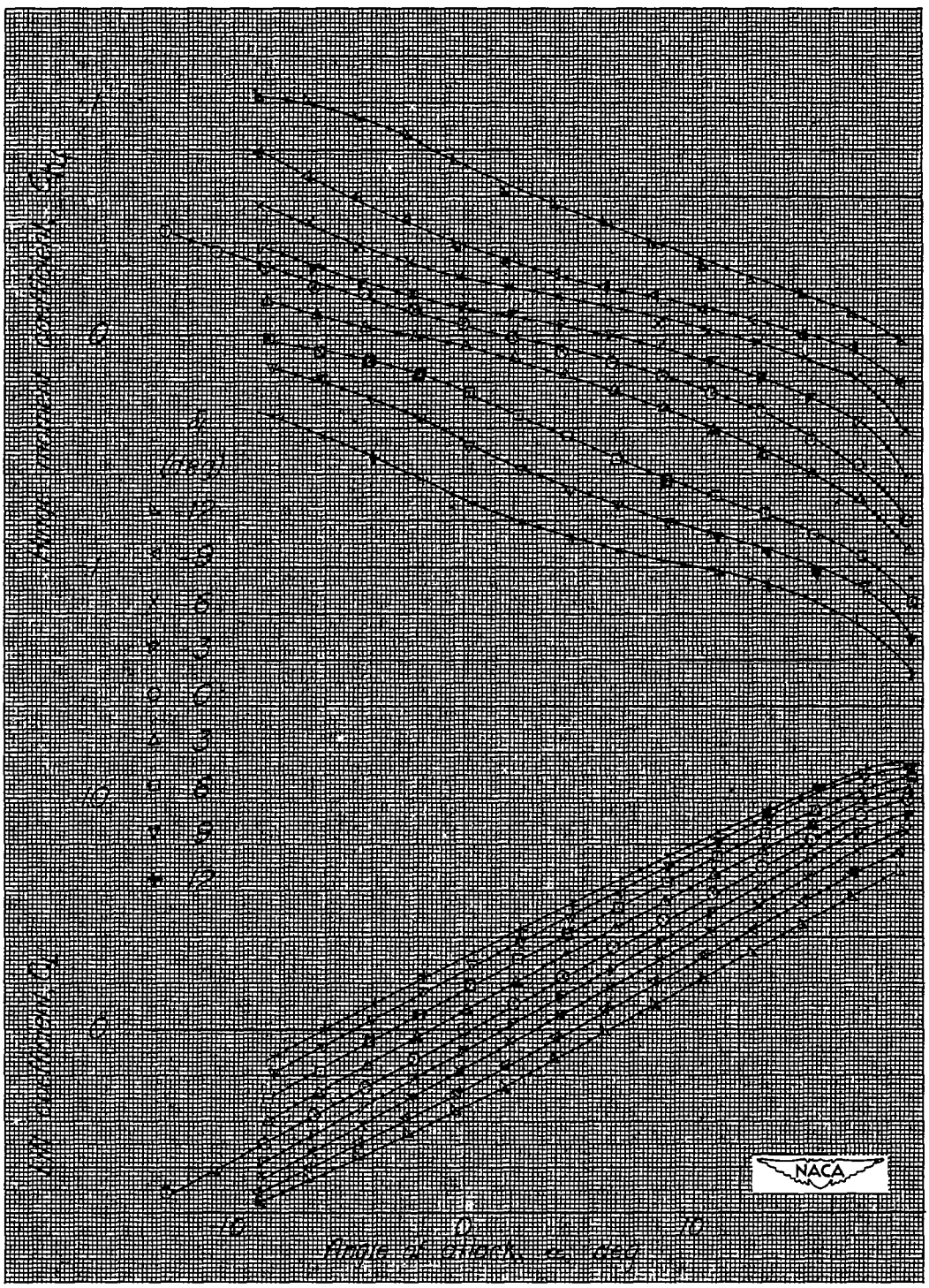

(b) $\delta_t/\delta_f = -0.5$.

Figure 29.- Concluded.

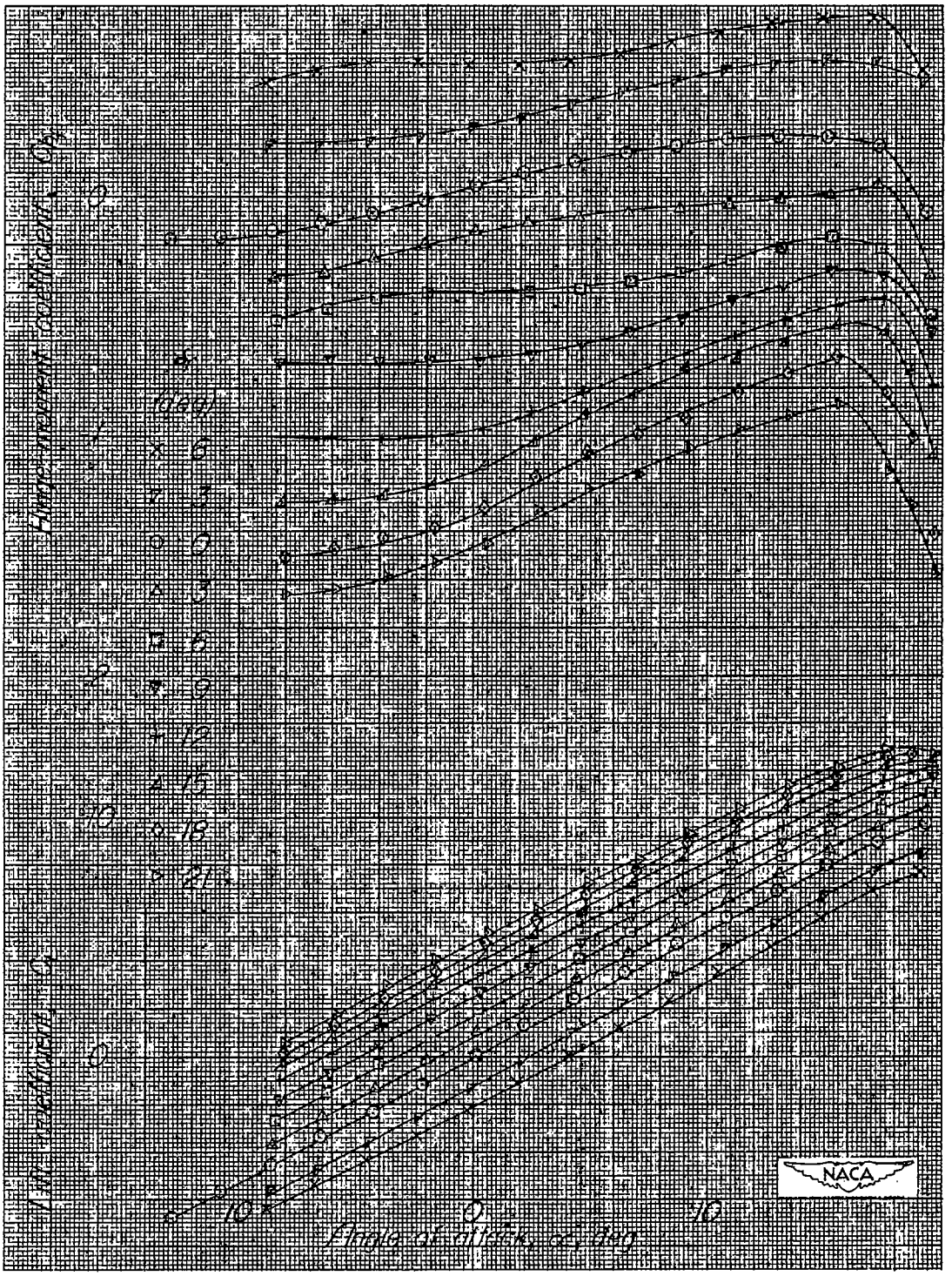

(a) Horn 1.

Figure 30.- NACA 66(215)-014 semispan tail surface. Taper ratio λ, 0.4; aspect ratio A, 3.36; 0.30c flap; 0.005c gap; δ_t/δ_f, 0.

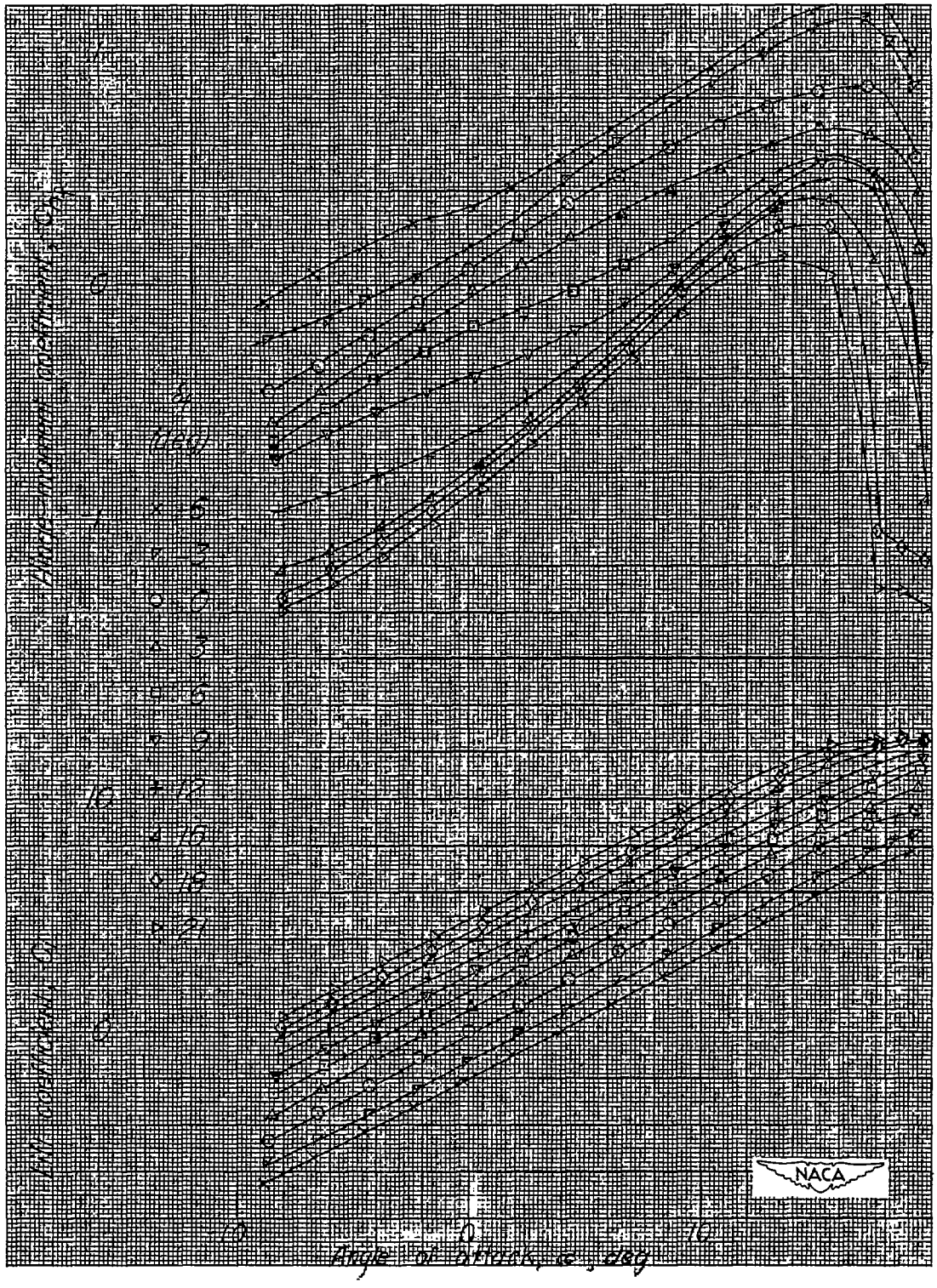

(b) Horn 2.

Figure 30.- Concluded.

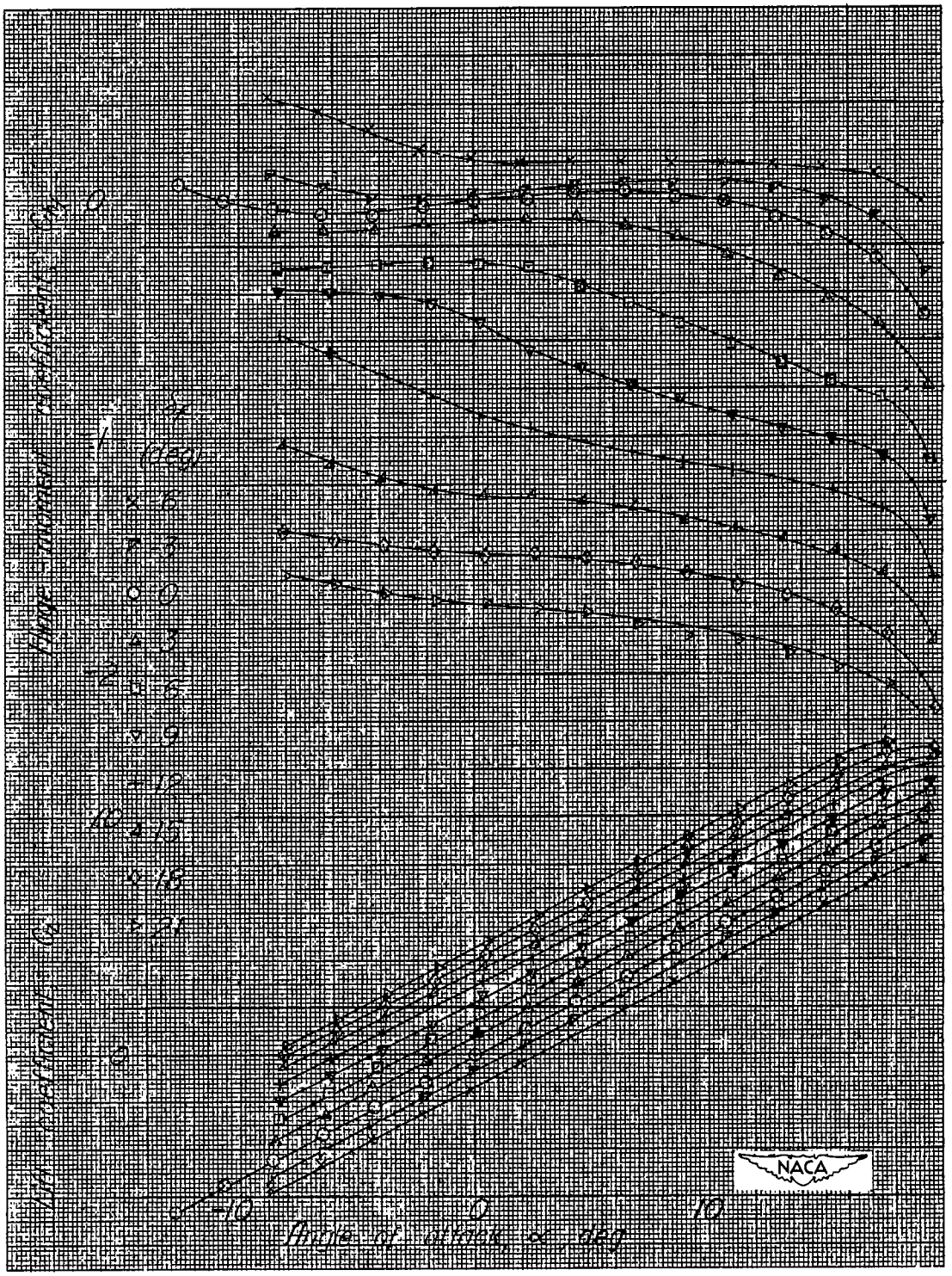

Figure 31.- NACA 66(215)-014 semispan tail surface. Taper ratio λ, 0.4; aspect ratio A, 3.36; 0.30c straight-contour flap; 0.005c gap; δ_t/δ_f, 0.

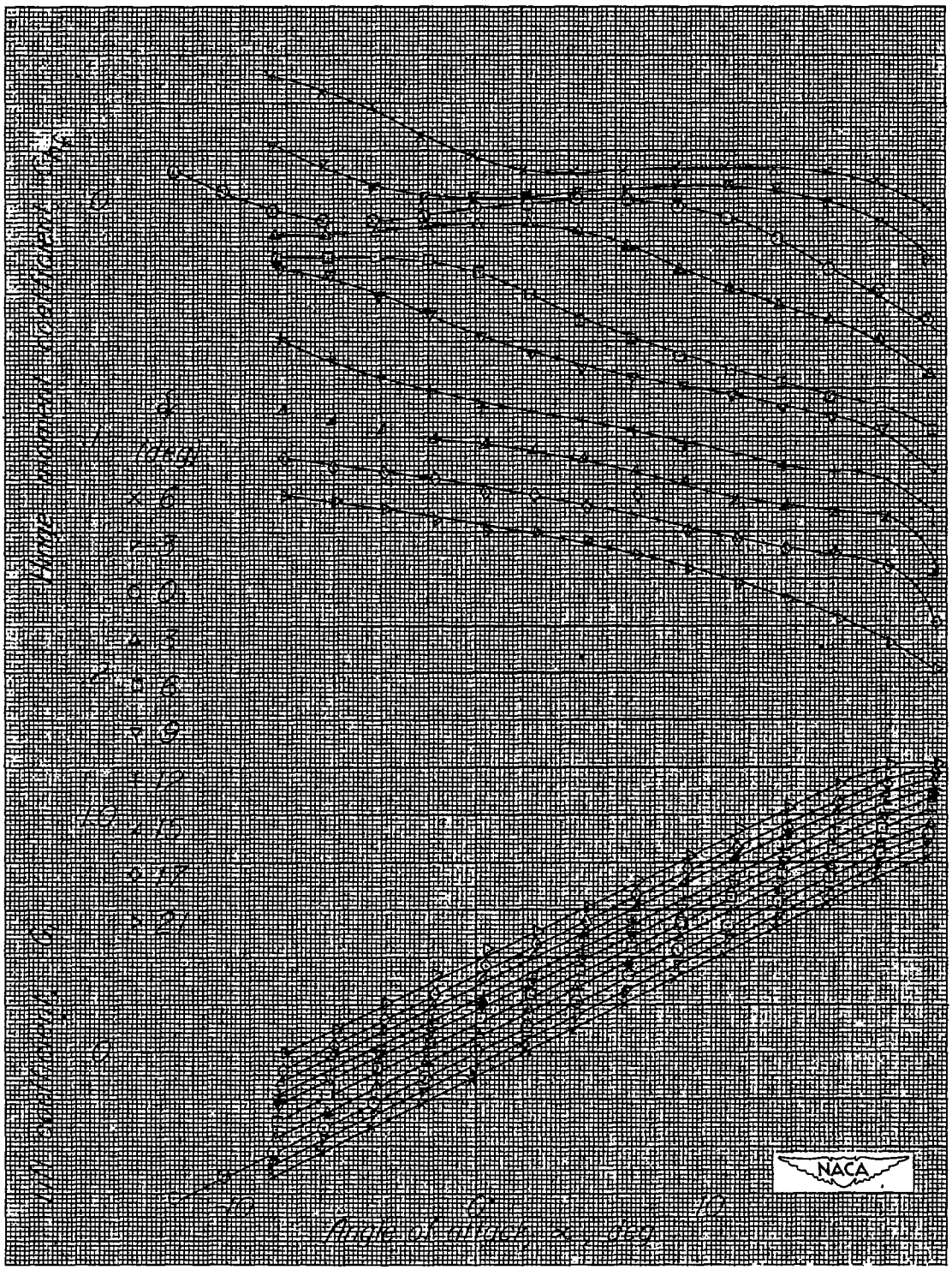

Figure 32.- NACA 66(215)-014 semispan tail surface. Taper ratio λ, 0.4; aspect ratio A, 3.36; 0.30c straight-contour flap with $0.35c_f$ elliptic overhang; 0.005c gap; δ_t/δ_f, 0.

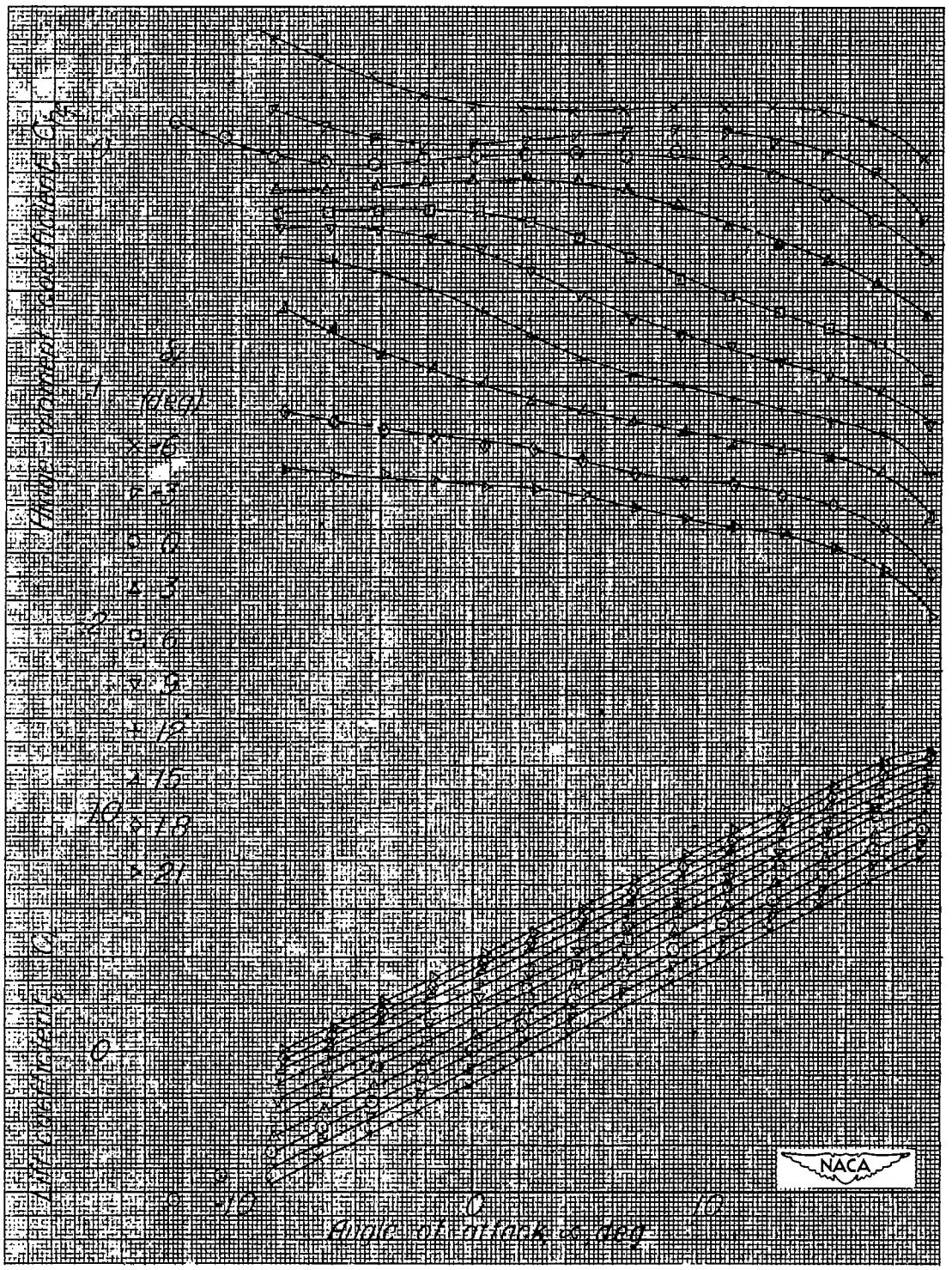

Figure 33.- NACA 66(215)-014 semispan tail surface. Taper ratio λ, 0.4; aspect ratio A, 3.36; 0.30c straight-contour flap with $0.35c_f$ sharp-nosed overhang; 0.005c gap; δ_t/δ_f, 0.

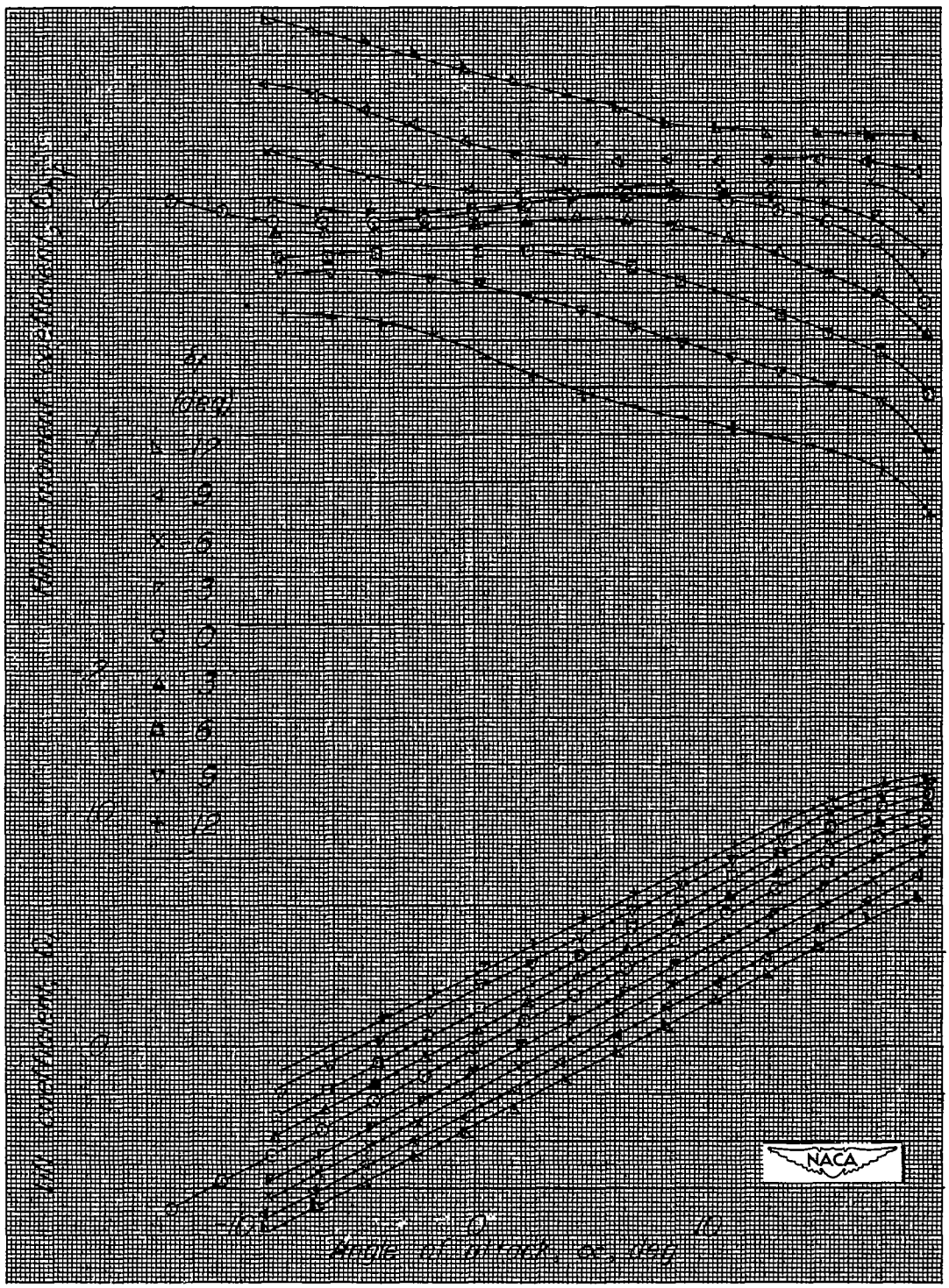

(a) $\delta_t/\delta_f = 0$.

Figure 34.- NACA 66(215)-014 semispan tail surface. Taper ratio λ, 0.4; aspect ratio A, 3.36; 0.30c straight-contour flap with $0.35c_f$ internal balance; sealed gap.

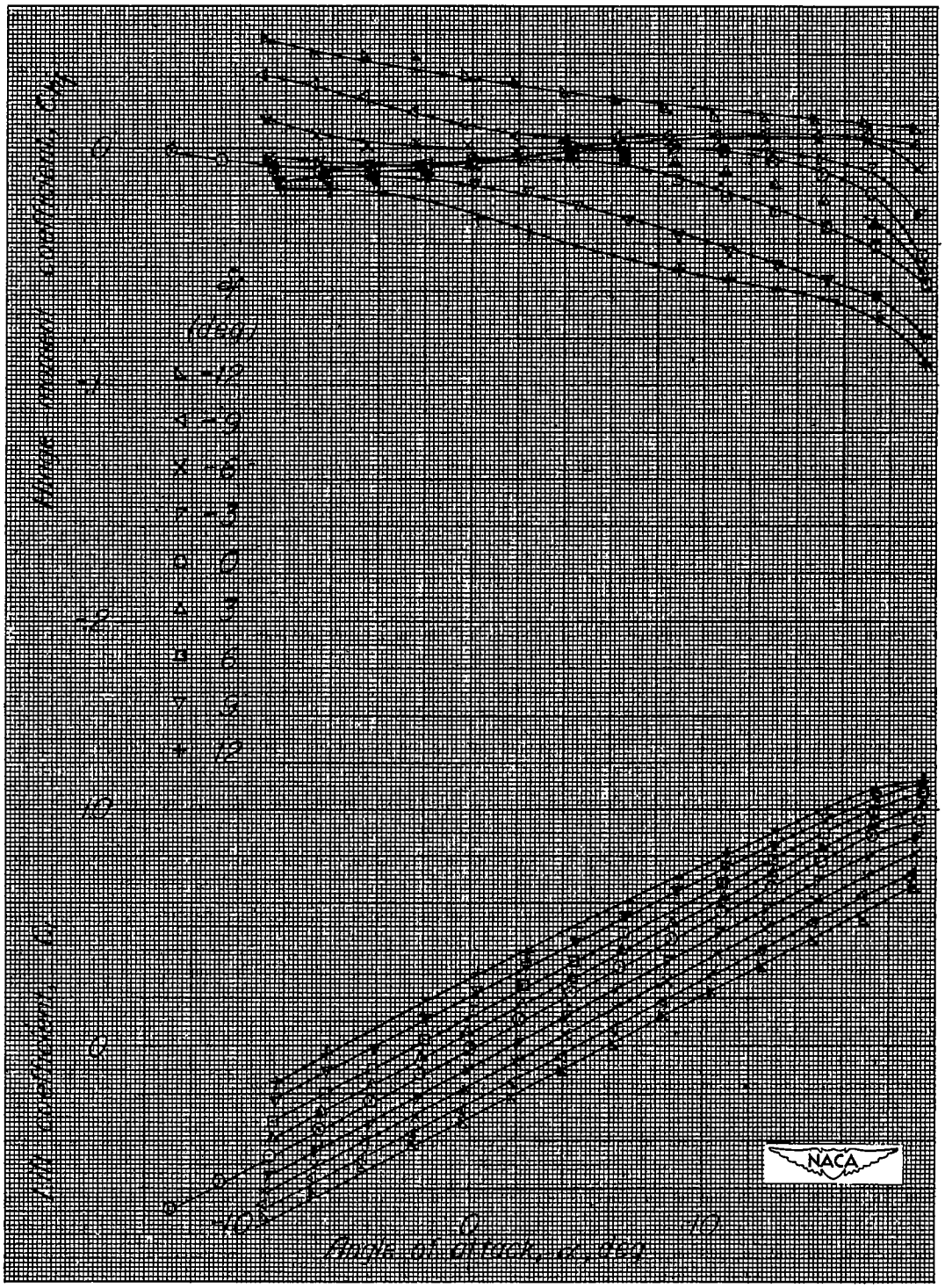

(b) $\delta_t/\delta_f = -0.5$.

Figure 34.- Concluded.

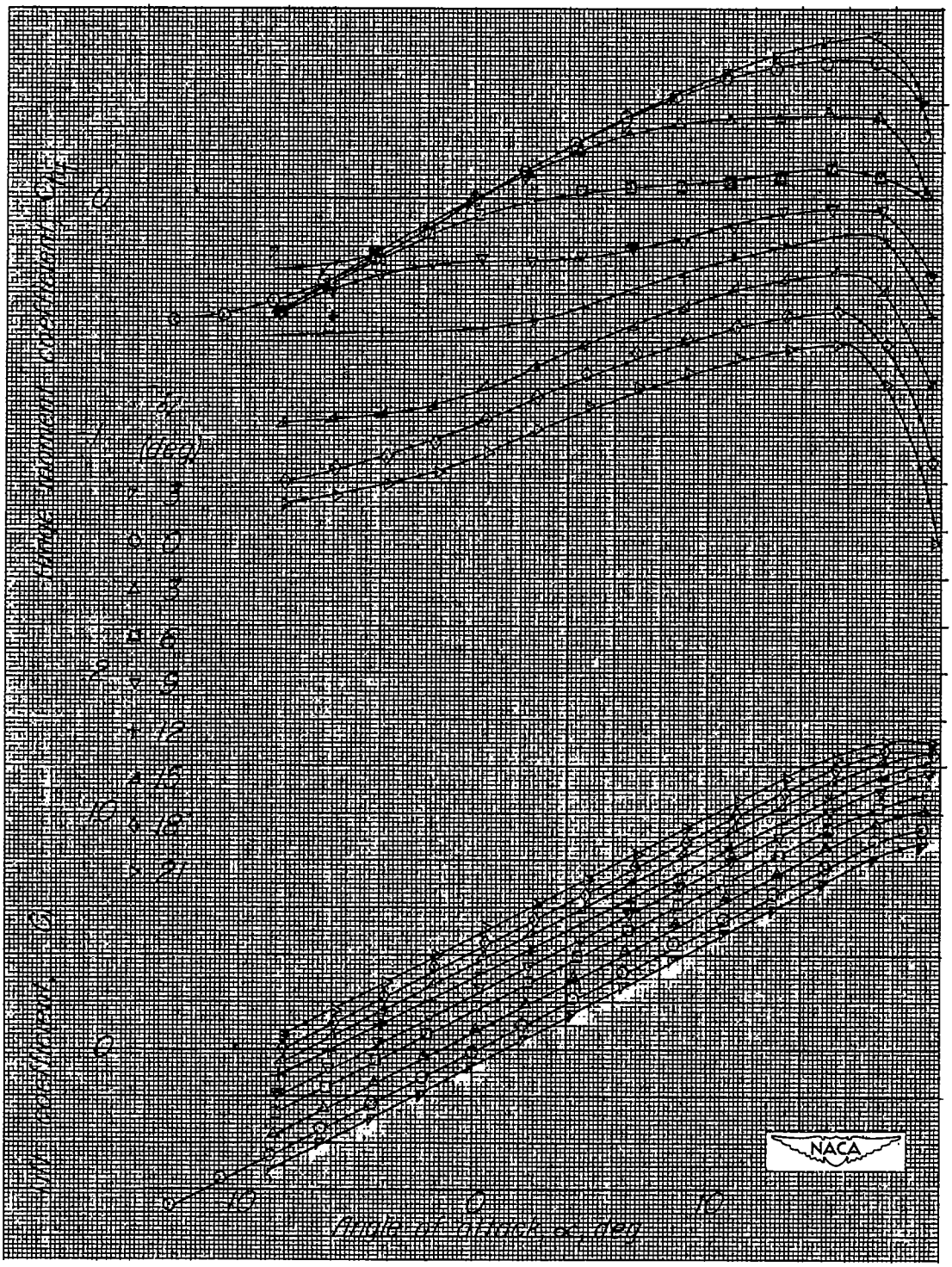

(a) Horn 1.

Figure 35.- NACA 66(215)-014 semispan tail surface. Taper ratio λ, 0.4; aspect ratio A, 3.36; 0.30c straight-contour flap; 0.005c gap; δ_t/δ_f, 0.

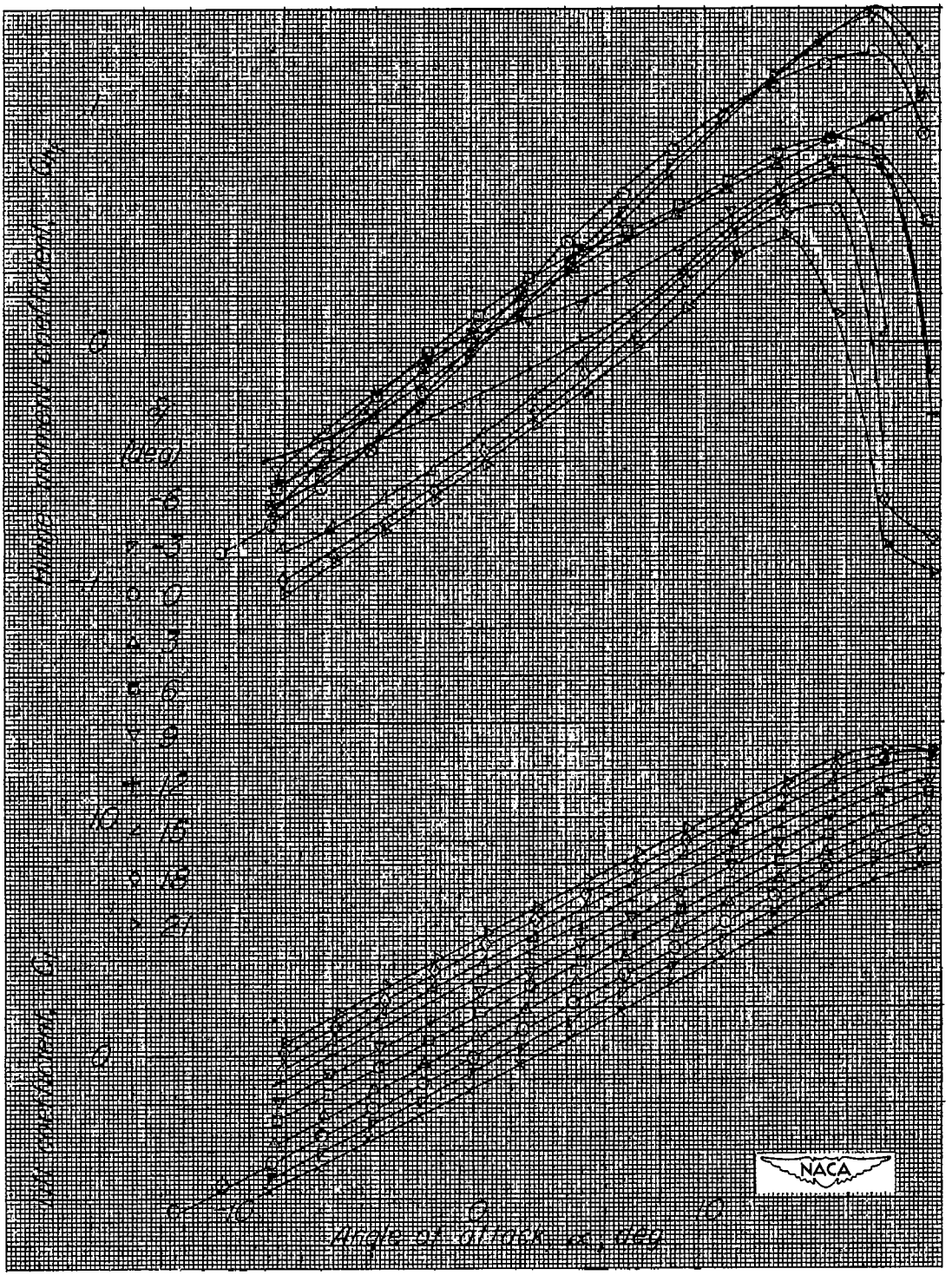

(b) Horn 2.

Figure 35.- Concluded.

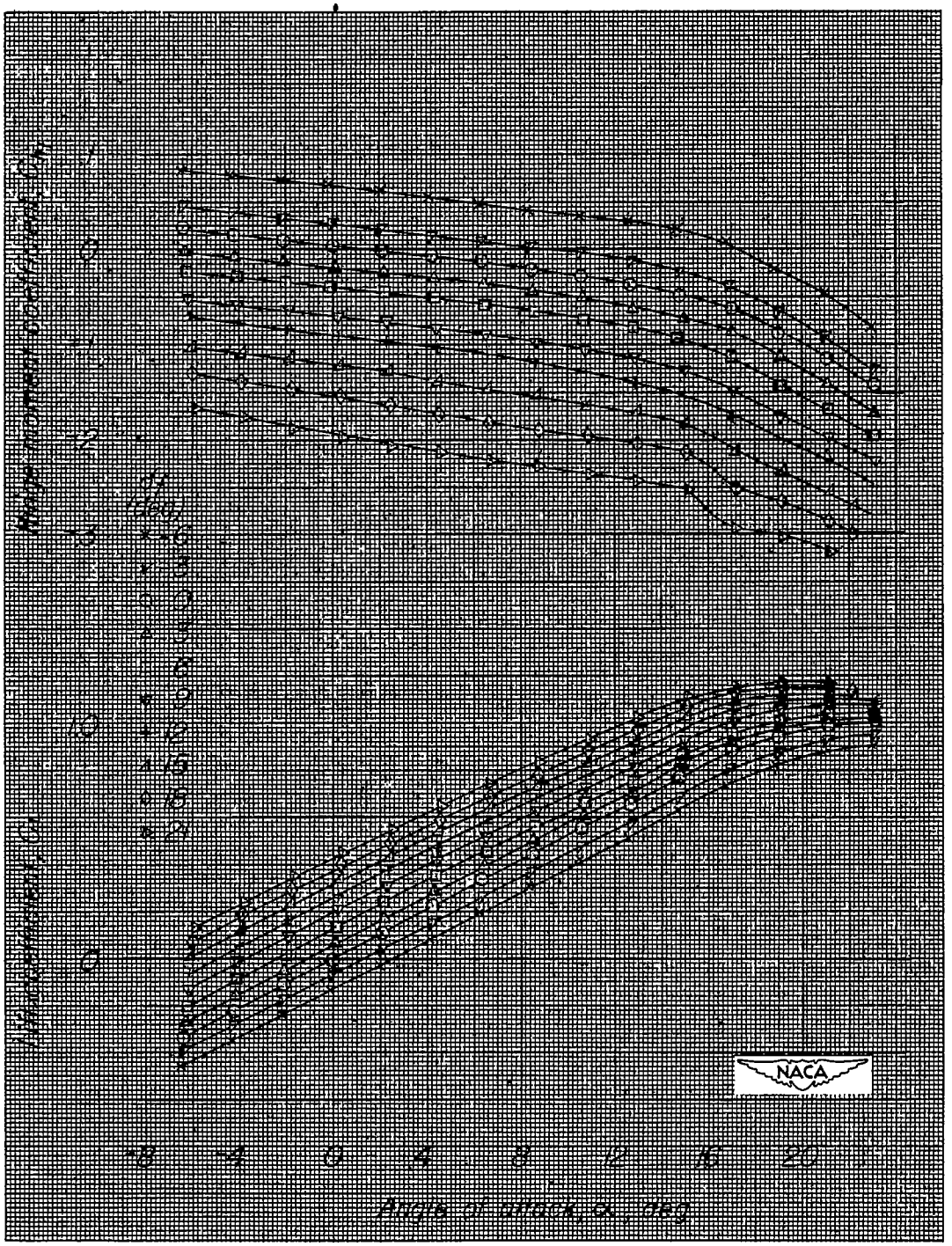

(a) Without transition wire; C_{h_f} and C_L against α.

Figure 36.- NACA 0009 semispan tail surface. Sweepback angle Λ, 40°; taper ratio λ, 0.4; aspect ratio A, 3.30; 0.30c flap with radius nose; 0.005c gap; δ_t/δ_f, 0.

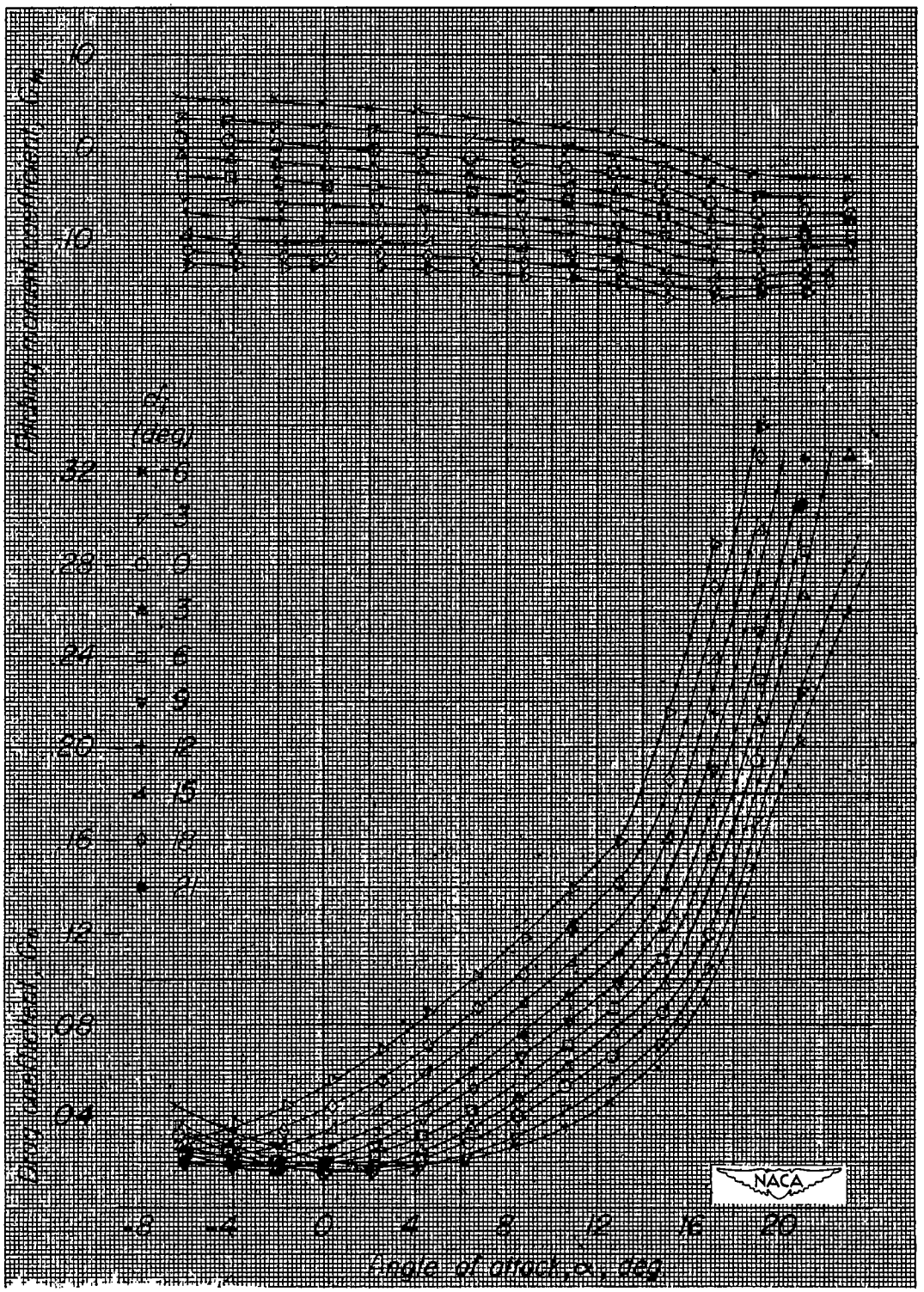

(b) Without transition wire; C_m and C_D against α.

Figure 36.- Continued.

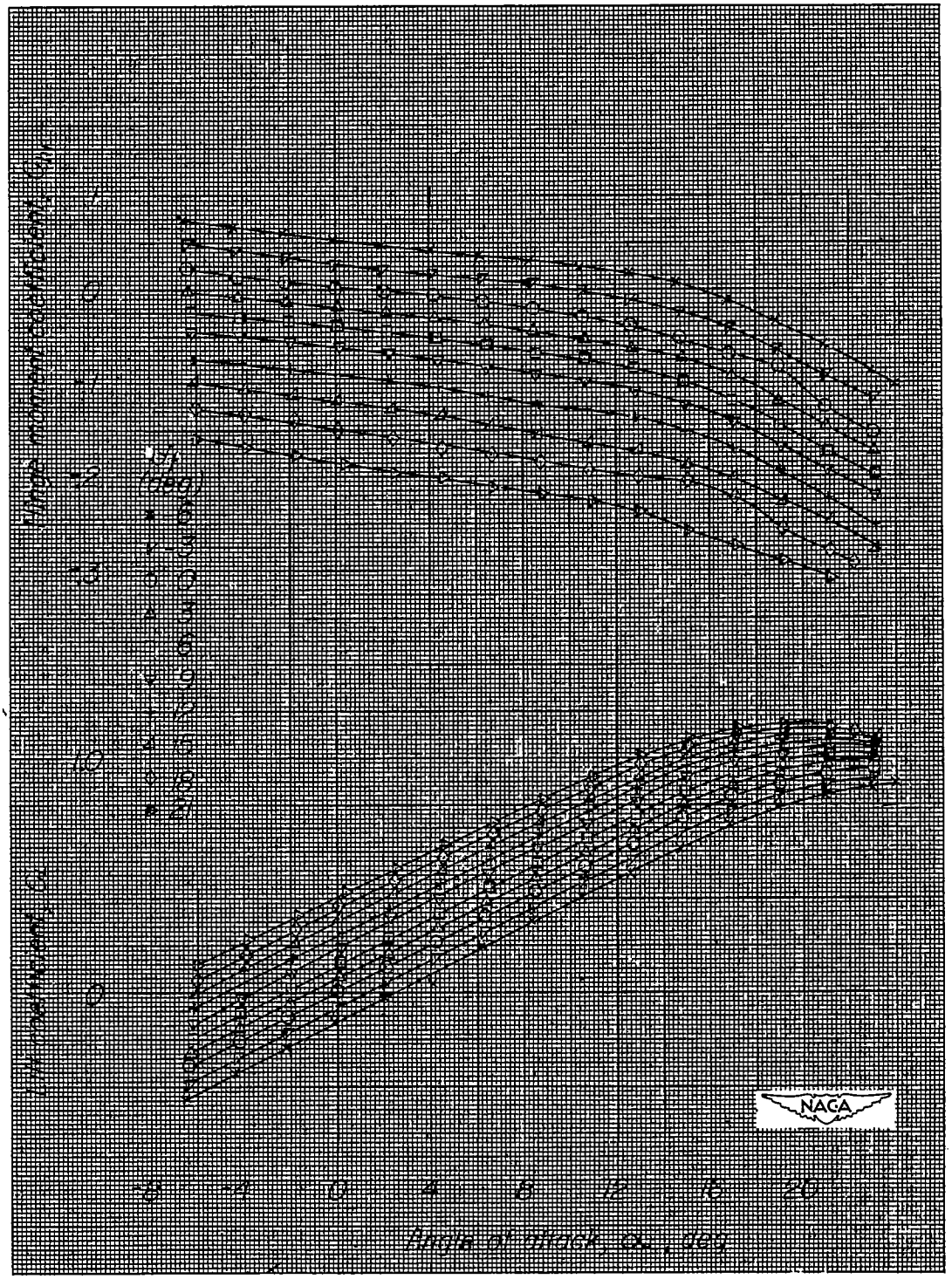

(c) 0.050-inch-diameter transition wire at 3 percent chord; C_{h_f} and C_L against α.

Figure 36.- Continued.

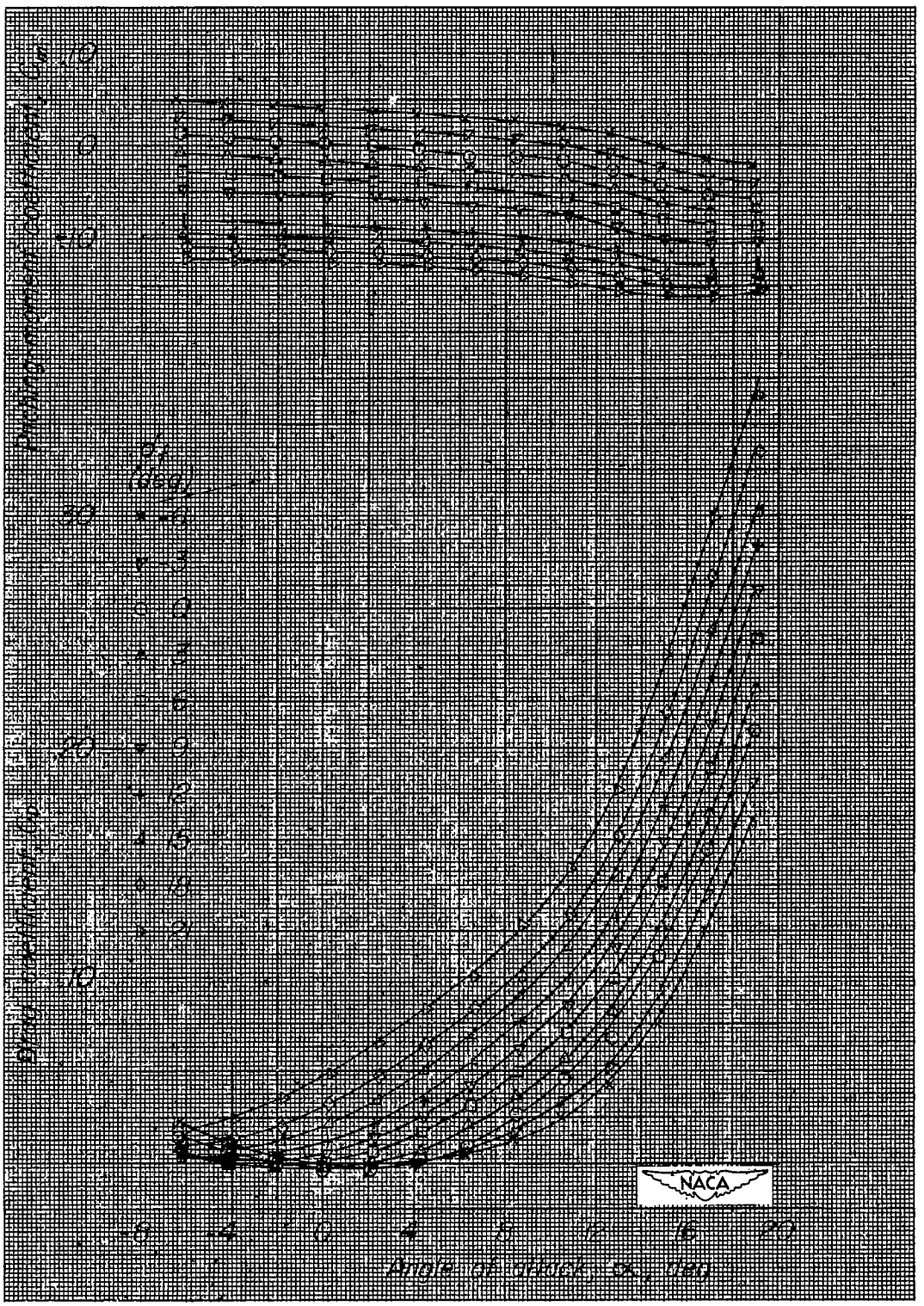

(d) 0.050-inch-diameter transition wire at 3 percent chord; C_m and C_D against α.

Figure 36.- Concluded.

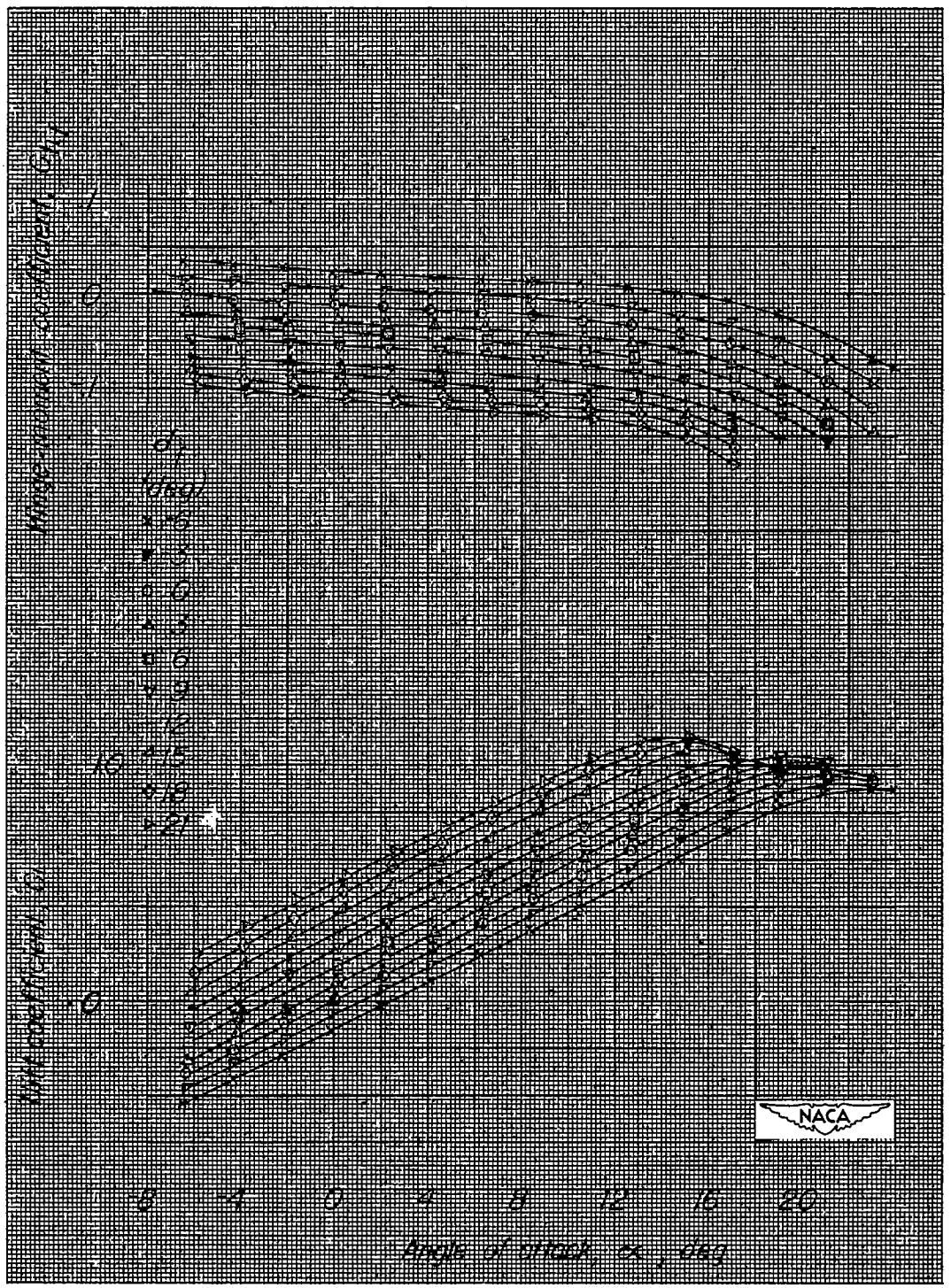

(a) C_{h_f} and C_L against α.

Figure 37.- NACA 0009 semispan tail surface. Sweepback angle Λ, 40°; taper ratio λ, 0.4; aspect ratio A, 3.30; 0.35c' flap with 0.319c_f' elliptic overhang; 0.005c gap; δ_t/δ_f, 0.

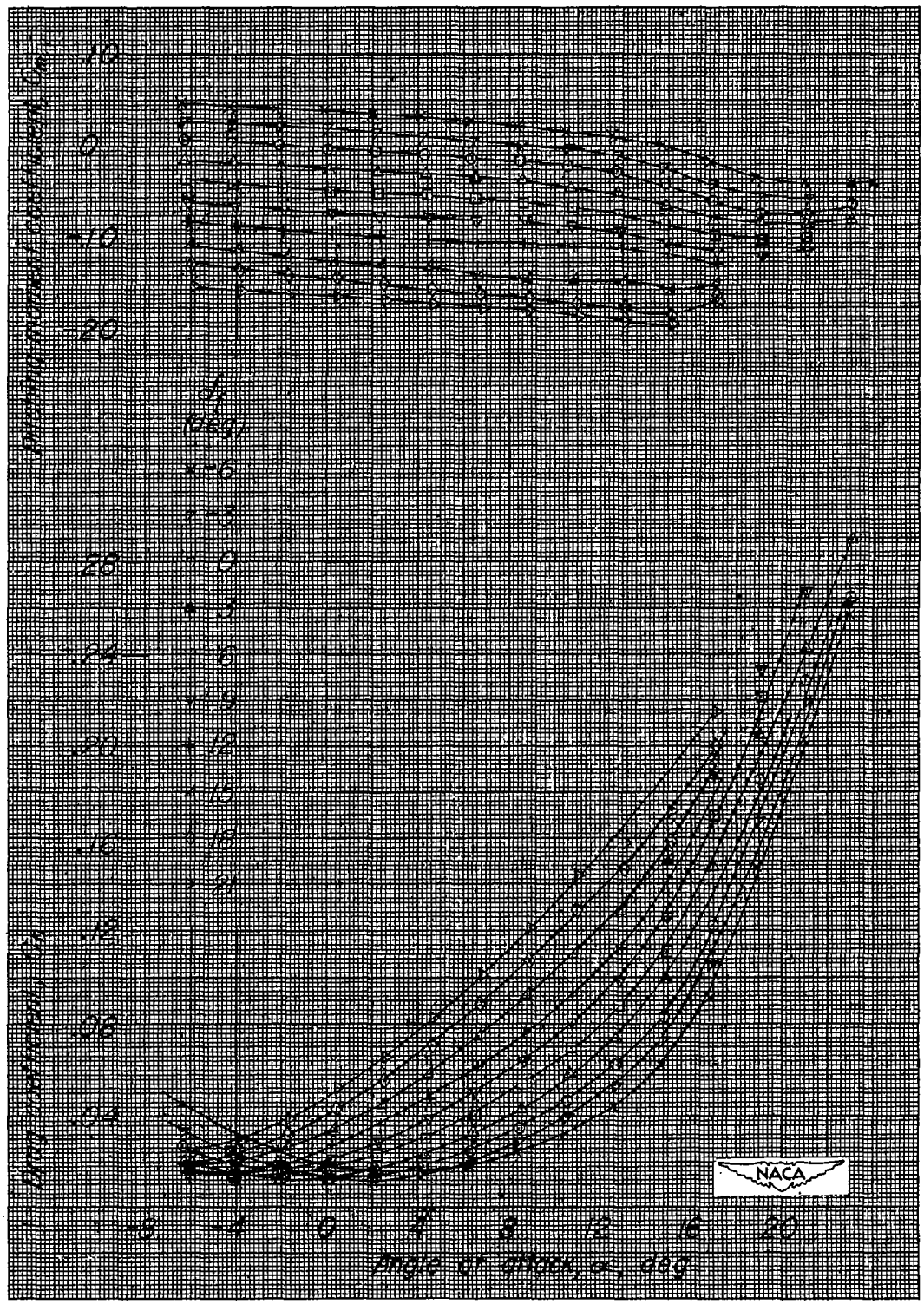

(b) C_m and C_D against α.

Figure 37.- Concluded.

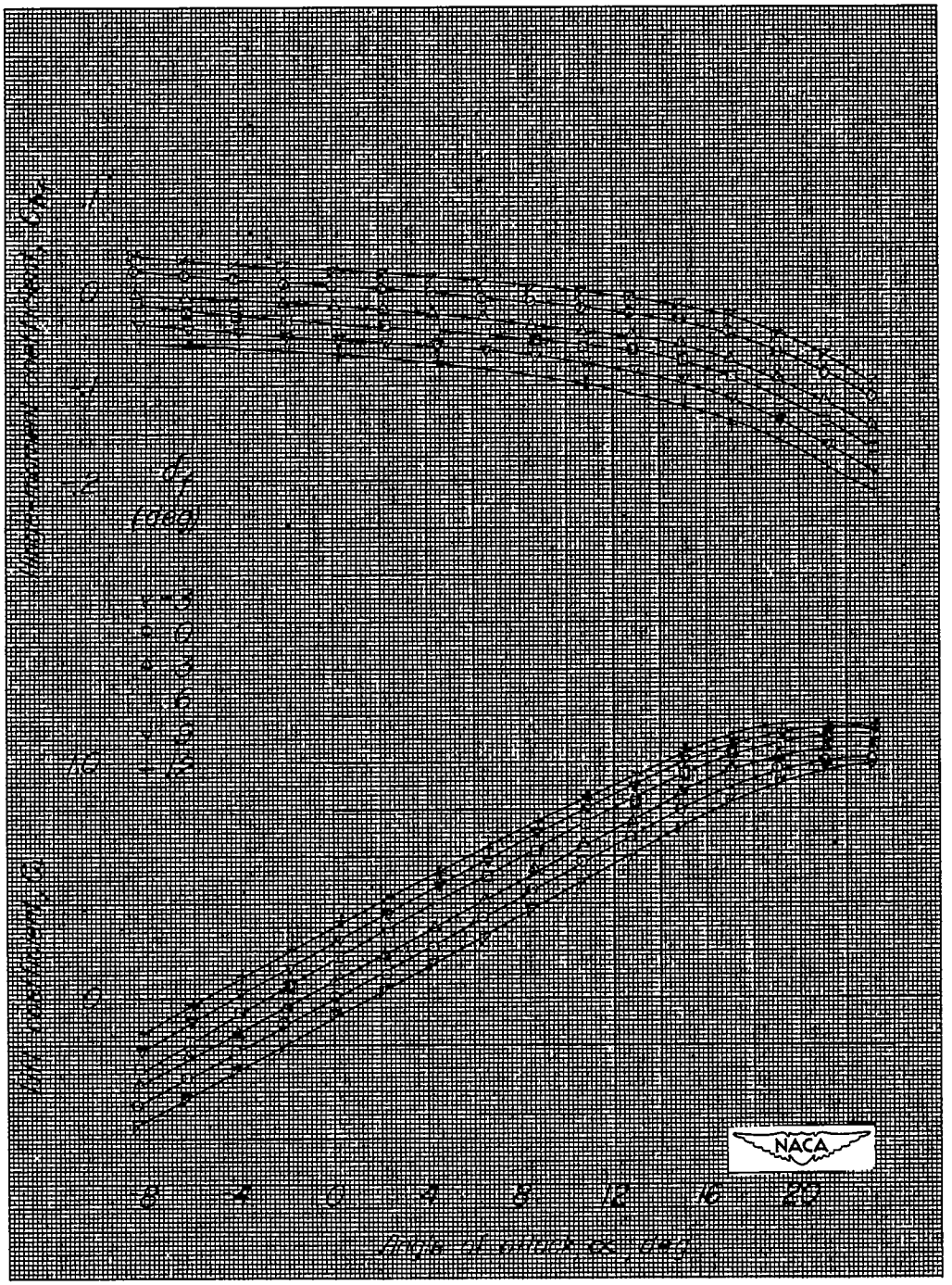

(a) $\delta_t/\delta_f = 0$; C_{h_f} and C_L against α.

Figure 38.- NACA 0009 semispan tail surface. Sweepback angle Λ, 40°; taper ratio λ, 0.4; aspect ratio A, 3.30; 0.35c' flap with 0.319c_f' sealed internal balance; 0.005c gap.

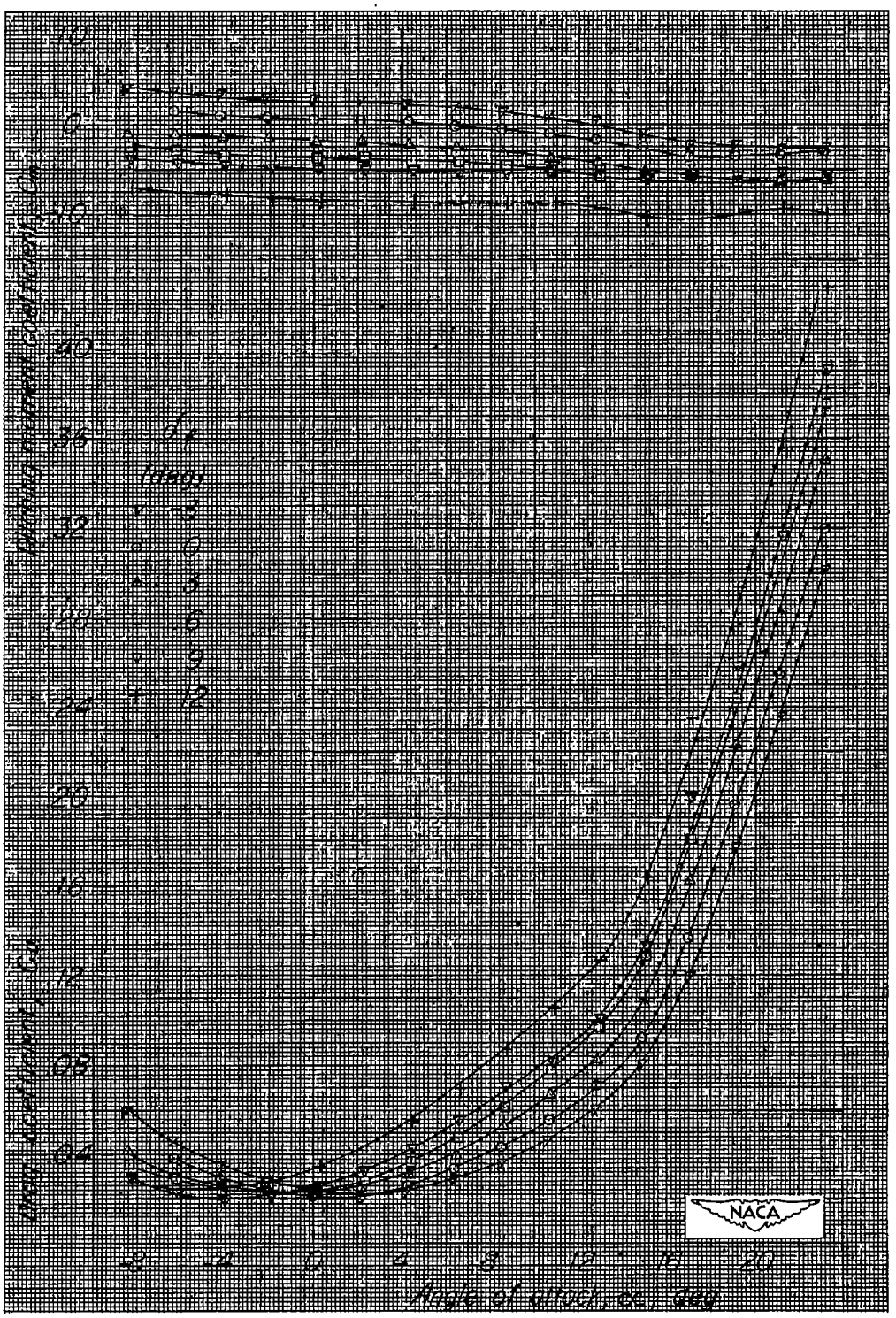

(b) $\delta_t/\delta_f = 0$; C_m and C_D against α.

Figure 38.- Continued.

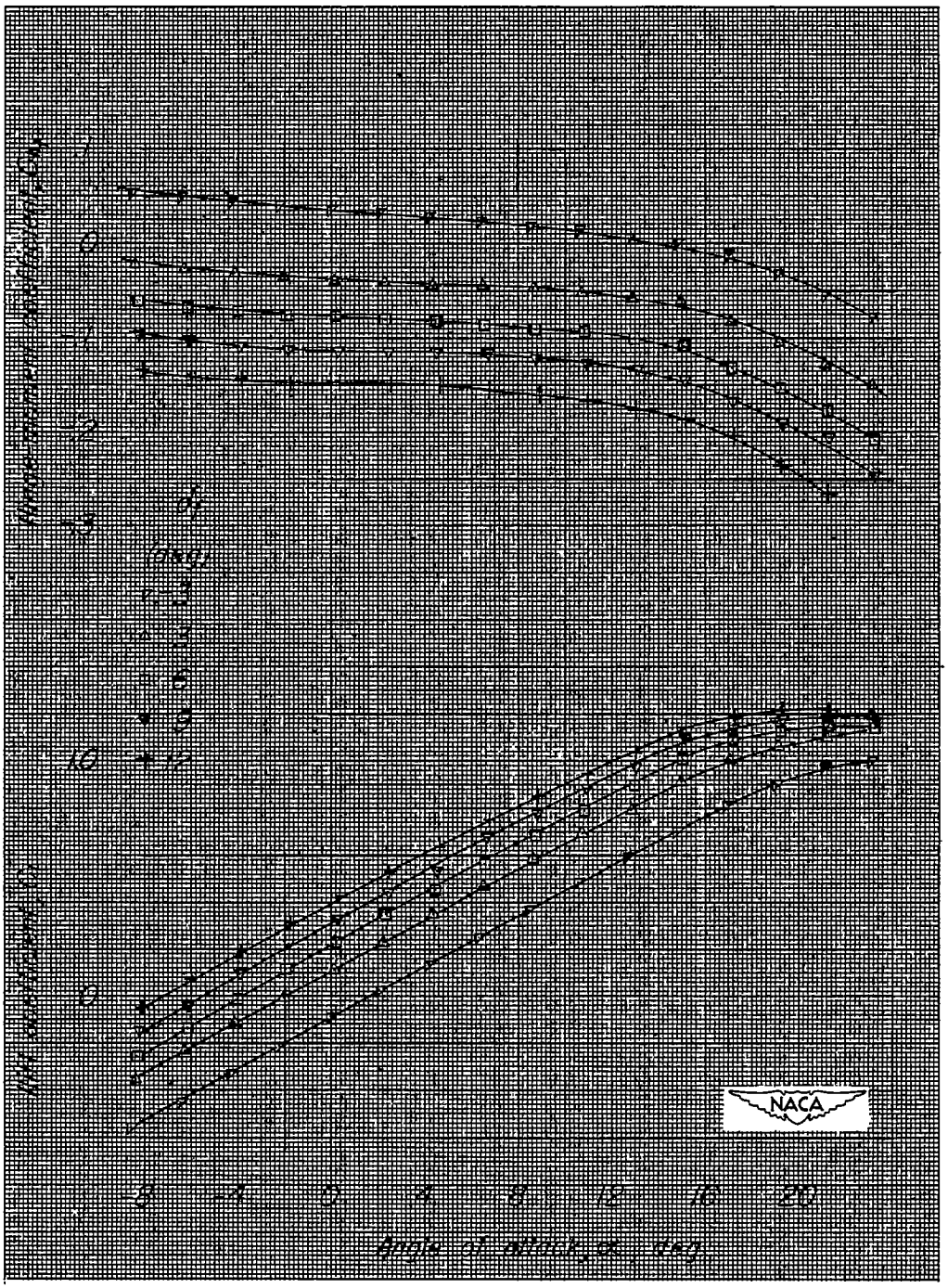

(c) $\delta_t/\delta_f = 1.0$; C_{h_f} and C_L against α.

Figure 38.- Continued.

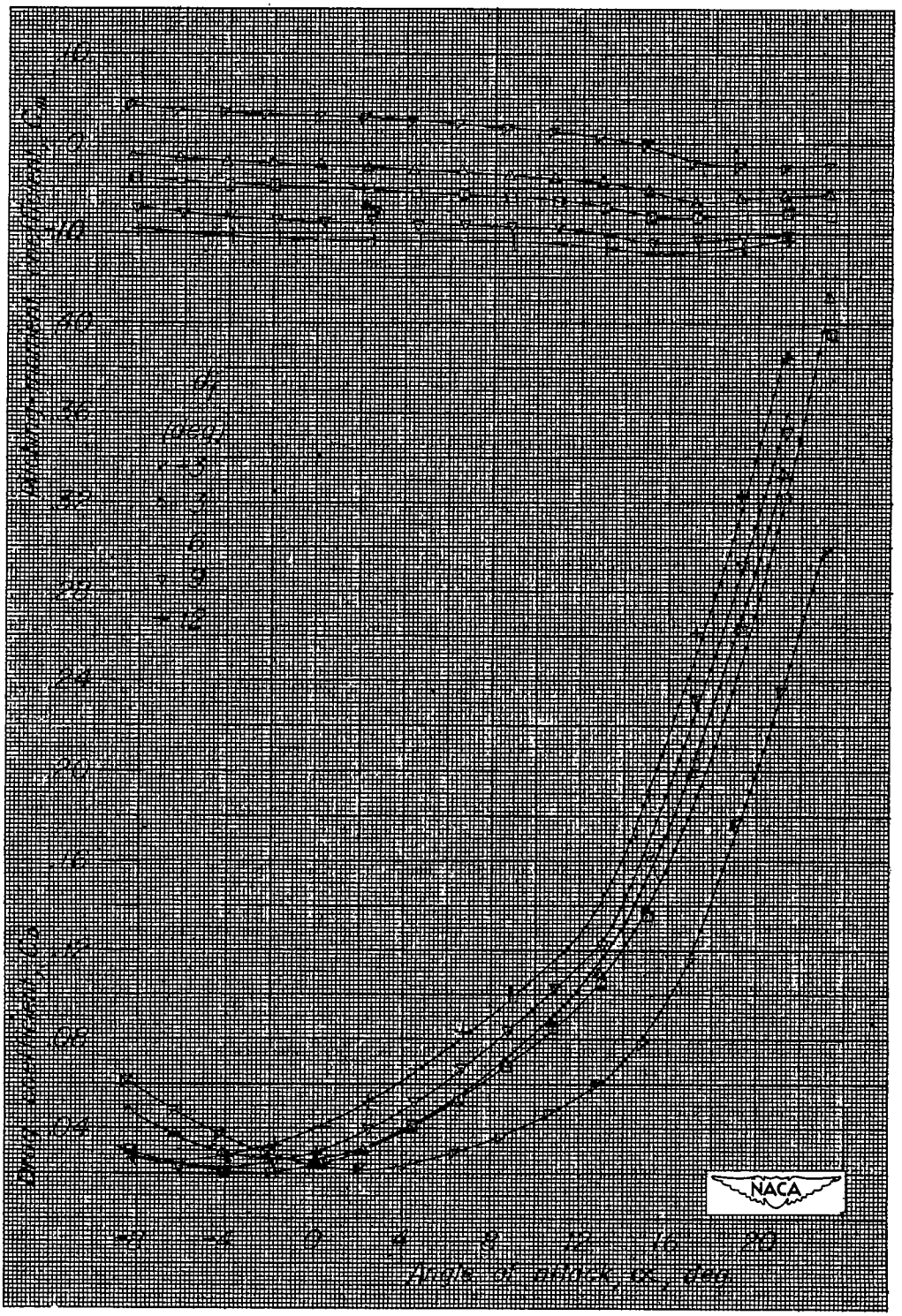

(d) $\delta_t/\delta_f = 1.0$; C_m and C_D against α.

Figure 38.- Continued.

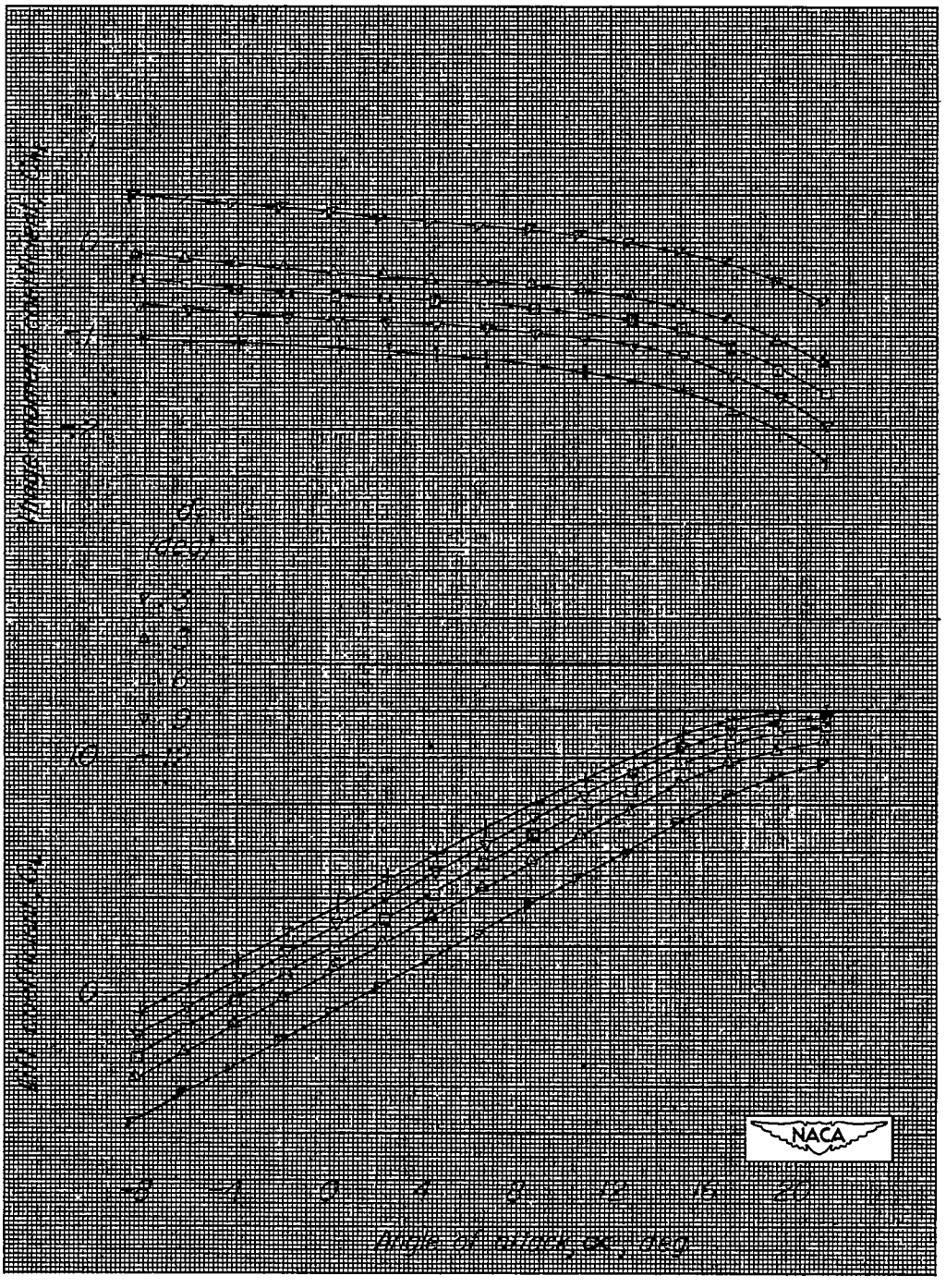

(e) $\delta_t/\delta_f = 0.5$; C_{h_f} and C_L against α.

Figure 38.- Continued.

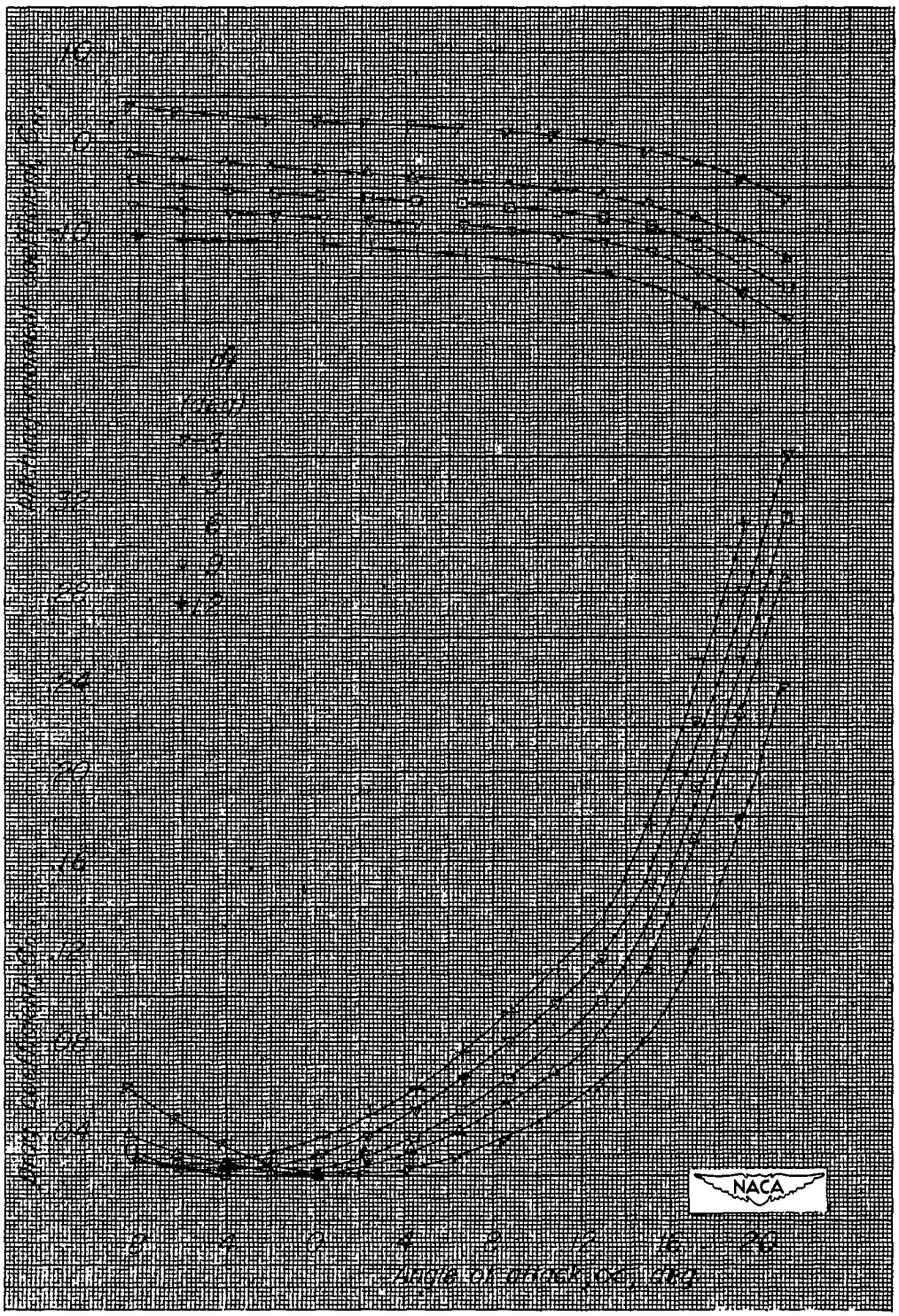

(f) $\delta_t/\delta_f = 0.5$; C_m and C_D against α.

Figure 38.- Continued.

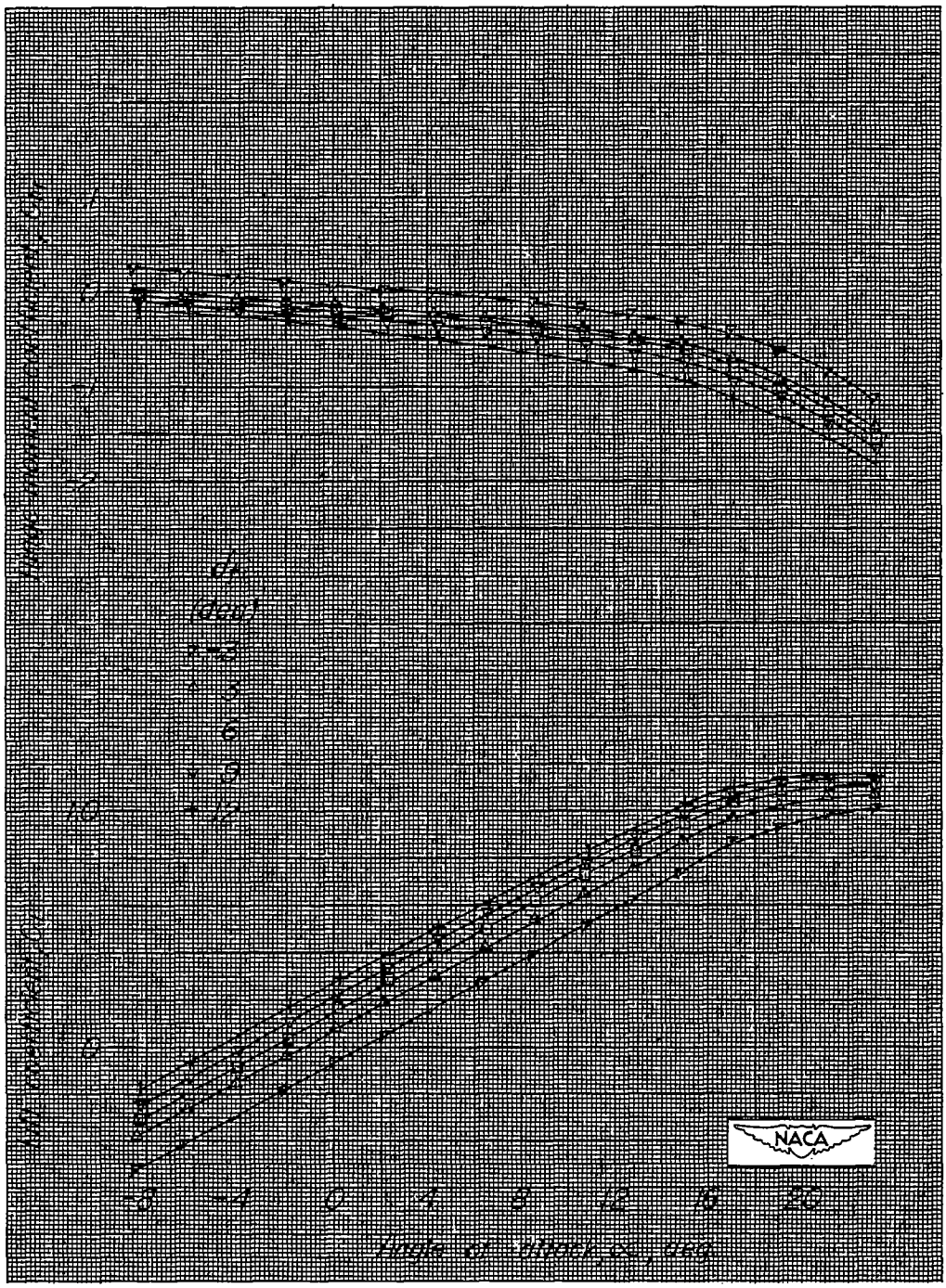

(g) $\delta_t/\delta_f = -0.5$; C_{h_f} and C_L against α.

Figure 38.- Continued.

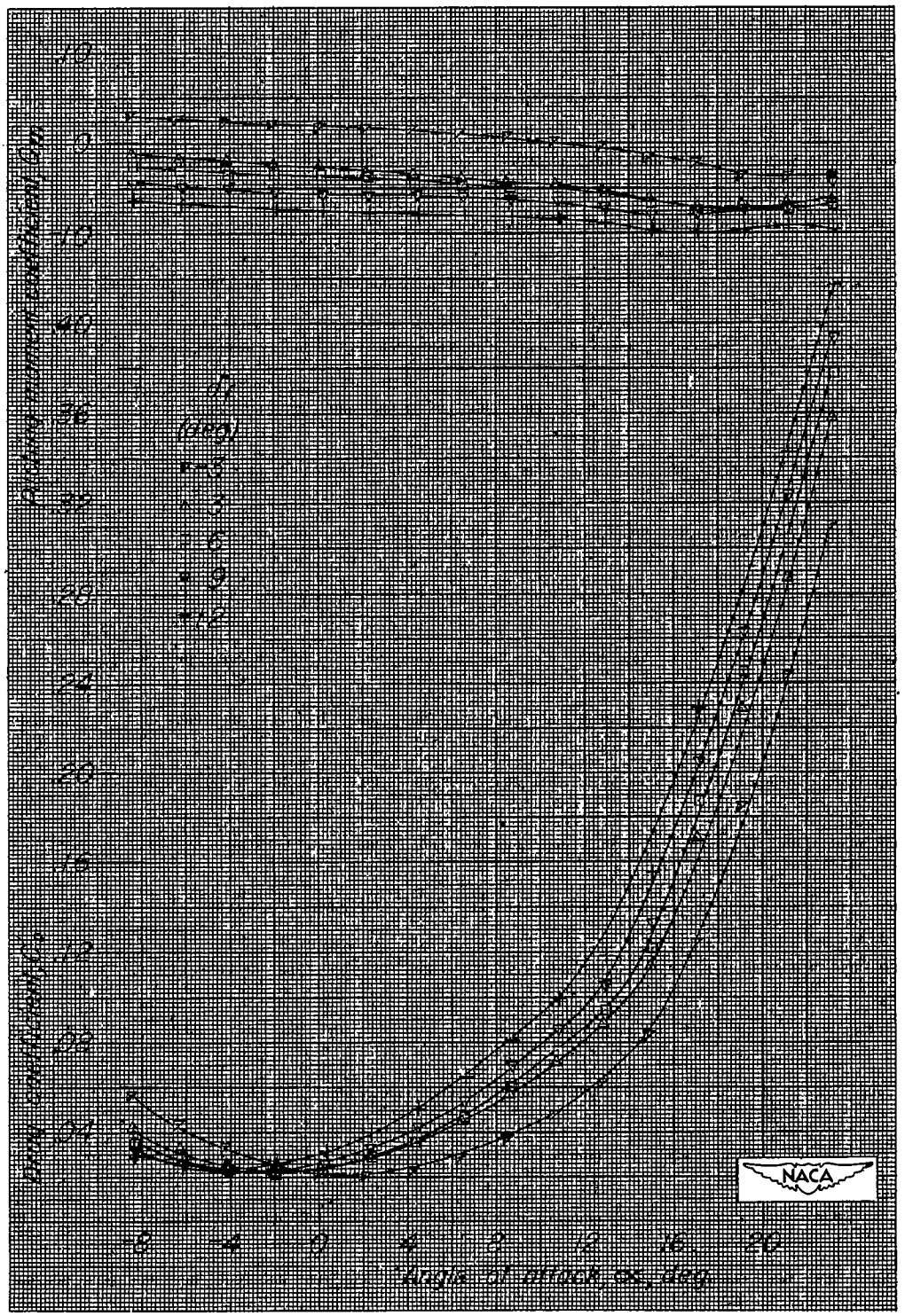

(h) $\delta_t/\delta_f = -0.5$; C_m and C_D against α.

Figure 38.- Continued.

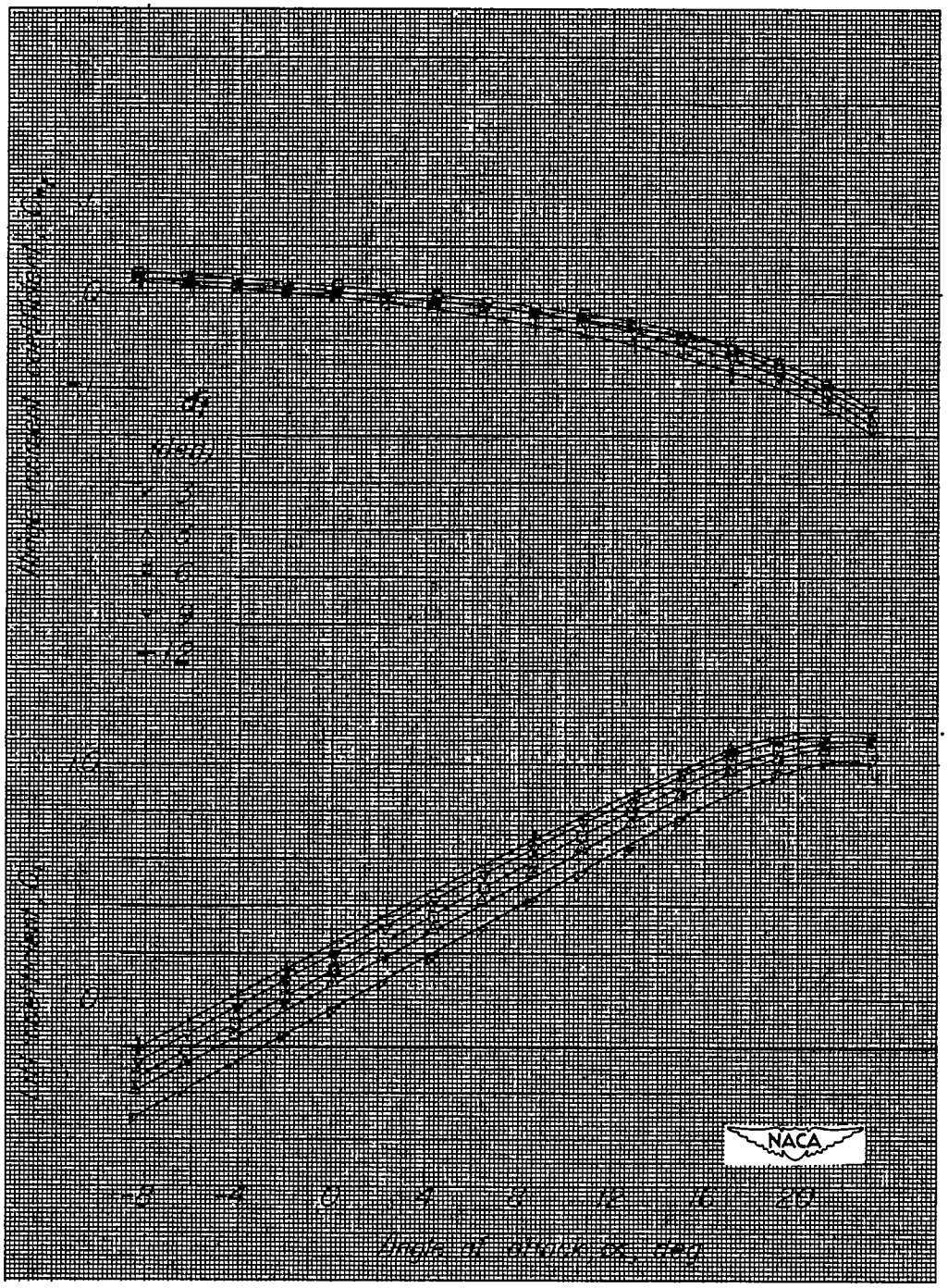

(i) $\delta_t/\delta_f = -1.0$; C_{h_f} and C_L against α.

Figure 38.- Continued.

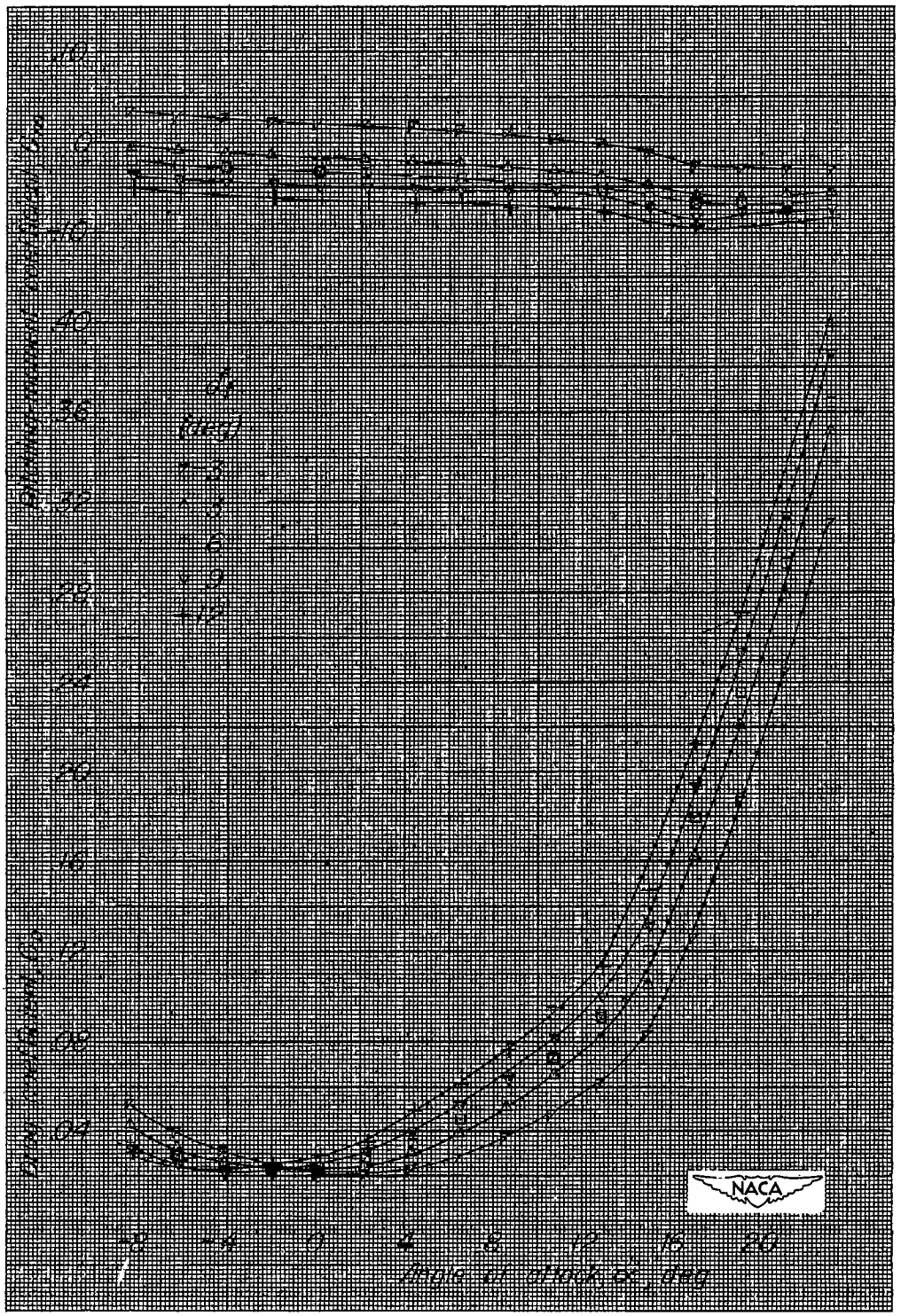

(j) $\delta_t/\delta_f = -1.0$; C_m and C_D against α.

Figure 38.- Concluded.

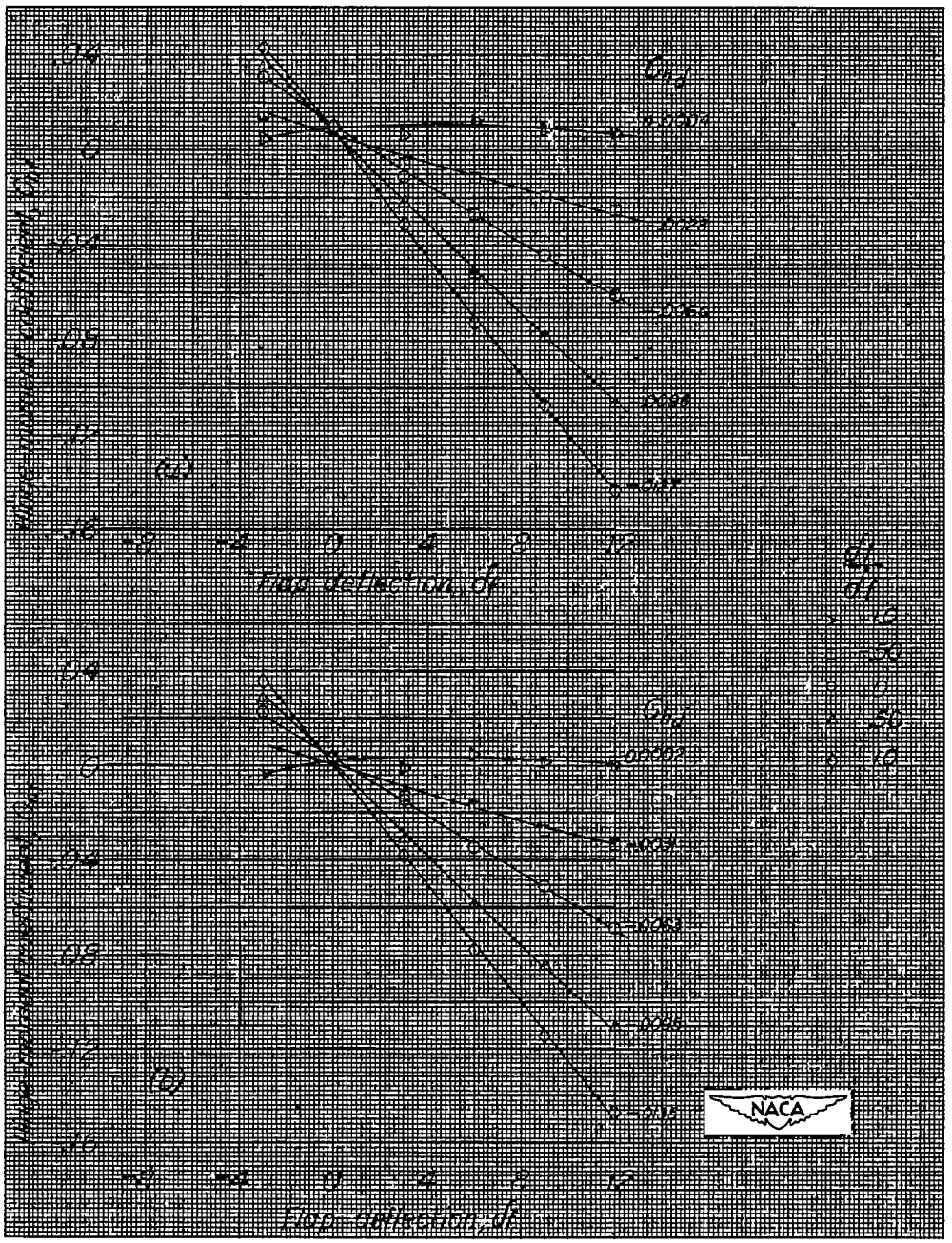

(a) $\alpha_u = -4^\circ$.

(b) $\alpha_u = 0^\circ$.

Figure 39.- Effect of tab deflection on control-surface hinge moment. NACA 0009 semispan tail surface; sweepback angle Λ, 40°; taper ratio λ, 0.4; aspect ratio A, 3.30; 0.35c' flap with 0.319c_f' sealed internal balance.

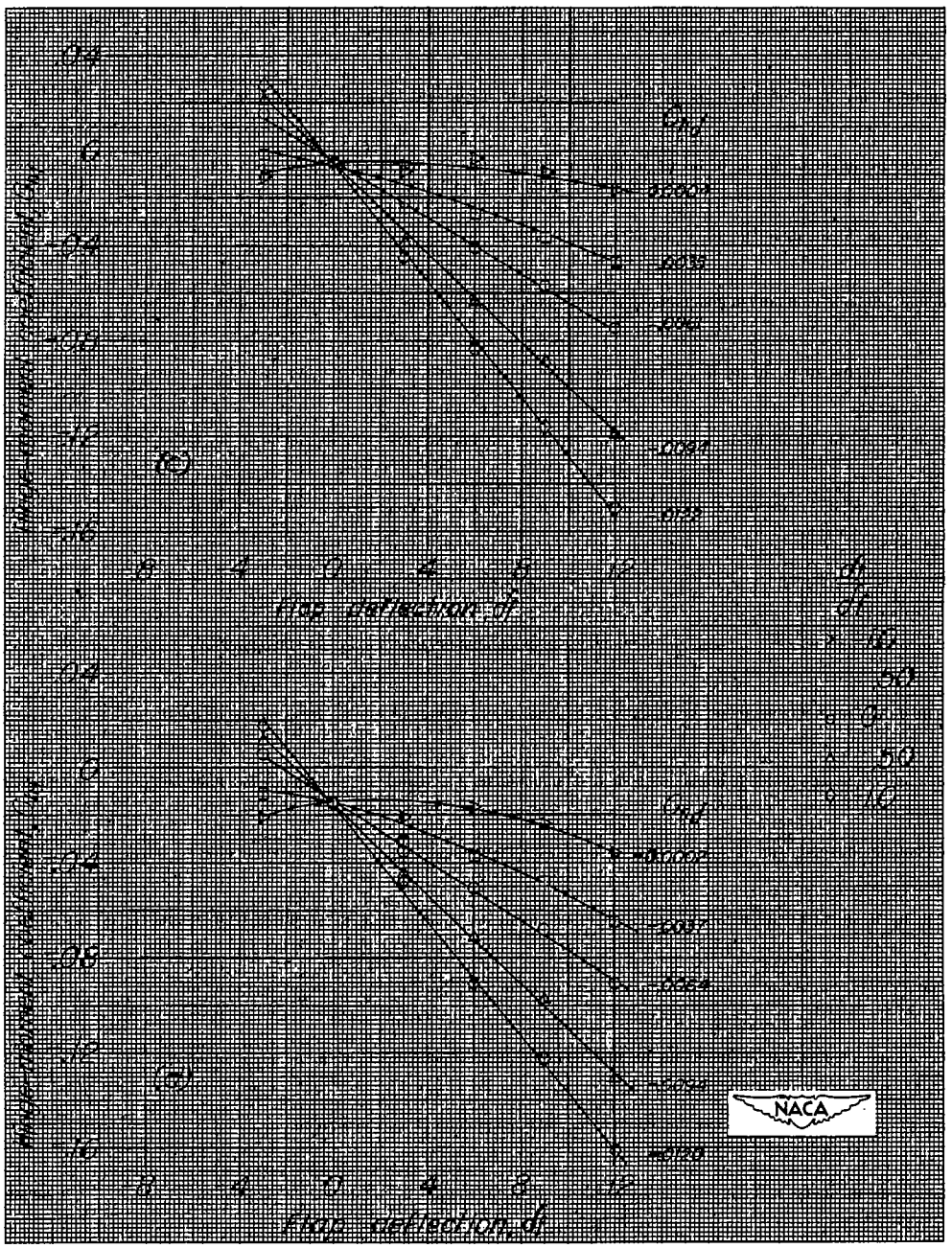

(c) $\alpha_u = 4°$.

(d) $\alpha_u = 8°$.

Figure 39.- Concluded.

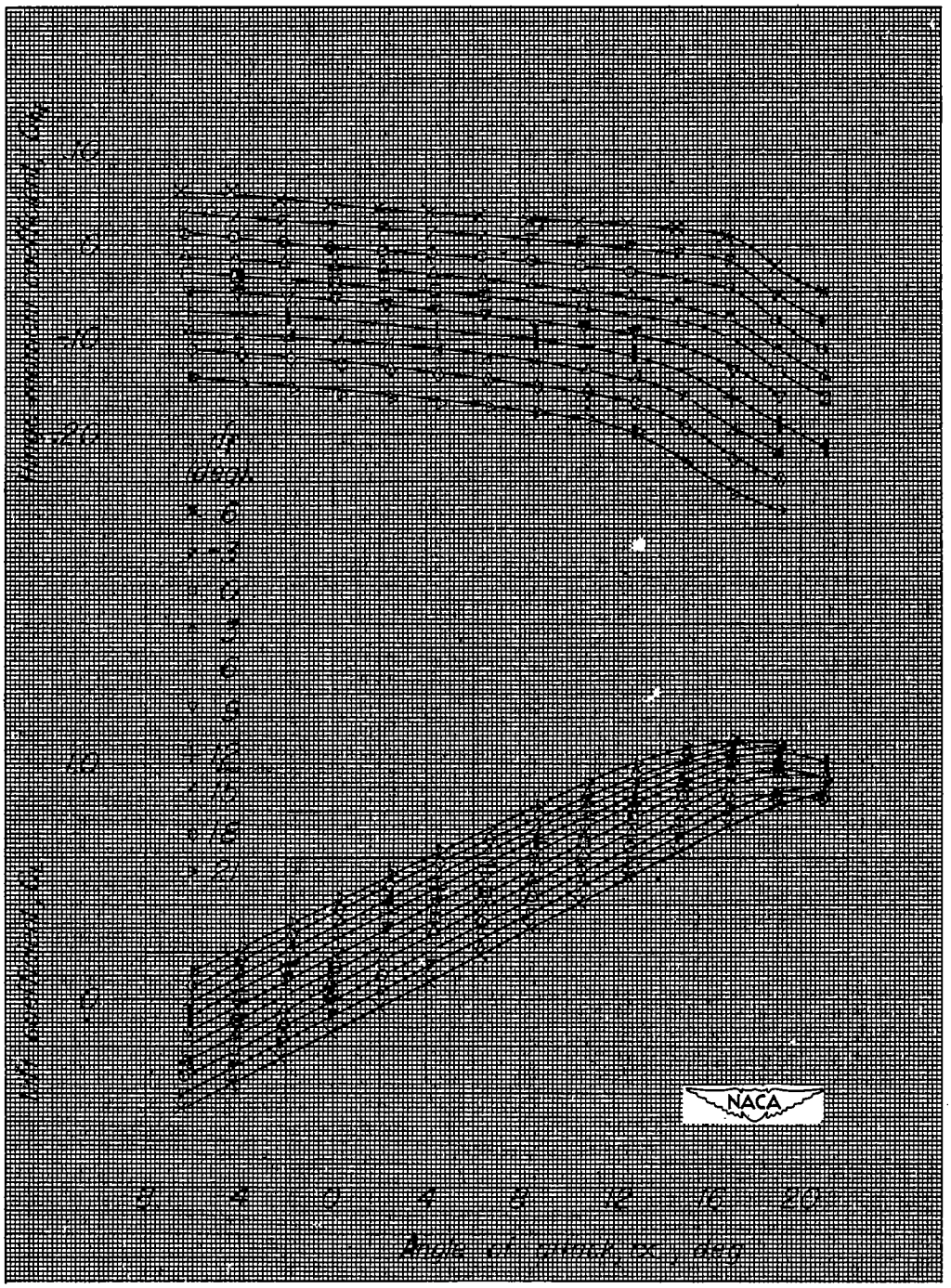

(a) C_{h_f} and C_L against α.

Figure 40.- NACA 0009 semispan tail surface. Sweepback angle Λ, 40°; taper ratio λ, 0.4; aspect ratio A, 3.30; 0.35c' flap with radius nose and horn; 0.005c gap; δ_t/δ_f, 0.

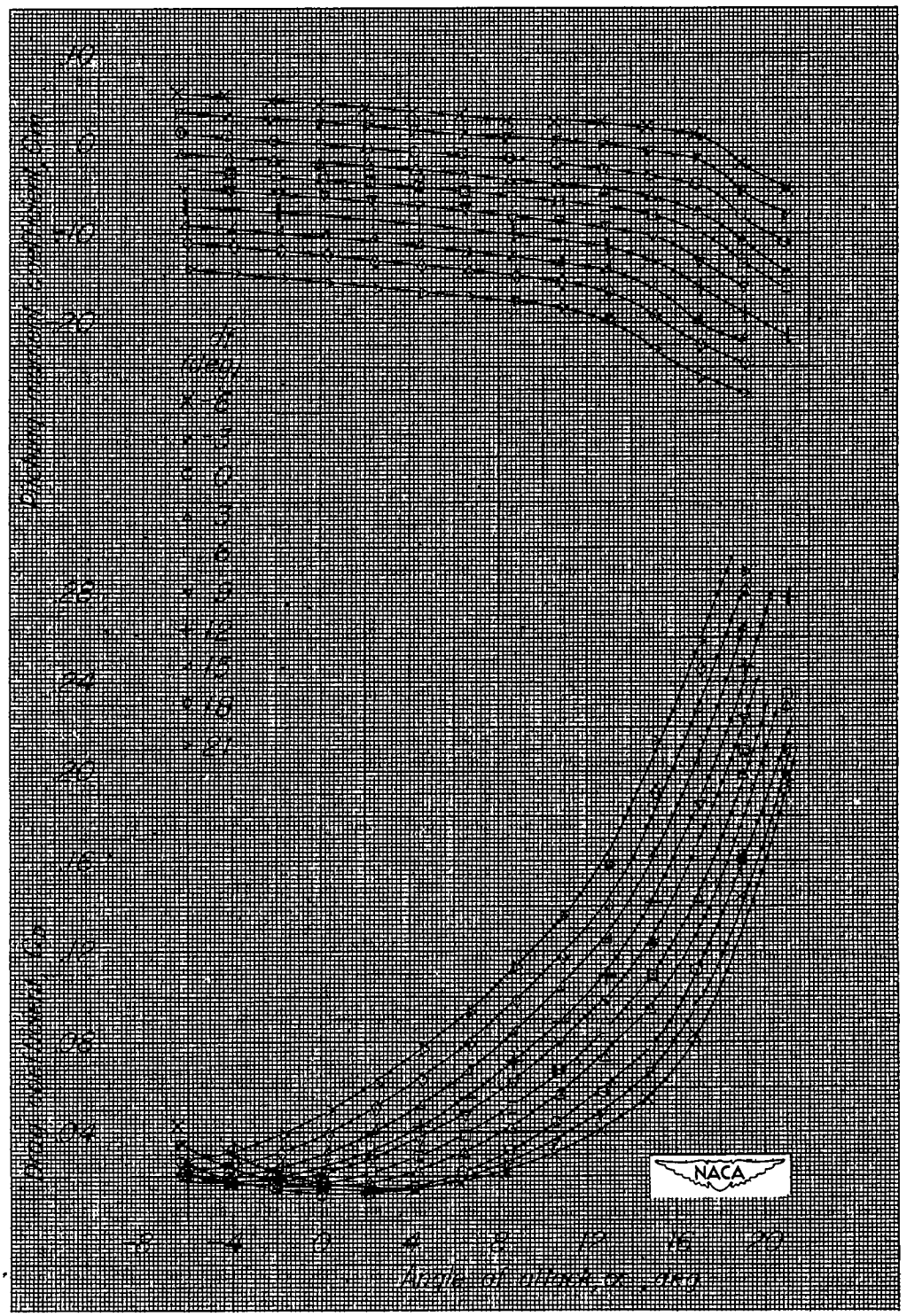

(b) C_m and C_D against α.

Figure 40.- Concluded.

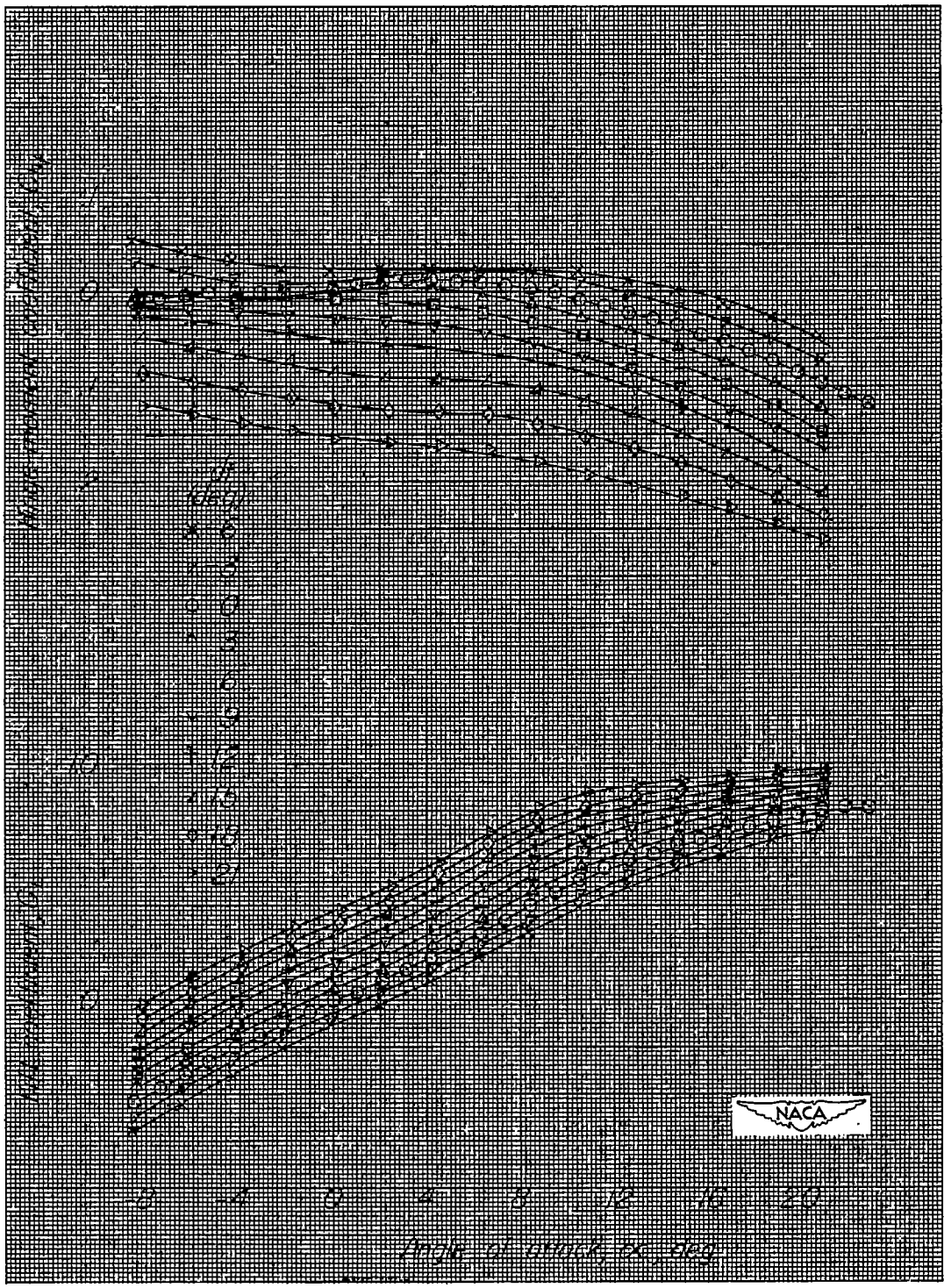

(a) C_{h_f} and C_L against α.

Figure 41.- Nine-percent-thick biconvex-arc semispan tail surface. Sweepback angle Λ, 40°; taper ratio λ, 0.4; aspect ratio A, 3.30; 0.35c' flap with radius nose; 0.005c gap; δ_t/δ_f, 0.

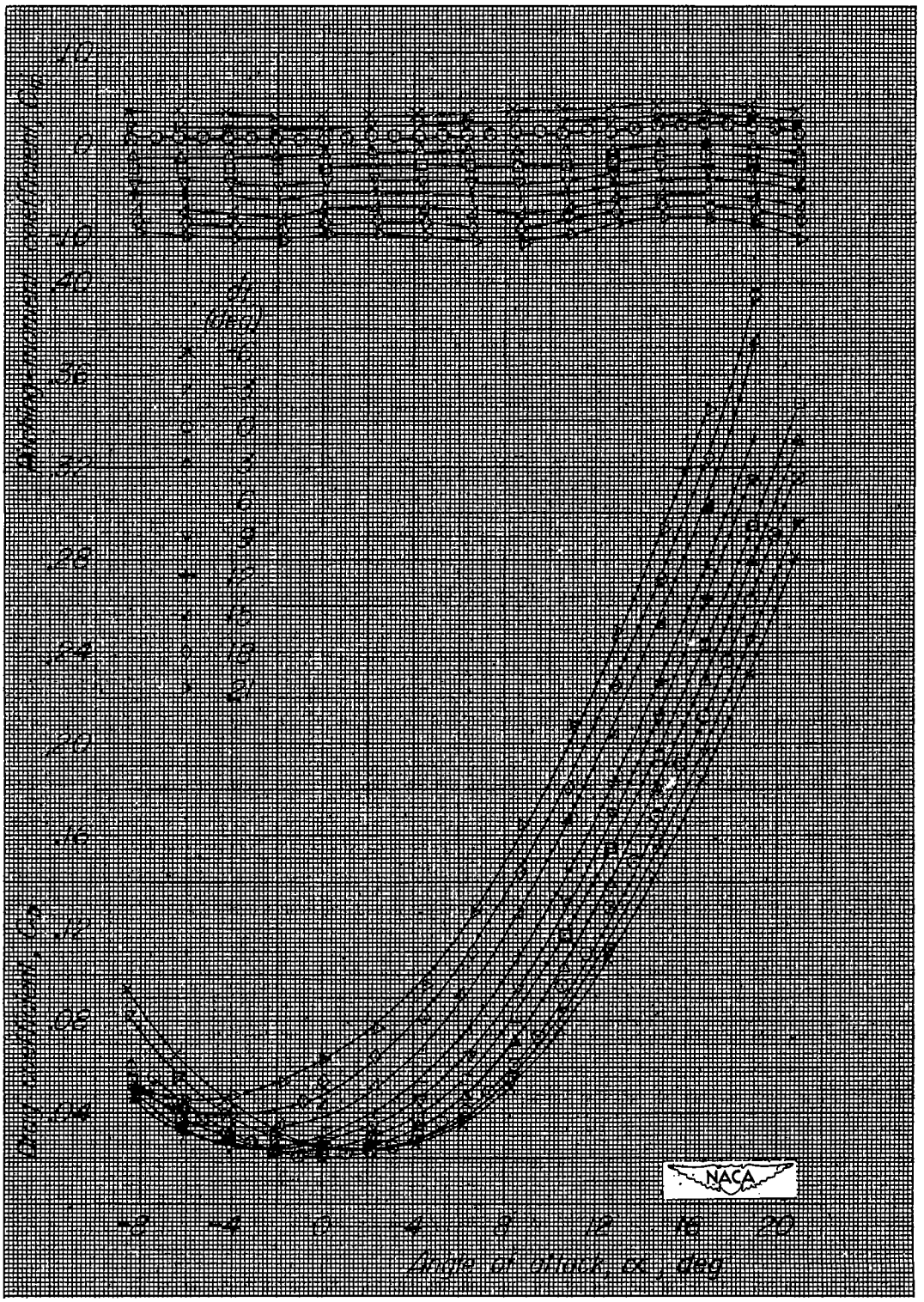

(b) C_m and C_D against α.

Figure 41.- Concluded.

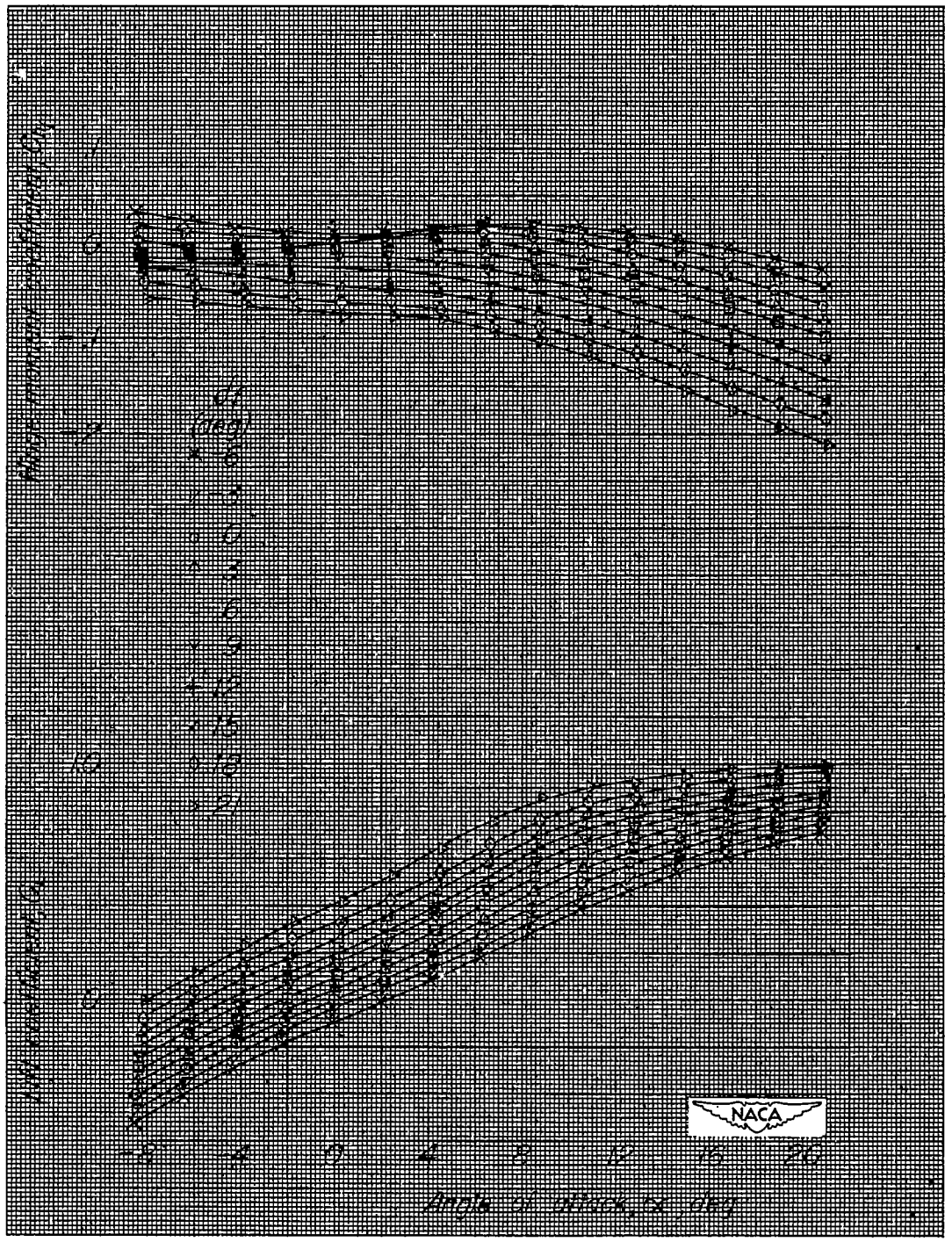

(a) C_{h_f} and C_L against α.

Figure 42.- Nine-percent-thick biconvex-arc semispan tail surface. Sweepback angle Λ, 40°; taper ratio λ, 0.4; aspect ratio A, 3.30; 0.35c' flap with 0.319c_f' elliptic overhang; 0.005c gap; δ_t/δ_f, 0.

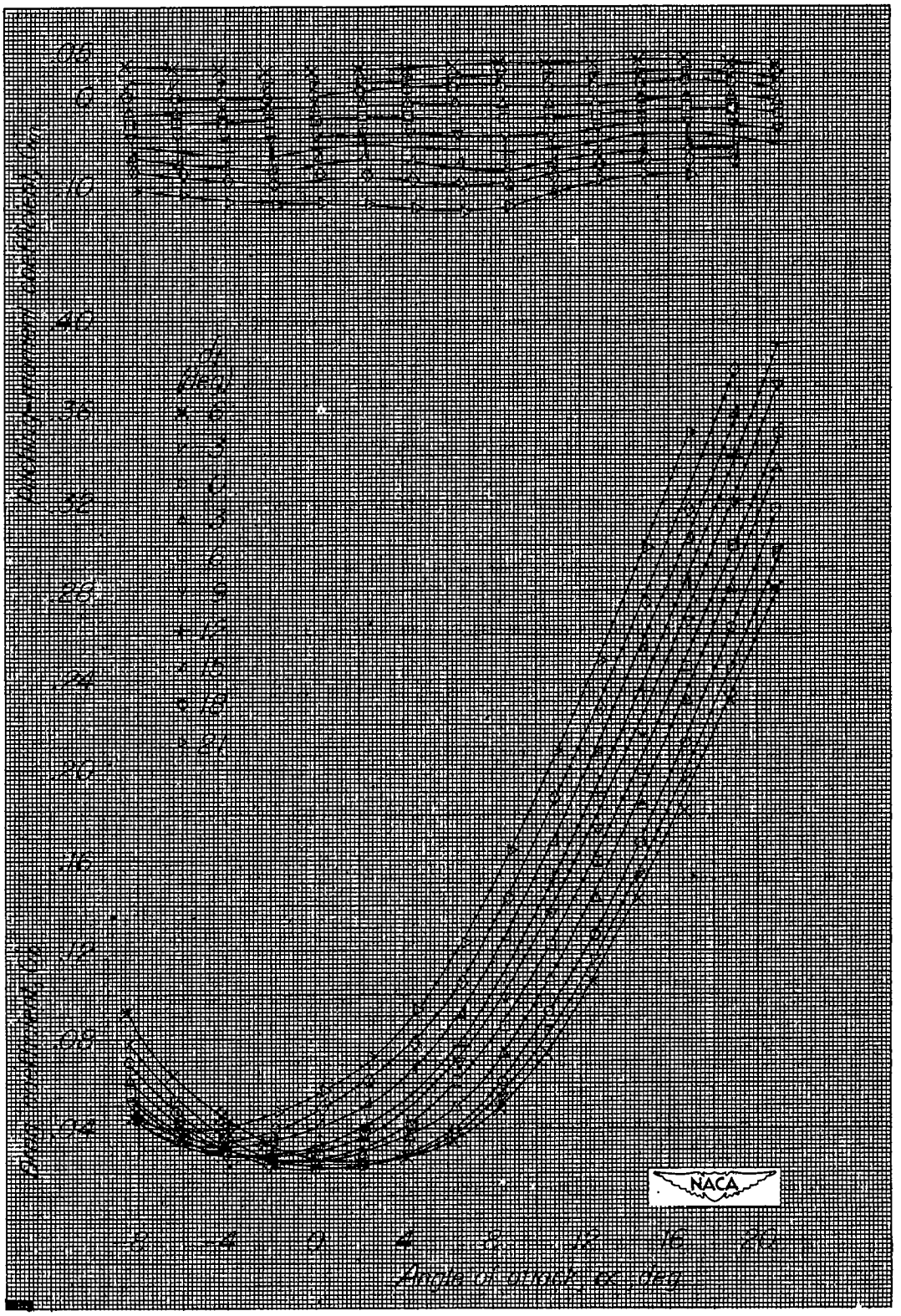

(b) C_m and C_D against α.

Figure 42.- Concluded.

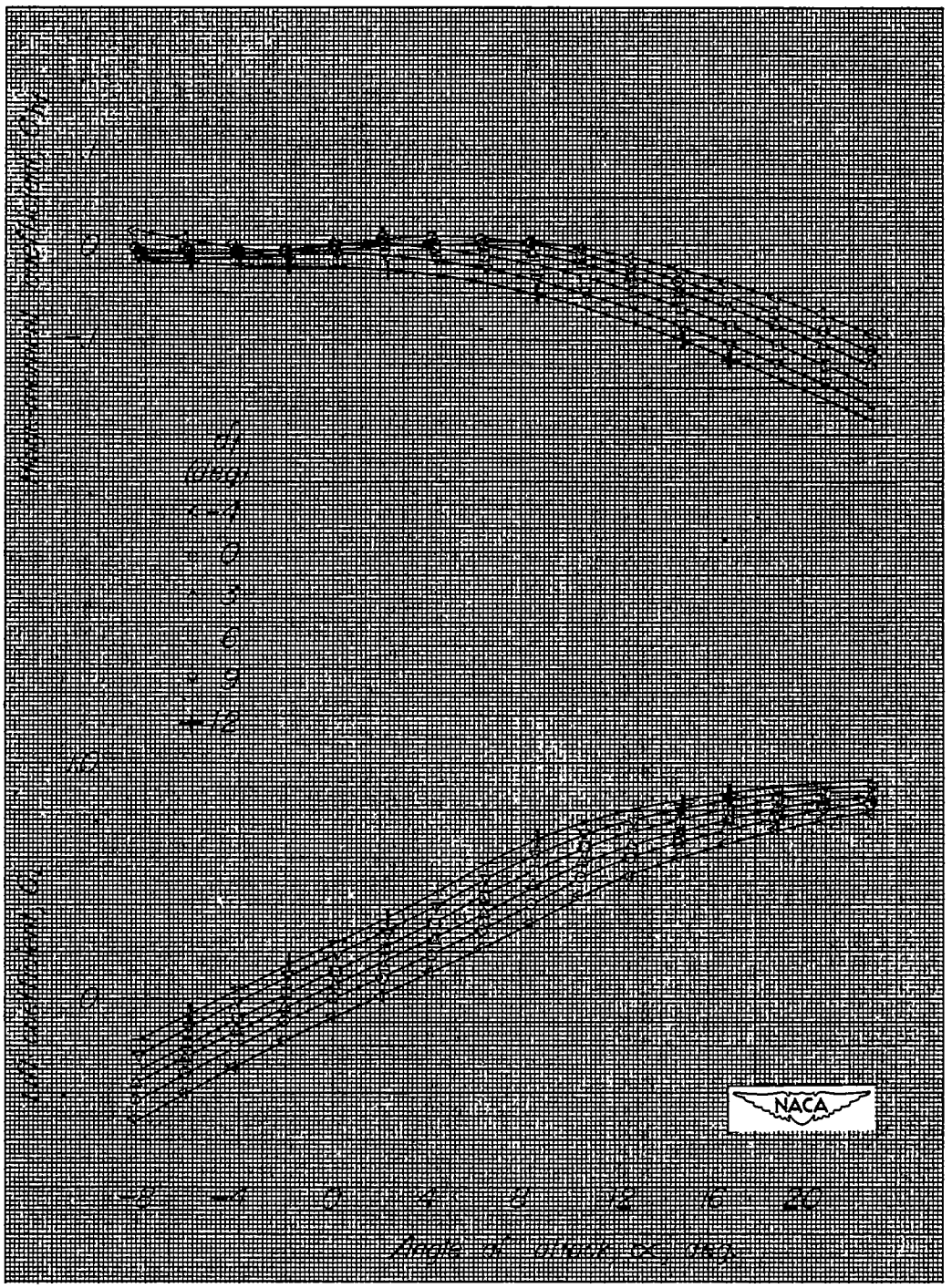

(a) $\delta_t/\delta_f = 0$; C_{h_f} and C_L against α.

Figure 43.- Nine-percent-thick biconvex-arc semispan tail surface. Sweepback angle Λ, 40°; taper ratio λ, 0.4; aspect ratio A, 3.30; 0.35c' flap with 0.319c_f' sealed internal balance; 0.005c gap.

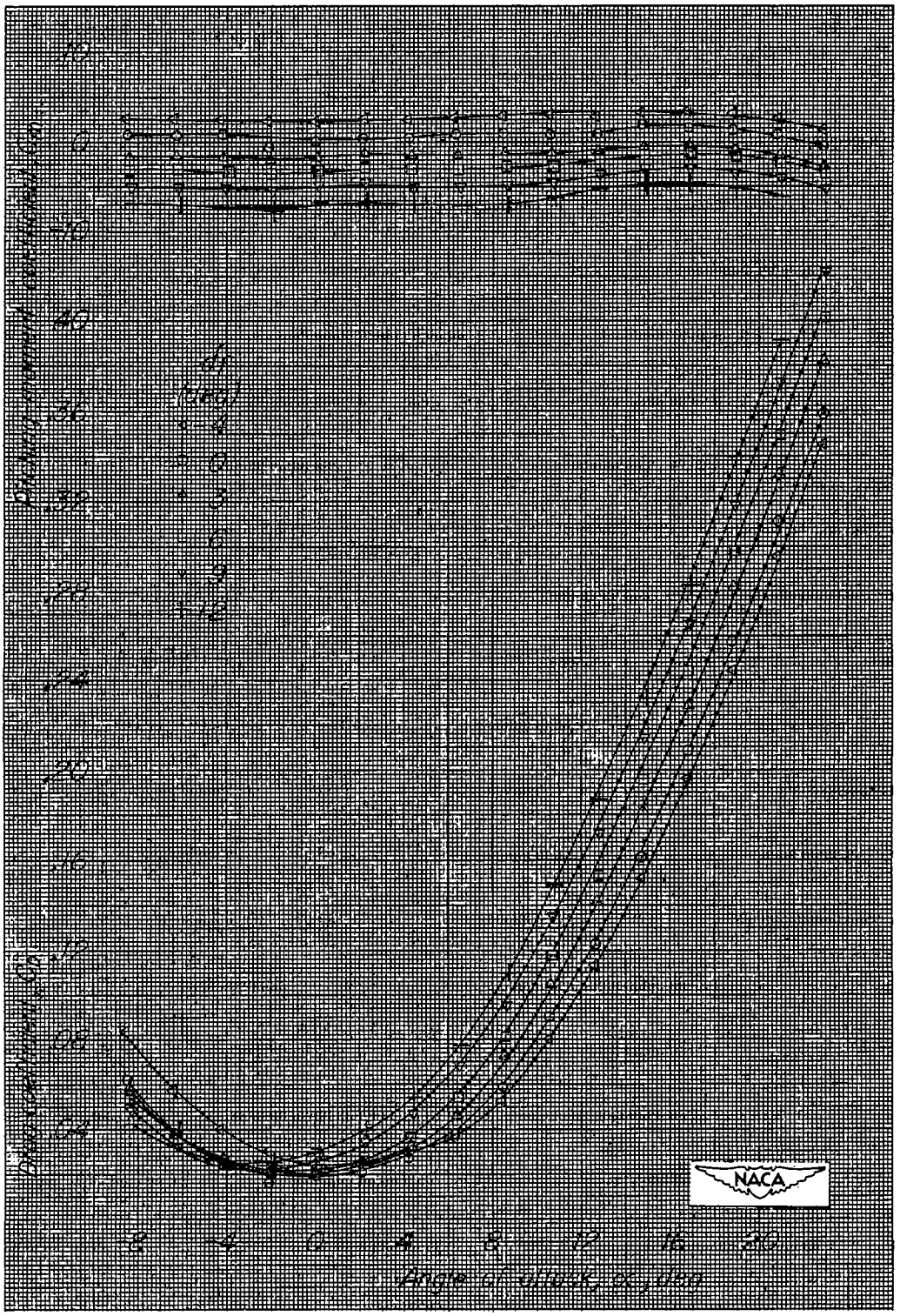

(b) $\delta_t/\delta_f = 0$; C_m and C_D against α.

Figure 43.- Continued.

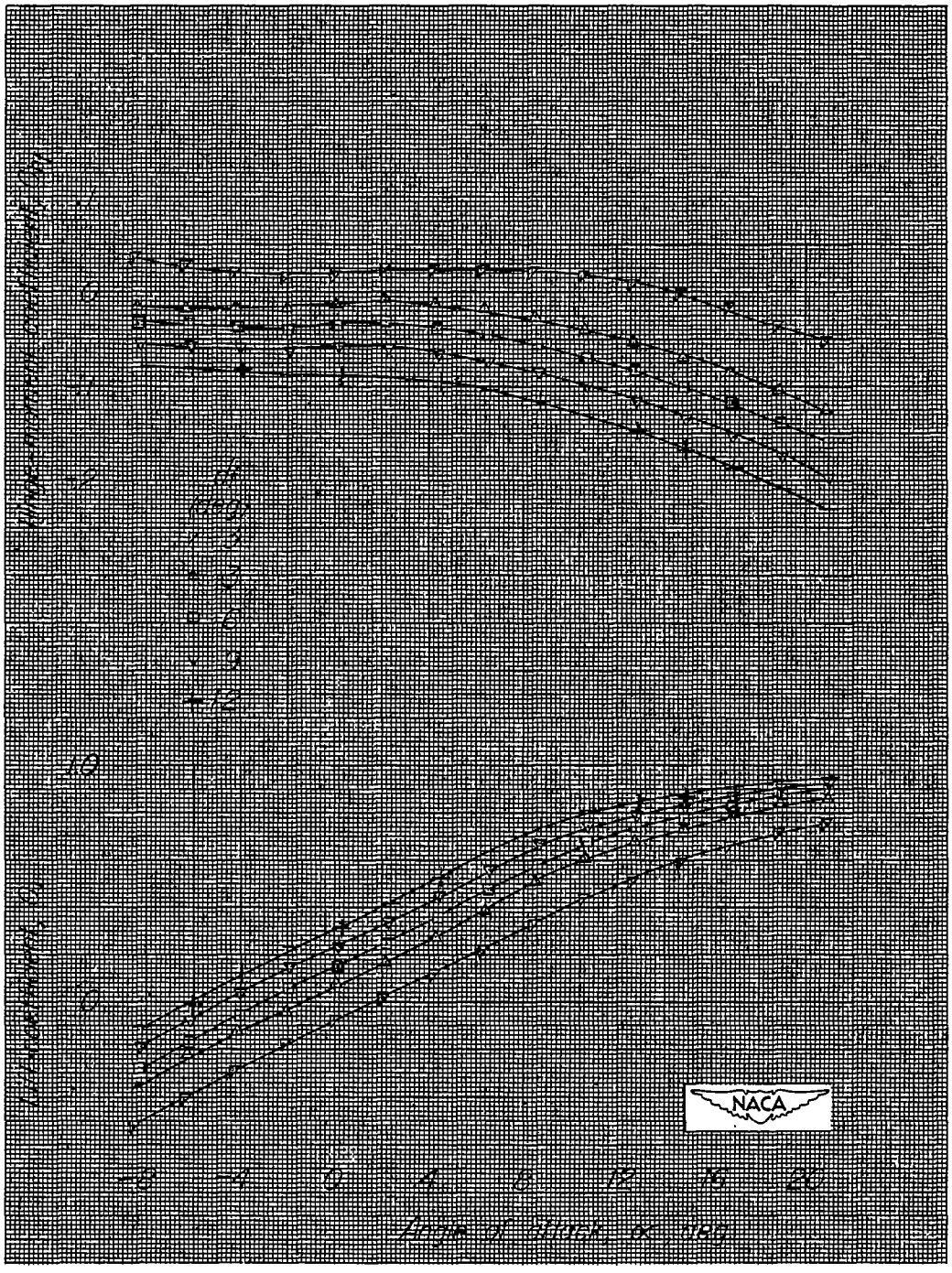

(c) $\delta_t/\delta_f = 1.0$; C_{h_f} and C_L against α.

Figure 43.- Continued.

(d) $\delta_t/\delta_f = 1.0$; C_m and C_D against α.

Figure 43.- Continued.

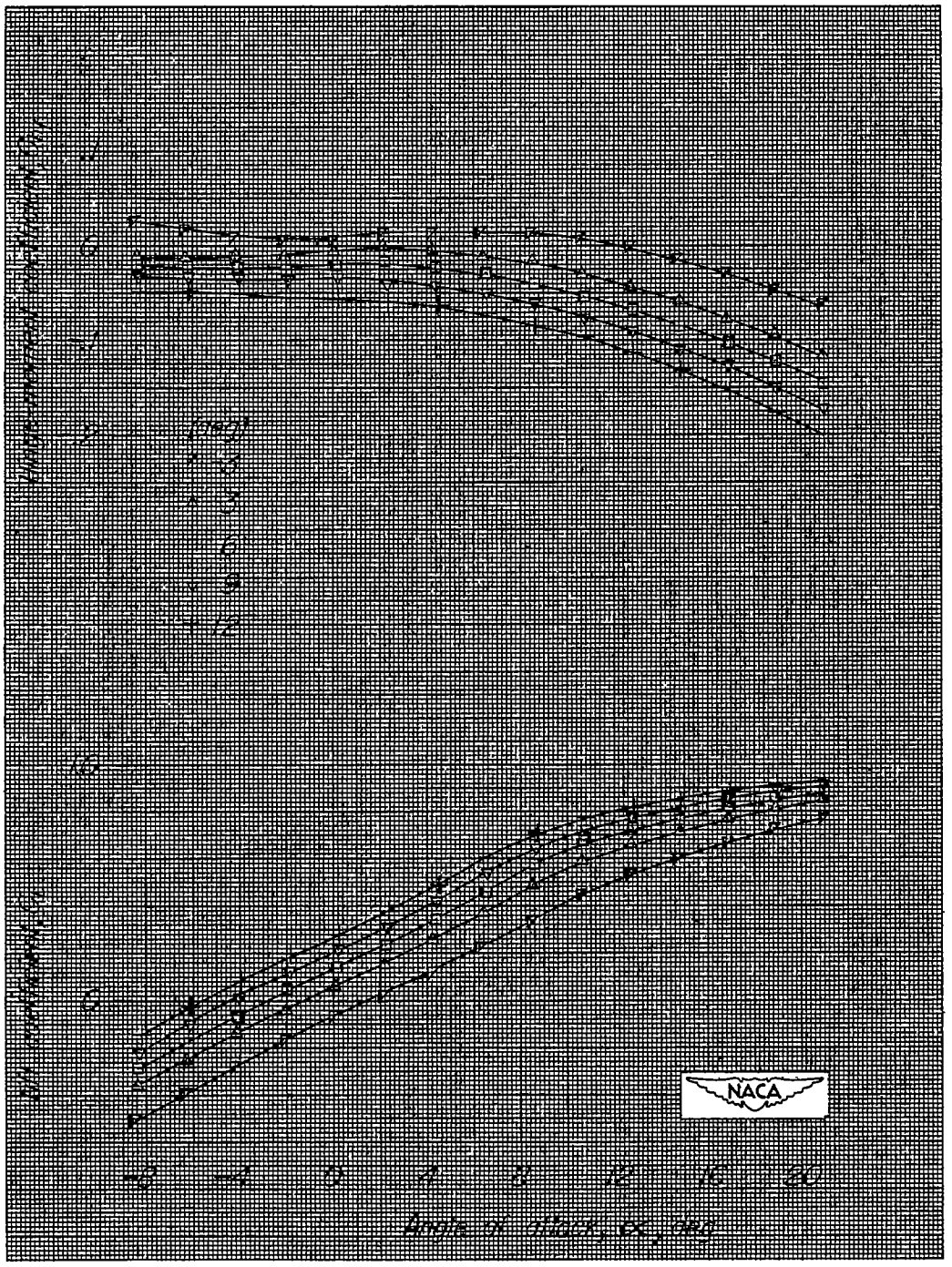

(e) $\delta_t/\delta_f = 0.5$; C_{h_f} and C_L against α.

Figure 43.- Continued.

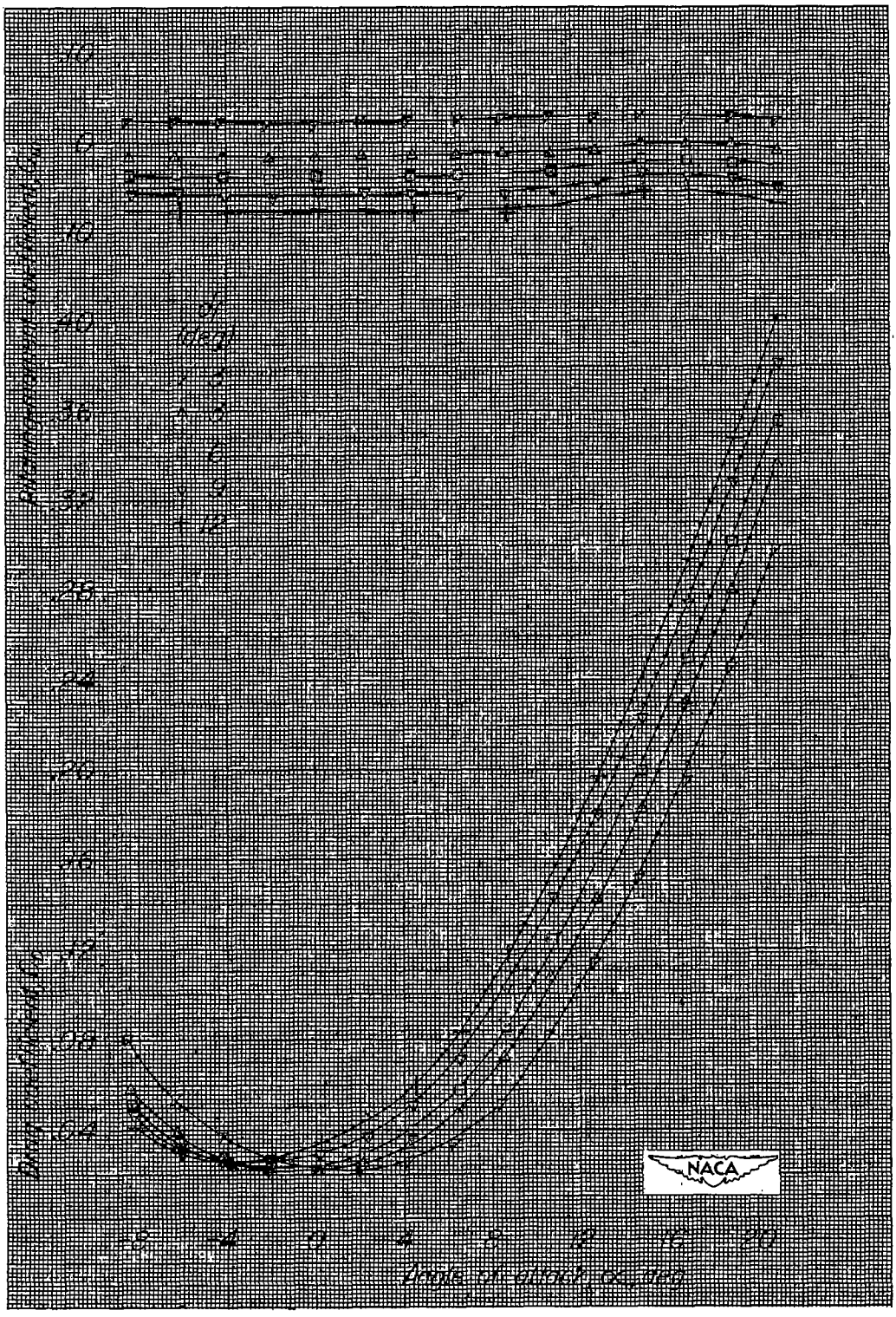

(f) $\delta_t/\delta_f = 0.5$; C_m and C_D against α.

Figure 43.- Continued.

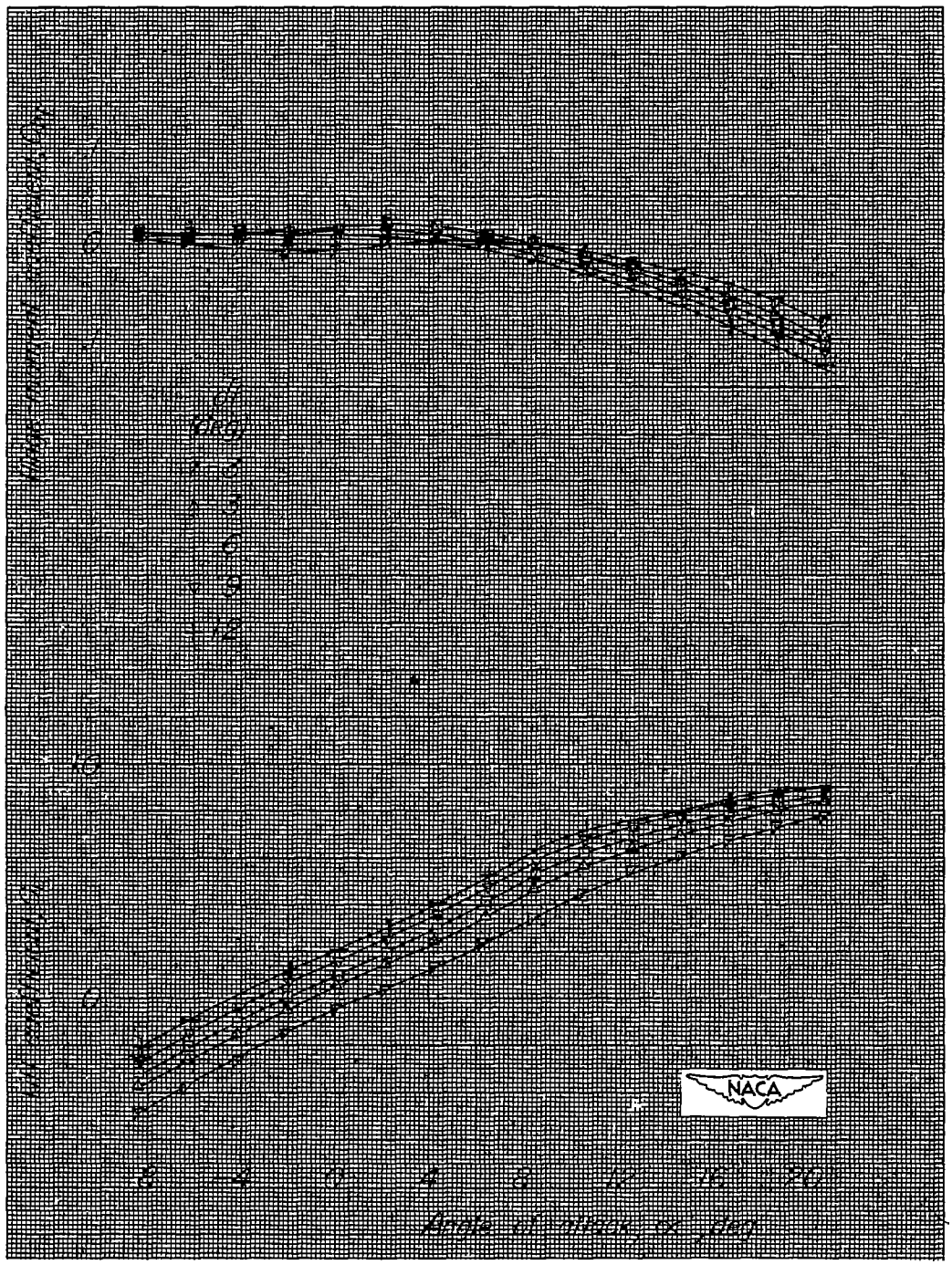

(g) $\delta_t/\delta_f = -0.5$; C_{h_f} and C_L against α.

Figure 43.- Continued.

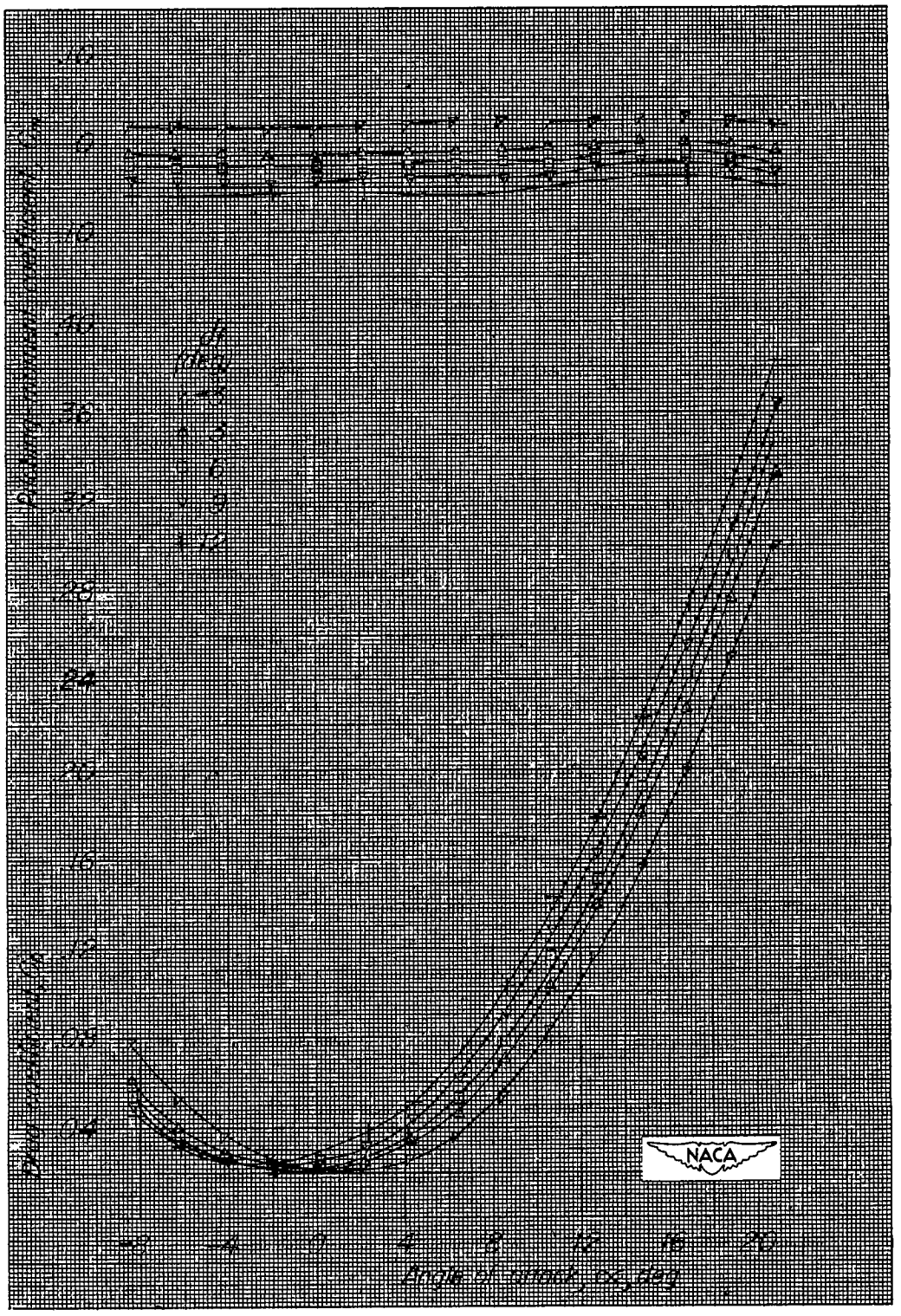

(h) $\delta_t/\delta_f = -0.5$; C_m and C_D against α.

Figure 43.- Continued.

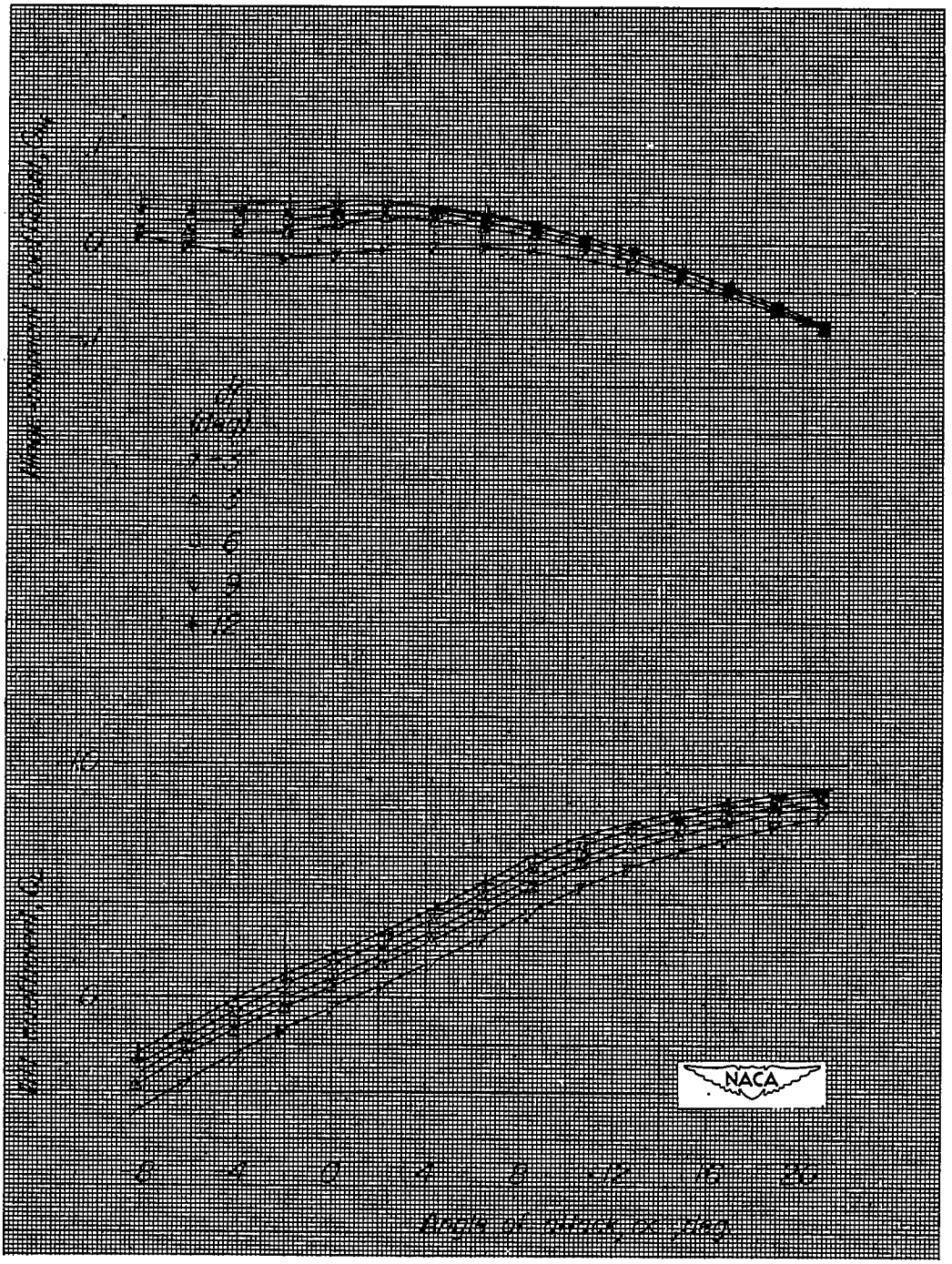

(i) $\delta_t/\delta_f = -1.0$; C_{h_f} and C_L against α.

Figure 43.- Continued.

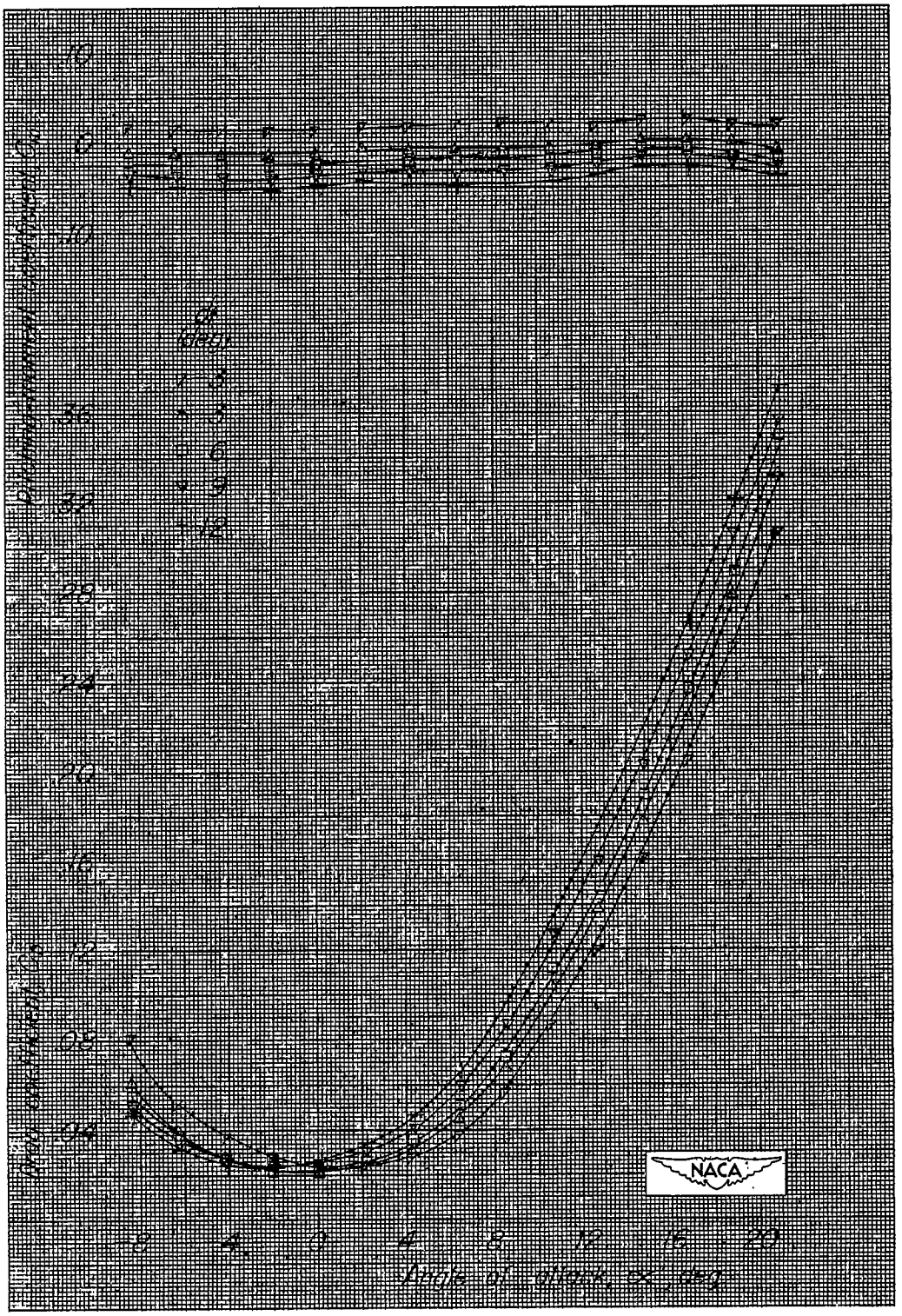

(j) $\delta_t/\delta_f = -1.0$; C_m and C_D against α.

Figure 43.- Concluded.

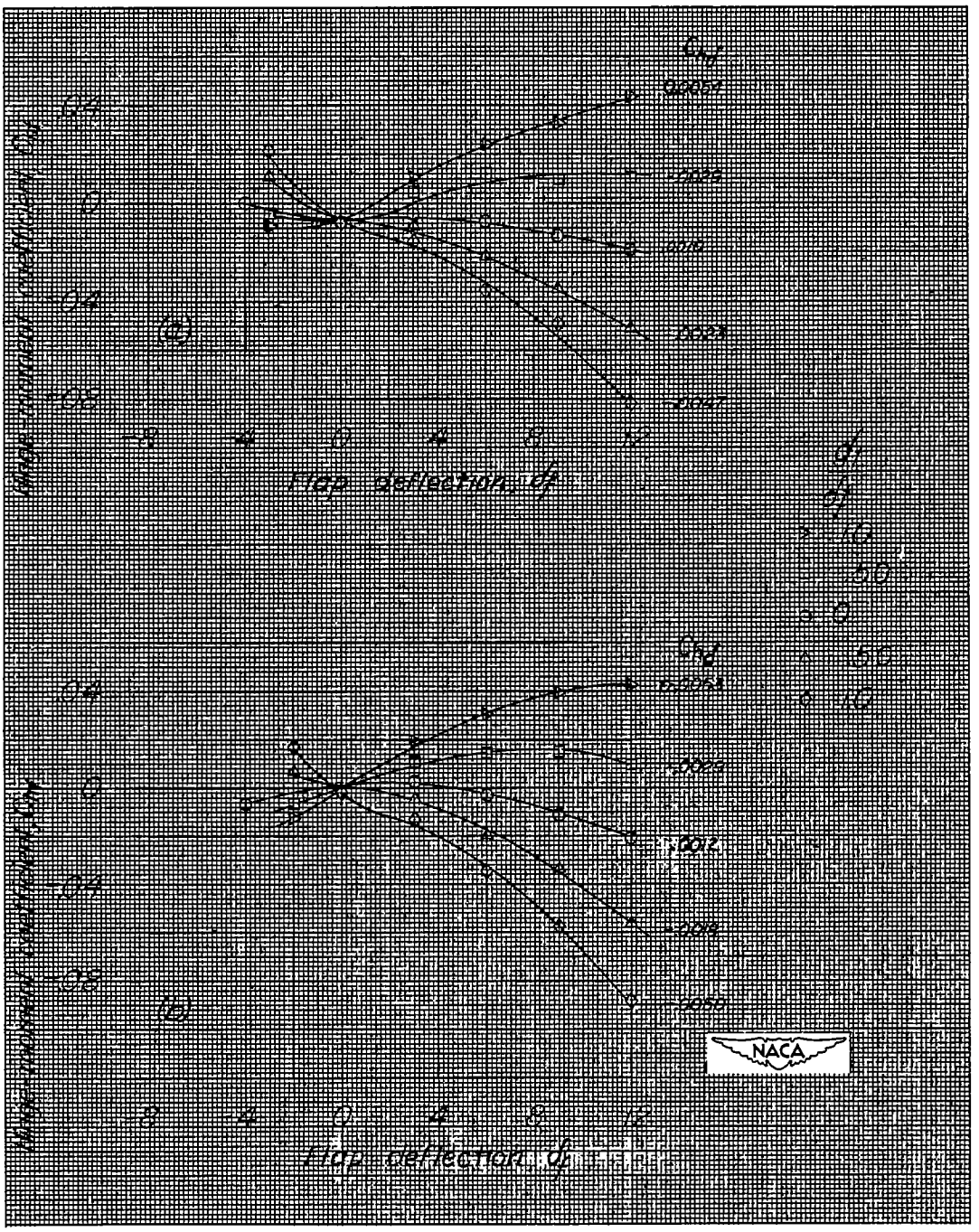

(a) $\alpha_u = -4^\circ$.

(b) $\alpha_u = 0^\circ$.

Figure 44.- Effect of tab deflection on control-surface hinge moment. 9-percent-thick biconvex-arc semispan tail surface; sweepback angle Λ, 40°; taper ratio λ, 0.4; aspect ratio A, 3.30; 0.35c' flap with 0.319c_f' sealed internal balance.

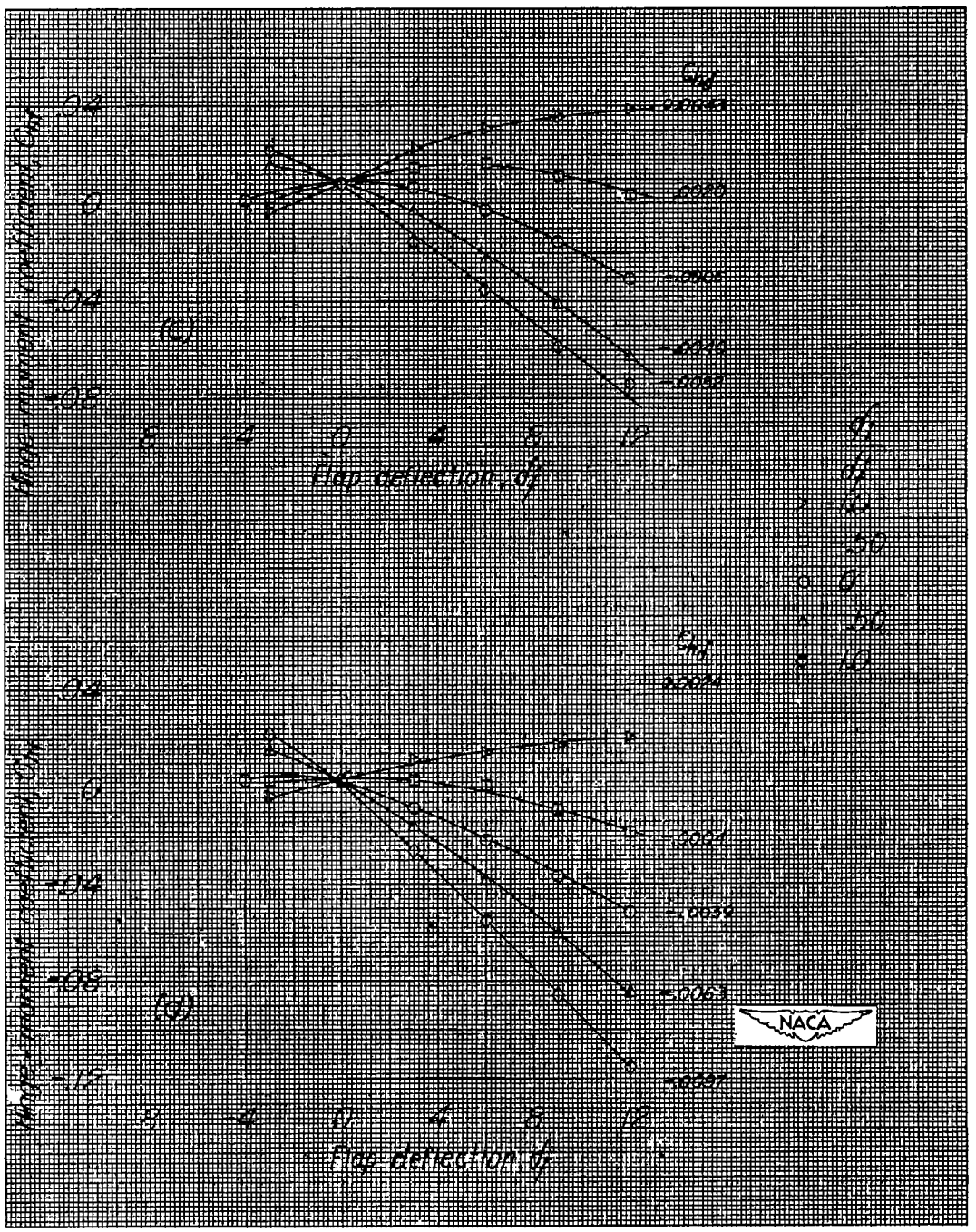

(c) $\alpha_u = 4°$.

(d) $\alpha_u = 8°$.

Figure 44.- Concluded.

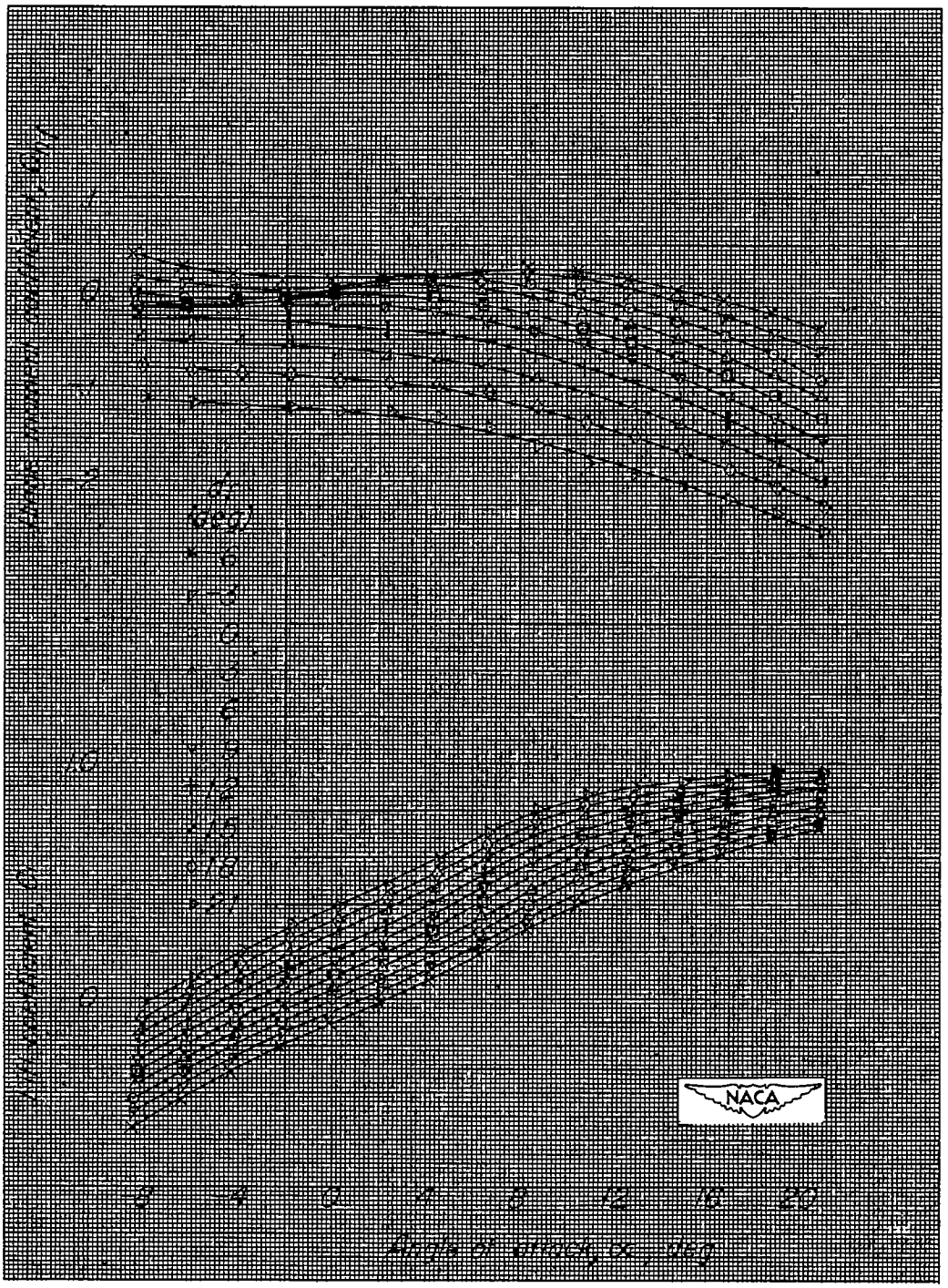

(a) C_{h_f} and C_L against α.

Figure 45.- Nine-percent-thick biconvex-arc semispan tail surface. Sweepback angle Λ, 40°; taper ratio λ, 0.4; aspect ratio A, 3.30; 0.35c' flap with radius nose and horn; 0.005c gap; δ_t/δ_f, 0.

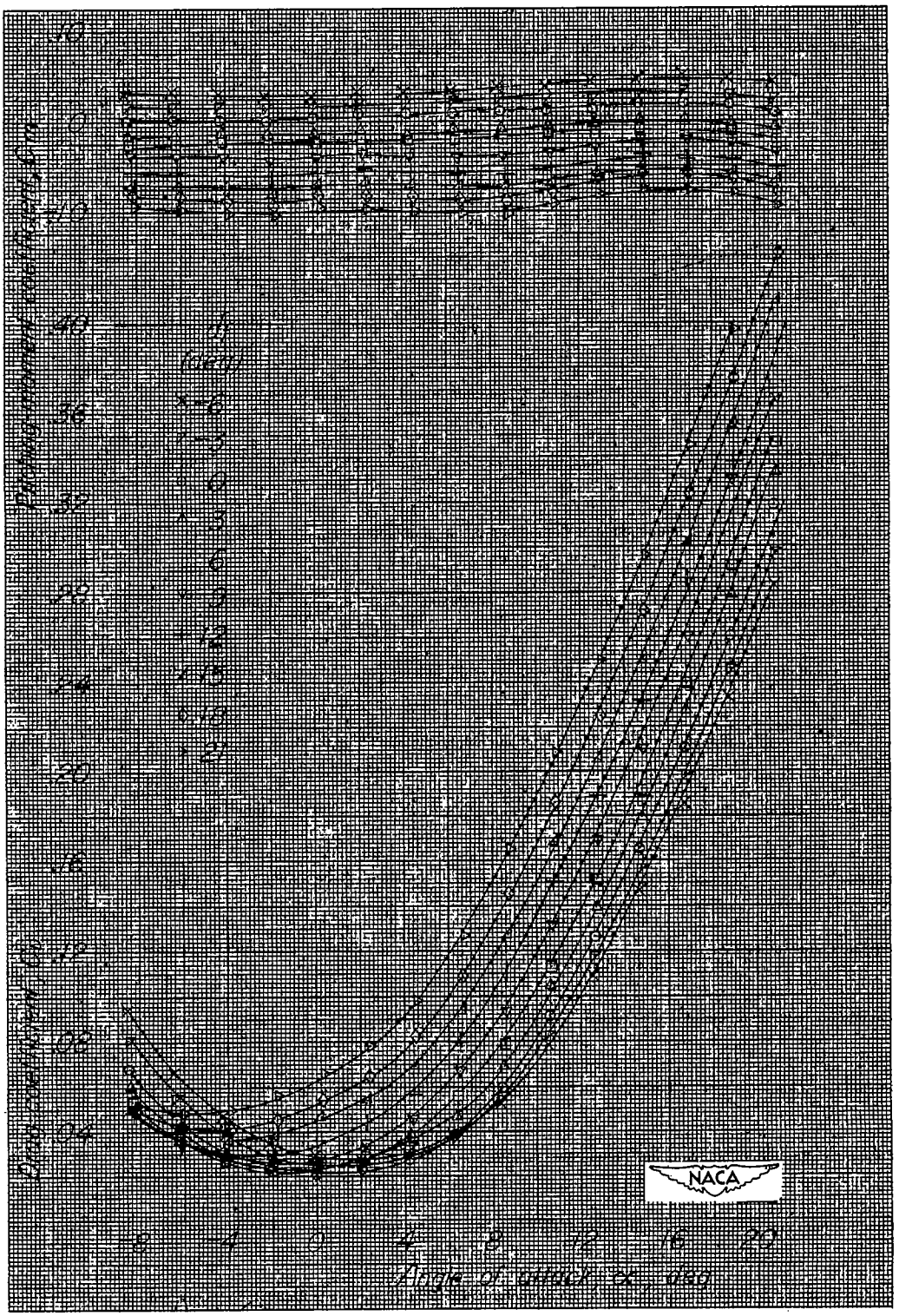

(b) C_m and C_D against α.

Figure 45.- Concluded.

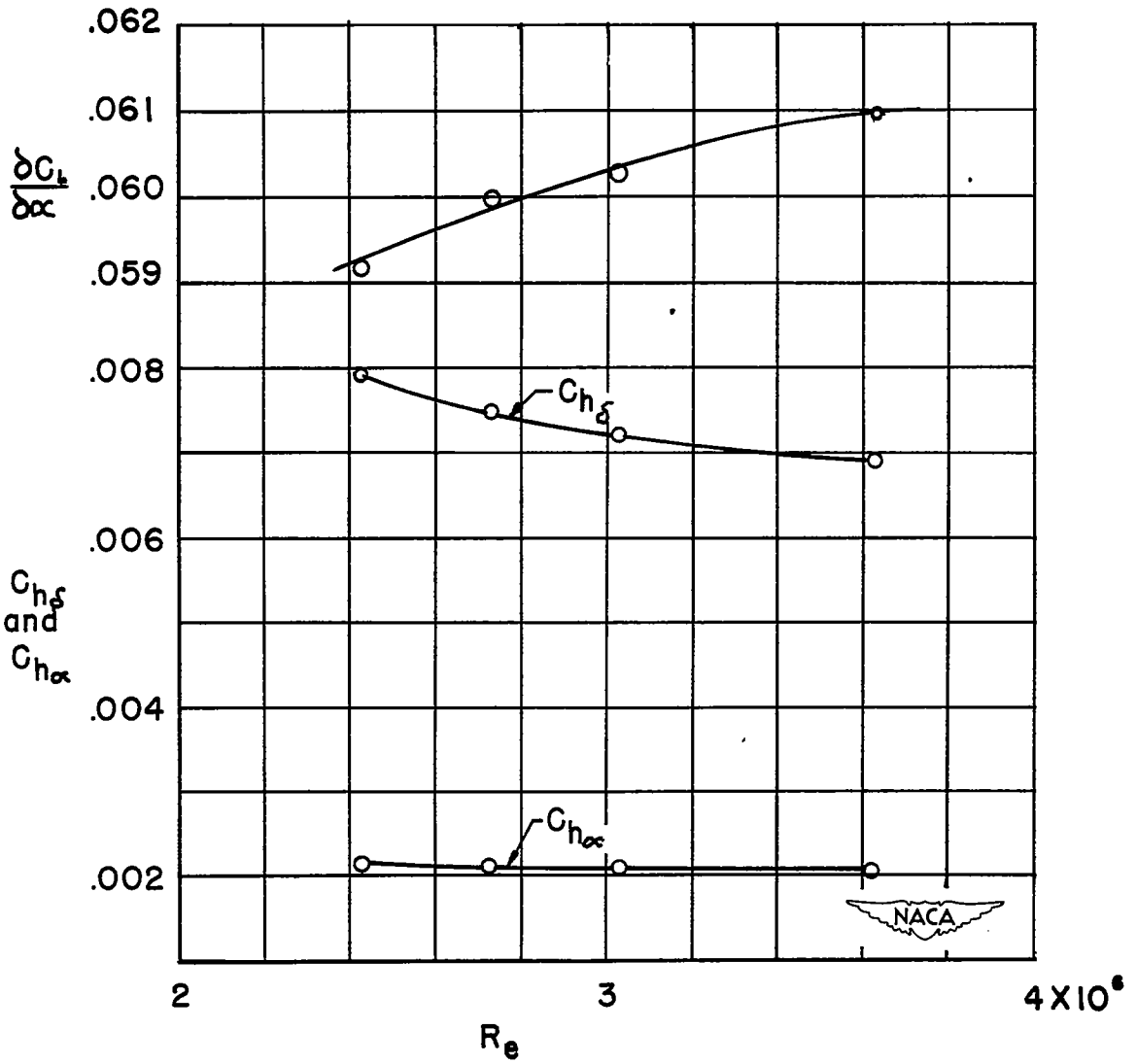

Figure 46.- Reynolds number effect. Data from unpublished results of tests on 9-percent-thick 35° sweptback horizontal-tail panel in 9-foot wind tunnel of Georgia Institute of Technology.

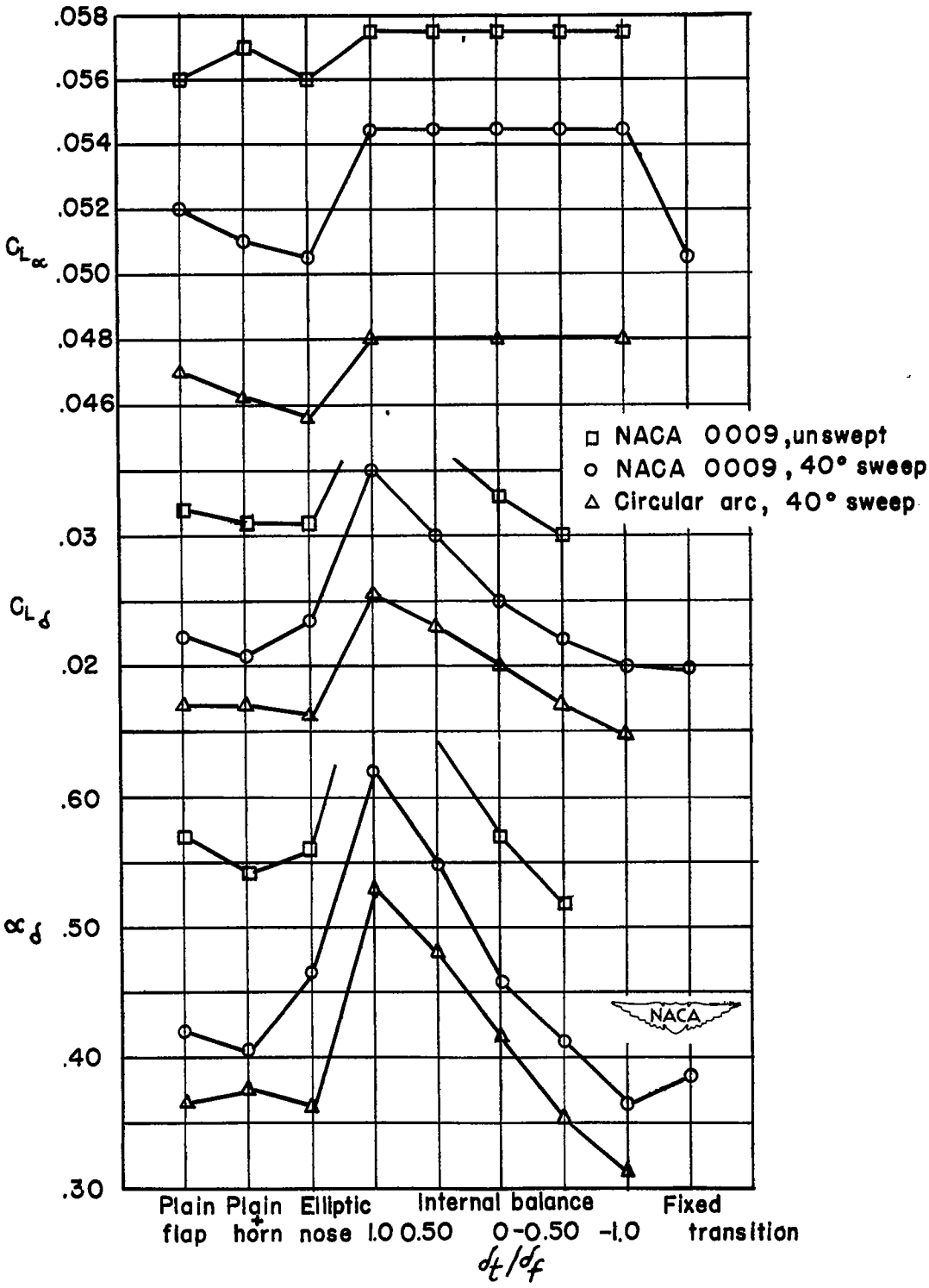

(a) C_{L_α}, C_{L_δ}, and α_δ.

Figure 47.- Graphical comparison of parameters.

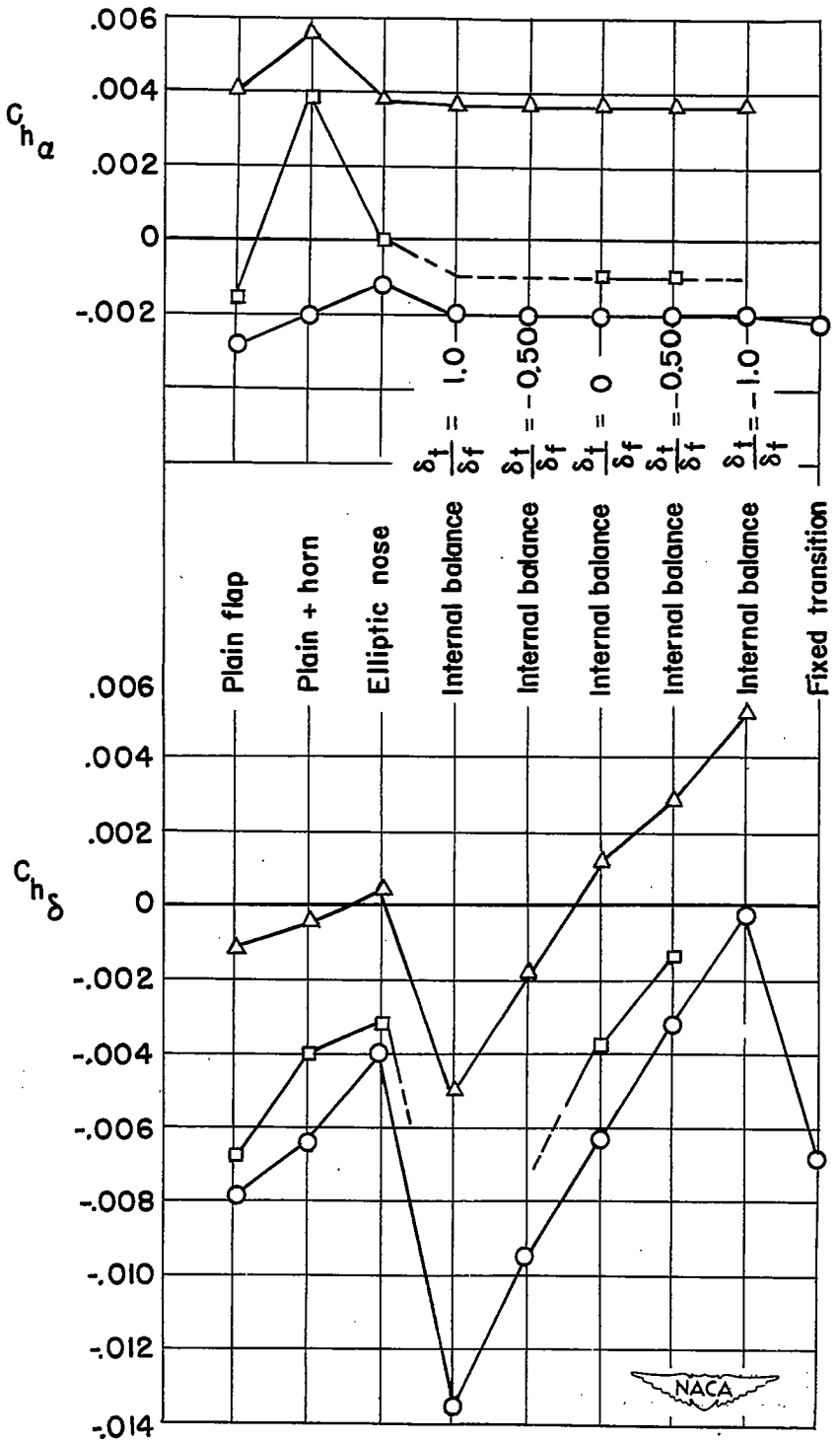

(b) C_{h_α} and C_{h_δ}.

Figure 47.- Concluded.

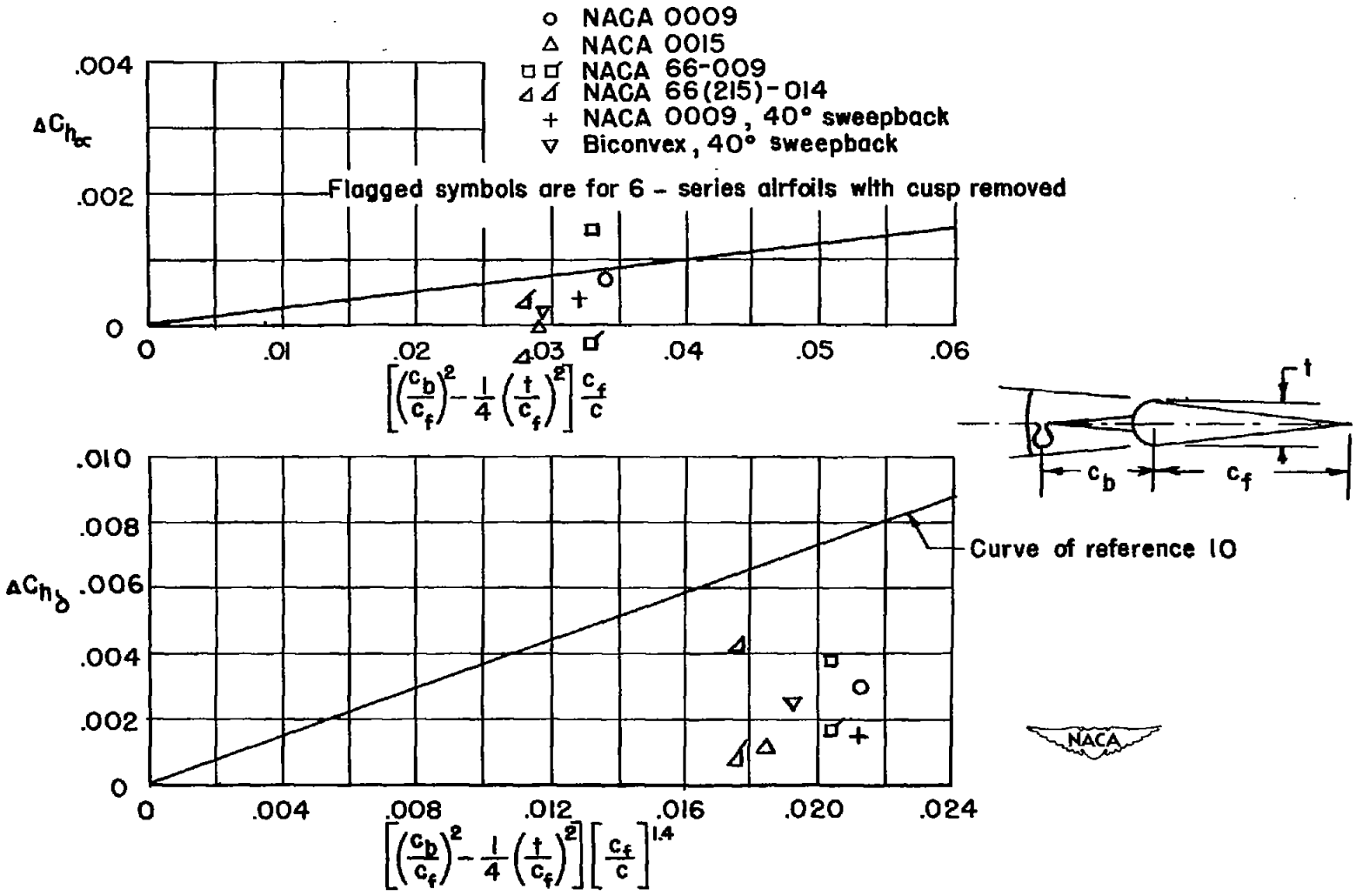

Figure 48.- Comparison of measured and estimated increments of hinge-moment slopes for internal balance.

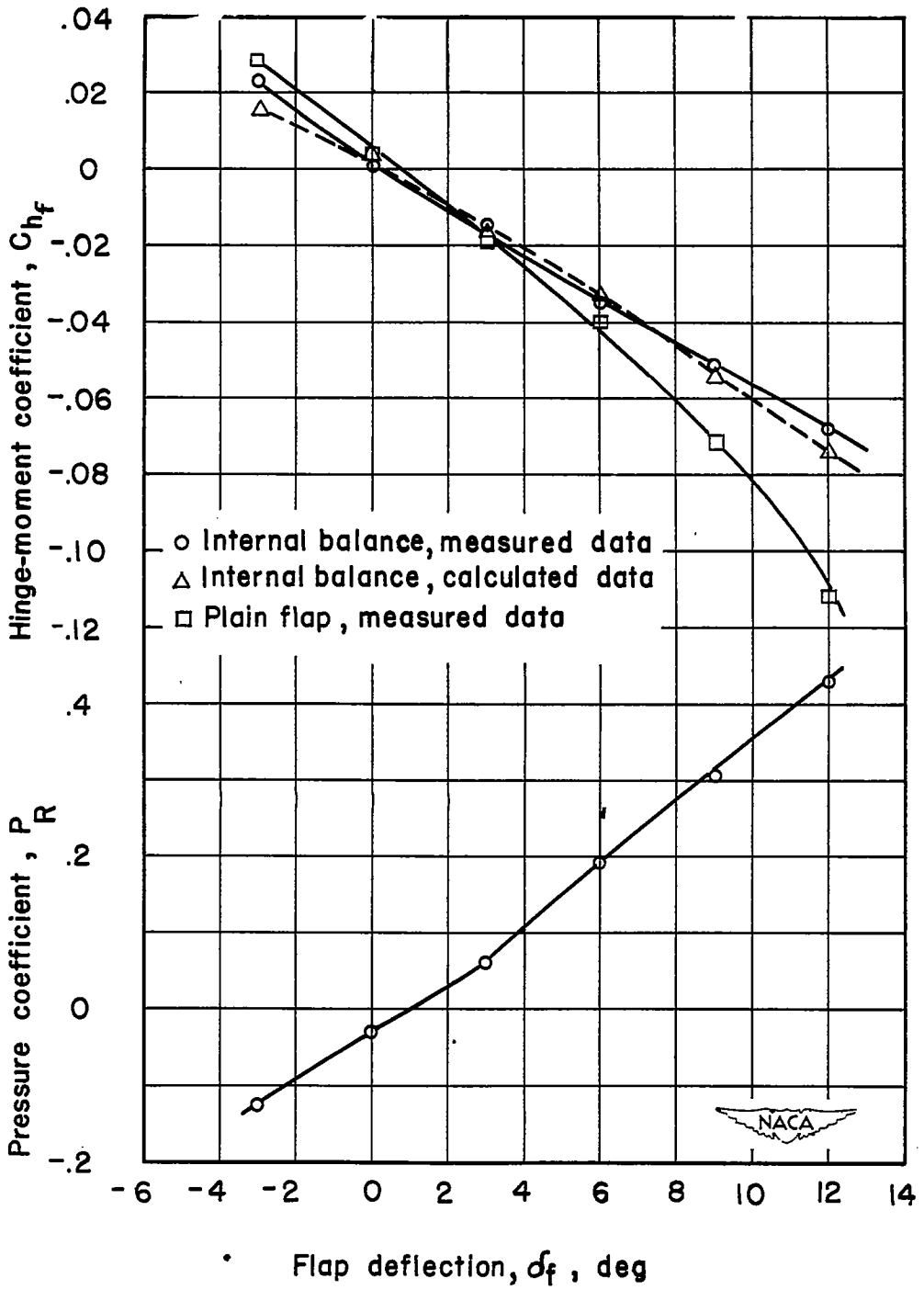

(a) NACA 0009 airfoil model.

Figure 49.- Comparison of measured hinge-moment coefficients with value calculated from balance-chamber pressure coefficient. Sweepback angle Λ, 40°; taper ratio λ, 0.4; aspect ratio A, 3.30; α, 0°.

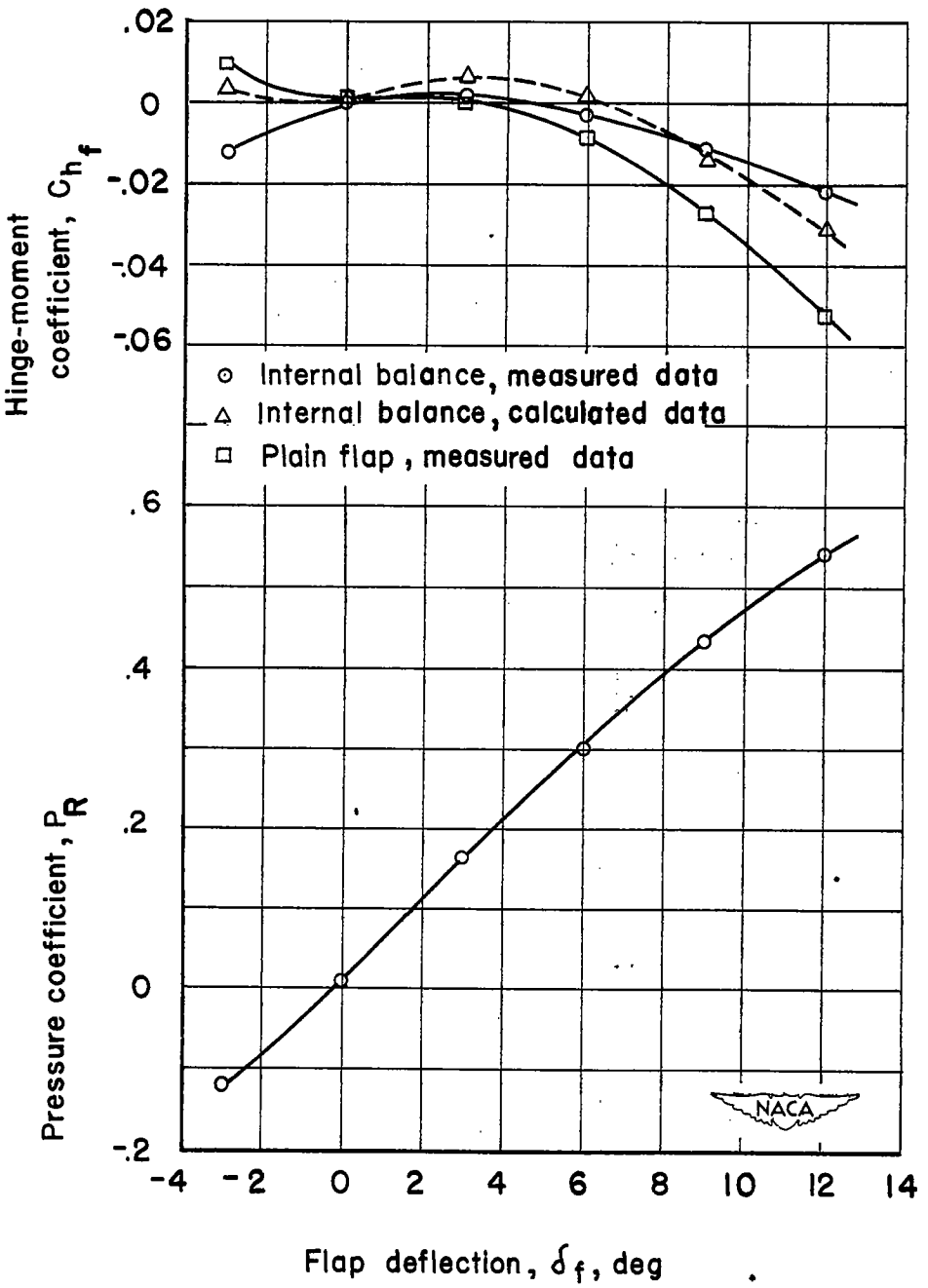

(b) 9-percent-thick biconvex-arc model.

Figure 49.- Concluded.

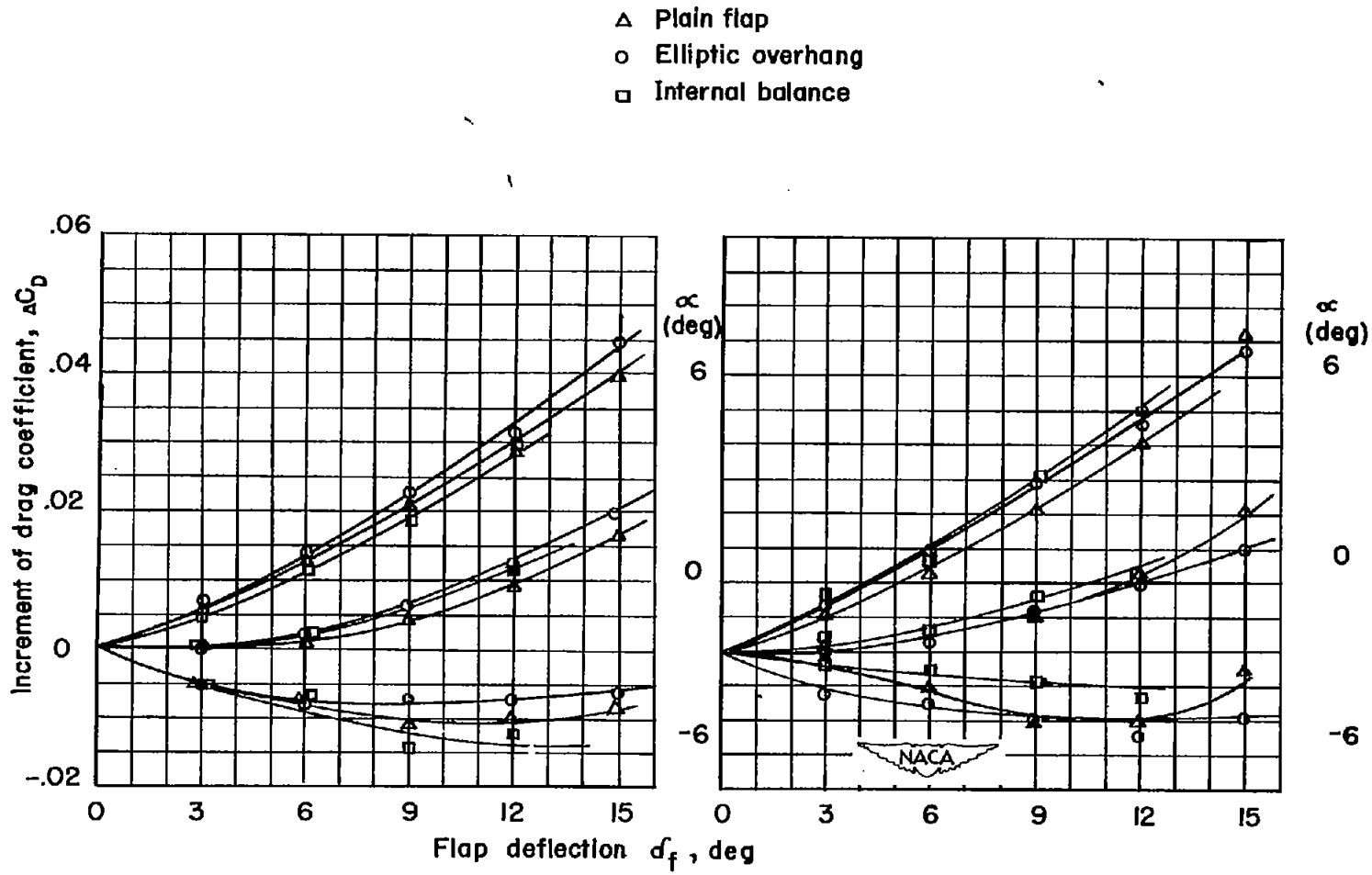

(a) NACA 0009 model; 40° sweepback. (b) Circular-arc model; 40° sweepback.

Figure 50.- Variation of ΔC_D with flap deflection at constant angle of attack.

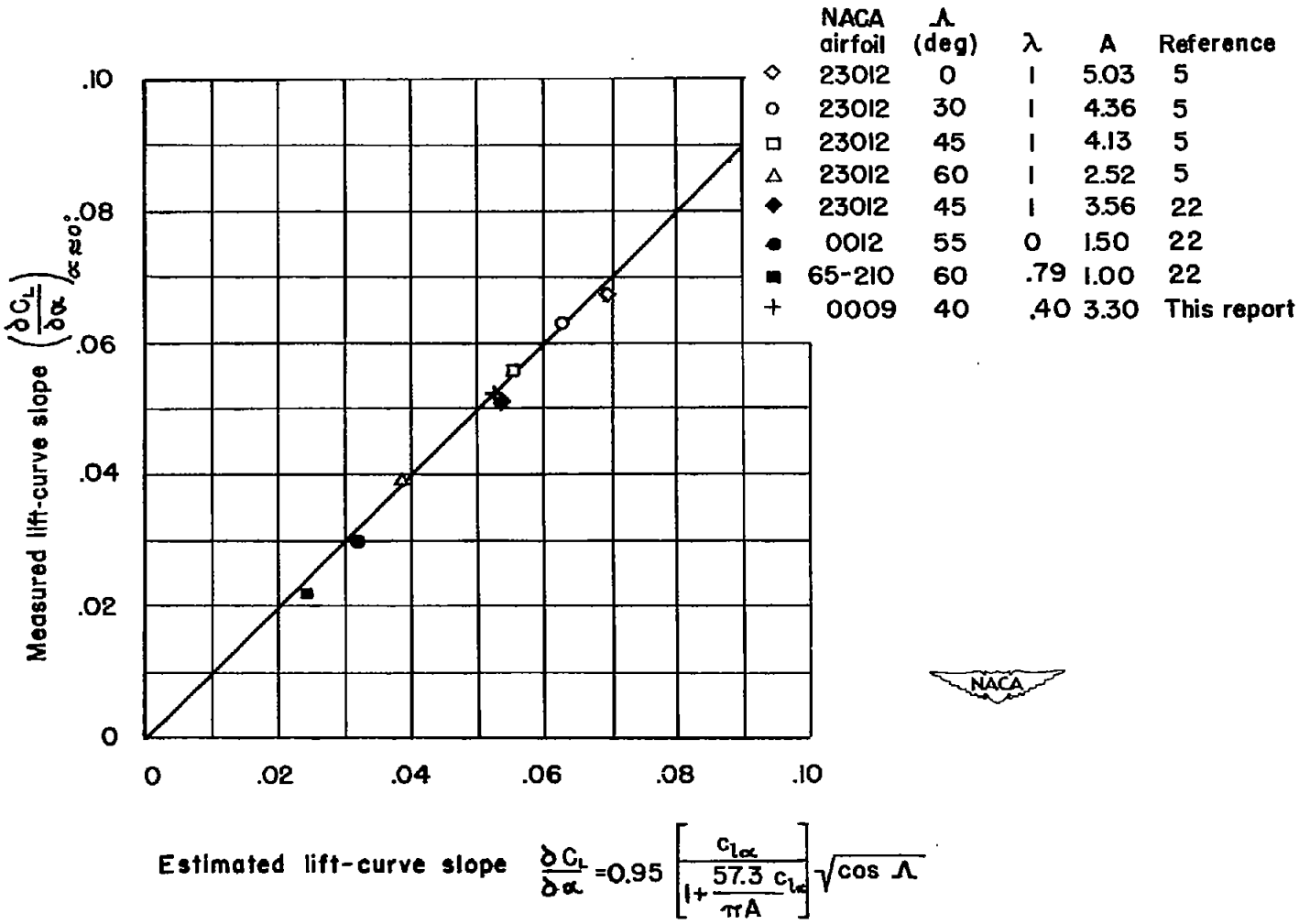

(a) Lift-curve slope C_{L_α}.

Figure 51.- Comparison of measured and estimated values of lift parameters.

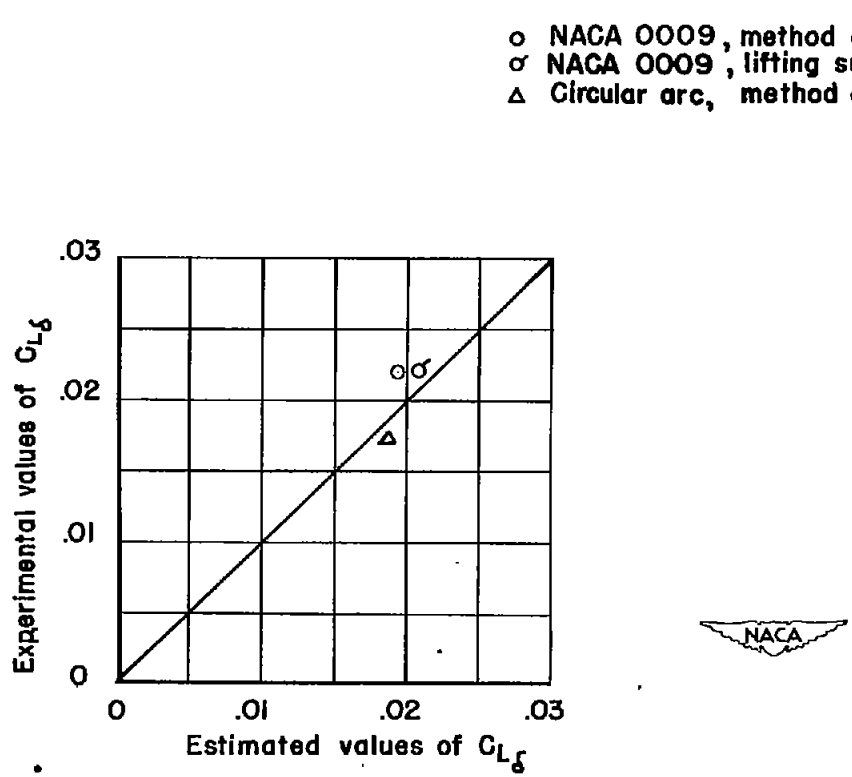

(b) Lift effectiveness parameter C_{L_δ}.

Figure 51.- Concluded.